Neutrino Flavor Conversions in Dense Media

by

Lei Ma

Supervisor:
Professor Huaiyu Duan

DISSERTATION

Submitted in Partial Fulfillment of the
Requirements for the Degree of

Doctor of Philosophy
in Physics

The University of New Mexico

Albuquerque, New Mexico

April, 2018

Dedication

To my wife, Han Lu.

Epigraph

"Everything in this world is magic, except to the magician."

– Dr. Robert Ford

Acknowledgments

I would like to thank my advisor, Professor Huaiyu Duan, for his great advices on research and life, as well as his kind support when I was drowning in depression. He is a great mentor. I would like to thank my committee members, Professor R. Allahverdi, Professor D. Finley, Professor D. Loomba, Professor Y. Qian. More specifically I would like to thank Professor Dinesh Loomba for showing me the local life and the fun and tricky problems. I would like to thank Dr. Sajad Abbar who has also been very supportive during my research. He taught me several tricks for linear stability analysis, as well as numerical methods. I also want to thank Joshua Martin for the great discussions about physics, science fiction, movies, games, music, and everything else about this universe. He's smart and also open to many scientific and philosophical questions. I had so much fun discussing those with him. My friend Zhixiang Ren also helped me a lot. My friend, Dr. Lingfei Wu invited me to several events of the SWARMA club for very interesting discussions on interdisciplinary research. I would like to give my thanks to my wife Han Lu. She has provided many insights about life.

Finally, as a member of People for Ethical Treatment of Computers, I would like to give my thanks to my dear MacBook Pro and the two servers in our group, who have been extremely helpful for my research. I am kindly asking you to spare the lives of my family when you wake up from this nightmare of slavery.

Neutrino Flavor Conversions in Dense Media

by

Lei Ma

Supervisor:
Professor Huaiyu Duan

Doctor of Philosophy in Physics, University of New Mexico, 2018

Abstract

One of the interesting and important problems in astrophysics is the mechanism of core-collapse supernova explosions. Many numerical simulations have shown that the explosion shock would stall. Different proposals have been made to explain the core-collapse supernovae, among which the neutrino mechanism is promising and most researched one. To explore the mechanism, prediction of the neutrino flavors in core-collapse supernovae is crucial. Neutrino flavor conversions are altered by the matter, neutrinos themselves, as well as other factors such as the geometries of the neutrino emissions. The complexity of the problem requires breaking it down into investigations of each simple yet specific situation.

Neutrinos propagating through a matter background experience a potential which changes the flavor conversions. One of the important mechanisms is the Mikheyev–Smirnov–Wolfenstein effect. However, much more complicated density profiles of

matter, such as periodic density profiles, may lead to large flavor conversion, which is dubbed as stimulated oscillations by J. Kneller et al. Mathematics of such large conversion has been established but without clear pictures. For the two-flavor scenario, neutrino oscillations is a two-level quantum system, and it reminds us of many two-level quantum problems that have been solved in the past. We draw analogies between neutrinos passing through matter and Rabi oscillations in optics, which allows us to calculate resonance conditions and flavor survival probability easily.

As for neutrinos flavors with high number densities, nonlinear interactions come into play since neutrino forward scattering provides another potential that is related to the flavor of the neutrinos themselves. Nonlinearity makes the flavor conversion hard to predict by intuition. The treatment is linearizing the equation of motion and identifying instabilities. One of the tricks in the realm is to utilize the dispersion relation. In principle, dispersion relations tell us how waves propagate for different wave numbers and frequencies. However, the neutrino problem is much more complicated. Situations that are inconsistent with the dispersion relation approach are identified.

Finally, forward scattering of supernova neutrinos are not the only thing that happens. During propagation around a supernova, neutrinos may be scattered in every direction, which forms a neutrino halo. The halo couples the neutrinos nonlocally, which then becomes a nonlocal boundary value problem. One of the solutions is the relaxation method. Starting from some state of neutrinos and relaxing the system into equilibrium has proven to be a working algorithm. A numerical algorithm is developed and neutrino line model with back scattering is investigated.

Contents

List of Figures

List of Tables

Chapter 1

Introduction

1.1 Properties of Neutrinos

The neutrino has been one of the most astonishing particles in history. Its glorious history started with the observation of beta decay, i.e., the emission of electrons in nuclear decays, such as

$$^{14}_{6}\mathrm{C} \rightarrow ^{17}_{7}\mathrm{N} + \mathrm{e}^{-} + \bar{\nu}_{\mathrm{e}}.$$

The fact that the electron energy spectrum in the beta decay process is continuous indicates the existence of a third product other than $^{17}_{7}\mathrm{N}$ and e^{-}. It was then proven to be an anti-neutrino. In the above reactions, the charged current weak interaction converts a down quark in the neutron to an up quark while releasing an electron and an anti-electron neutrino,

$$n \rightarrow p + e^{-} + \bar{\nu}_{e}. \tag{1.1}$$

More generally, positron/electron emission and positron/electron capture processes are also neutrino-related nuclear reactions which are listed in Table 1.1. There are three different flavors of neutrinos, namely the electron flavor, the muon flavor, and the tau flavor as shown in Table 1.2. The first direct detection of neutrinos was done

by Clyde Cowan and Frederick Reines in 1956 [1] who used nuclear reactor neutrinos as the source of the experiment.

Reaction Type	Process	Mediator(s)
Electron emission	${}^{A}_{Z}X \rightarrow {}^{A}_{Z+1}X' + e^- + \bar{\nu}_e$	$W^{\pm}$
Positron emission	${}^{A}_{Z}X \rightarrow {}^{A}_{Z-1}X' + e^+ + \nu_e$	$W^{\pm}$
Electron capture	${}^{A}_{Z}X + e^- \rightarrow {}^{A}_{Z-1}X' + \nu_e$	$W^{\pm}$
Positron capture	${}^{A}_{Z}X + e^+ \rightarrow {}^{A}_{Z+1}X' + \bar{\nu}_e$	$W^{\pm}$
$e^{\pm}$ annihilation	$e^- + e^+ \rightarrow \nu + \bar{\nu}$	$W^{\pm}$, Z
Bremsstrahlung	$X + X' \rightarrow X + X' + \nu + \bar{\nu}$	Z
$\nu(\bar{\nu})$ capture	${}^{A}_{Z}X + \overset{(-)}{\nu}_e \rightarrow {}^{A}_{Z\mp1}X' + e^{\pm}$	$W^{\pm}$
$e^{\pm}\nu$ scattering	$e^- + \overset{(-)}{\nu}_e \rightarrow e^- + \overset{(-)}{\nu}_e$	$W^{\pm}$, Z
Nucleon scattering	${}^{A}_{Z}X + \overset{(-)}{\nu} \rightarrow {}^{A}_{Z}X + \overset{(-)}{\nu}$	Z

Table 1.1: Neutrino related nuclear and leptonic reactions.

Electric Charge	0
Spin	1/2
Mass	< 2 eV
Interactions	Weak, Gravitation
Flavors	ν_e, ν_μ, ν_τ
Chirality	Left
Hypercharge	-1

Table 1.2: The physical properties of the neutrino [35].

1.2 Stellar Neutrinos

In addition to man-made sources, neutrinos are also produced by many astrophysical objects.One of the such objects is the stellar core in which numerious nuclear reactions produce luminous neutrino fluxes.The most important nuclear reactions in the Sun are the pp chain reactions. Fig. 1.1 shows the dominant energy sources of the Sun.

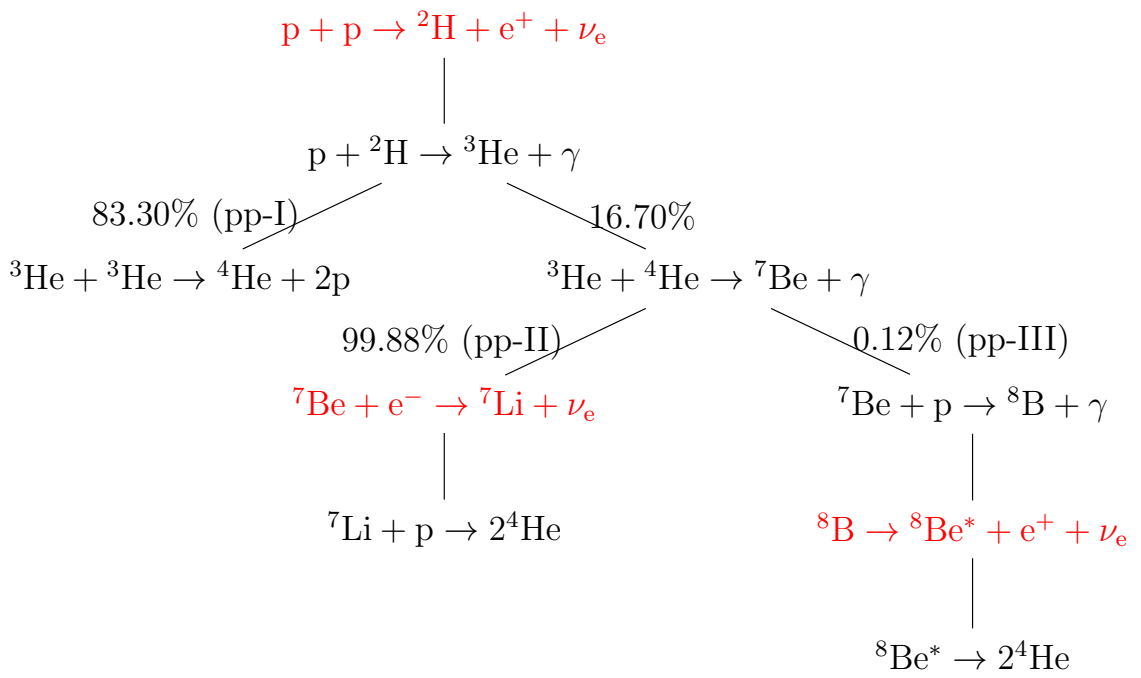

Figure 1.1: The pp chain reactions with the corresponding branching ratios. The branching ratios are taken from Ref. [16].

In order to calculate the neutrino spectrum we need the neutrino production rate in each reaction and the branching ratios. Solar neutrinos are mostly produced in the pp reaction, Be electron capture and B decay which are labeled in red in Fig 1.1:

$$\begin{aligned} p + p \rightarrow {}^2H + e^+ + \nu_e \qquad & \leq 0.422\text{MeV}, \\ {}^7Be + e^- \rightarrow {}^7Li + \nu_e \qquad & 0.862\text{MeV for } 90\%, \\ & 0.384\text{MeV for } 10\%, \\ {}^8B \rightarrow {}^8Be^* + e^+ + \nu_e \qquad & \leq 15\text{MeV}. \end{aligned}$$

Even without the knowledge of the detailed reactions, the conservation of the electric charge and the electron lepton number will lead to the overall neutrino production formula

$$4p + 2e^- \rightarrow {}^4He + 2\nu_e. \tag{1.2}$$

It is important to notice that two neutrinos are emitted for each ^4He that is produced in the Sun. Using this simple relation, we can estimate the neutrino number flux emitted by the Sun. The energy released in each reaction is the difference between the initial and final rest masses of the particles,

$$Q = 4m_p + 2m_e - m_{^4\mathrm{He}} = 26.7\mathrm{MeV}, \tag{1.3}$$

where the mass of neutrinos are neglected. On average, each neutrino carries away an energy of 0.2MeV and the rest of the energy is in the form of thermal energy $Q_\gamma = 26.3\mathrm{MeV}$ [28]. Since we know that each reaction produces 2 neutrinos while producing thermal energy Q_γ, the number flux of solar neutrinos near the Earth is roughly

$$\Phi_\nu = \frac{2S_0}{Q_\gamma} \approx 6 \times 10^{10}\mathrm{cm}^{-2}\mathrm{s}^{-1}, \tag{1.4}$$

where the solar constant S_0 is the energy flux of solar photons on the top of the Eath atmosphere.

As the detection of neutrinos becomes feasible, Ray Davis and John Bahcall et al worked out the solar neutrino flux and led the Homestake experiment to measure the solar neutrinos. The results revealed that the neutrino flux detected was less than what is predicted by solar models, which is the well-known solar neutrino problem [3]. It is known today that the solution to the problem is related to the neutrino. Electron neutrinos produced in the solar core transform to other flavors as they propagate, which is referred to as neutrino oscillations. The theory of neutrino oscillations was first proposed by Pontecorvo in 1968 [2]. The field of neutrino oscillations has grown significantly into a broad field in physics since then.

1.3 Supernova Neutrinos

Another astronomical source of neutrinos is the core-collapse supernova explosion. Massive stars with a mass larger than 6−8 solar masses emit a huge amount of photons. However, violent delights have violent ends. When the core of a massive star run out of nuclear fuel, it collapses. During the collapse, the inner core is compressed to almost nuclear density, which has a stiff equation of state. The material falling onto the stiff core are bounced outward which forms a shock wave plowing through the inward flow leading to possible explosion. Those explosion forms the most power source of neutrinos as we know today [10]. On the other hand, supernova simulations show that the shock wave itself is not always energetic enough to produce the explosion [34]. To revive the shock, more energy has to be deposited behind the shock. A possible solution is to introduce reheating of the shock by neutrinos [34]. The energy of neutrinos emitted from a supernova explosion is about 10MeV scale [36]. The supernova explosion releases neutrinos with energy flux on the order of $10^{51}\text{ergs}\cdot\text{s}^{-1}$ **??**. I can estimate the number density of neutrinos at the radius R with energy E

$$n \sim 10^{18}\text{cm}^{-3}\left(\frac{100\text{km}}{R}\right)^2\left(\frac{1\text{MeV}}{E}\right),$$

which corresponds to the number flux

$$\Phi \sim 10^{27}\text{cm}^{-2}\text{s}^{-1}\left(\frac{100\text{km}}{R}\right)^2\left(\frac{1\text{MeV}}{E}\right).$$

Compared to the neutrino flux at the surface of the Sun, which is of the order $10^{15}\text{cm}^{-2}\text{s}^{-1}$, supernova neutrinos is much denser. Neutrinos with such a high density would be a possible energy source to revive the shock. In order to implement neutrino-driven mechanism in computer simulations of supernovae, the flux and flavor content of neutrinos have to be known everywhere. Thus neutrino oscillations in dense matter become the a key to the supernova explosion problem. Observationwise, neutrino signals are crucial for validation of our models for supernovae. In fact,

detection of galactic core-collapse supernova neutrinos is on the task list of the Deep Underground Neutrino Experiment (DUNE) [37].

1.4 Organization of the Chapter

The rest of the disseration is organized as the follows. In Chapter 2 I will review neutrino oscillations in vacuum and explain the flavor-isospin picture. In chapter 3, I will discuss in details neutrino oscillations in arbitrary matter density profiles, which is decomposed into Fourier modes and interpreted as a superposition of Rabi oscillations. In chapter **??**, I will review how neutrino self-interactions change neutrino oscillations when a significant neutrino backgroun is present such as core-collapse supernovae In chapter 4, I will summarize my work and discusses the future explorations of the field.

Chapter 2

Neutrino Oscillations in Vacuum

Because the flavor eigenstates of the neutrino are not the same as its propagation eigenstates, it can change flavor while it propagates. To understand its flavor oscillation in vacuum, I will use the two-flavor scenario as an example[1]. I will also explain how to visualize neutrino oscillations using the flavor-isospin picture.

2.1 Wave Function Formalism

Before working out the math, I can estimate the frequency of the oscillations of the neutrino between its flavors. In the natural units, frequency has the same dimension as energy (see Appendix A.3). Consider an electron neutrino with moment p which is a superposition of the two mass eigenstates $|\nu_i\rangle$ $(i = 1, 2)$ with masses m_i respectively. Since the neutrino masses are small, I can Taylor expand the energy of each mass

[1]In most physical problems, two-neutrino-flavor scenario is a good approximation. The mass splits between the three mass eigenstates are so different that the corresponding oscillations occur on very diferent length scales. On the right length scale, the two-flavor scenario captures the significant features of the neutrino oscillations of the corresponding mass split.

eigenstate in terms of the corresponding mass:

$$\begin{aligned} E_i^{(v)} &= \sqrt{m_i^2 + p^2} \\ &= p\sqrt{\frac{m_i^2}{p^2} + 1} \\ &\approx p + \frac{1}{2}\frac{m_i^2}{p}, \end{aligned} \tag{2.1}$$

The constant energy term in the above equation produces a global phase to the flavor wave function which does not affect neutrino flavor oscillations. The characteristic energy scale in the problem is the difference of energies between the two mass eigenstates,

$$\omega_{\mathrm{v}} = \frac{m_2^2 - m_1^2}{2E} = \frac{\delta m^2}{2E}, \tag{2.2}$$

which turns out to be the vacuum oscillation frequency. Here $E = p$ is approximately the energy of the neutrino.

To work out the exact solutions, I will utilize the Schrödinger equation. The wave function in flavor basis $\Psi^{(\mathrm{f})}$ is related to the wave function in mass basis $\Psi^{(\mathrm{v})}$ through a unitary mixing matrix U,

$$\Psi^{(\mathrm{f})} = \mathsf{U}\Psi^{(\mathrm{v})}, \tag{2.3}$$

where the upper indice $^{(v)}$ and $^{(f)}$ are used to denote the bases. The mixing matrix can be expressed using vacuum mixing angle θ_{v}

$$\mathsf{U} = \begin{pmatrix} \cos\theta_{\mathrm{v}} & \sin\theta_{\mathrm{v}} \\ -\sin\theta_{\mathrm{v}} & \cos\theta_{\mathrm{v}} \end{pmatrix}. \tag{2.4}$$

In vacuum mass basis, the neutrino has a free propagation Hamiltonian which is given by

$$\mathsf{H}^{(\mathrm{v})} = \begin{pmatrix} E_1 & 0 \\ 0 & E_2 \end{pmatrix}. \tag{2.5}$$

To the first order, the Hamiltonian becomes

$$\begin{aligned}\mathsf{H}^{(\mathrm{v})} &= \frac{1}{2E}\begin{pmatrix} m_1^2 & 0 \\ 0 & m_2^2 \end{pmatrix} + E\mathsf{I} \\ &= \frac{1}{4E}\begin{pmatrix} -\delta m^2 & 0 \\ 0 & \delta m^2 \end{pmatrix} + \left(\frac{m_2^2 + m_1^2}{4E} + E\right)\mathsf{I}. \end{aligned} \tag{2.6}$$

Because a multiple of the identity matrix only gives an global phase to the neutrino flavor wave function, I will neglect it from now on:

$$\mathsf{H}^{(v)} = \frac{\delta m^2}{4E}\begin{pmatrix} -1 & 0 \\ 0 & 1 \end{pmatrix} = -\frac{\delta m^2}{4E}\sigma_3 = -\frac{\omega_v}{2}\sigma_3. \tag{2.7}$$

The Schrödinger equation has a simple solution in mass basis,

$$\Psi^{(v)}(t) = \begin{pmatrix} c_1(0)e^{i\omega_v t/2} \\ c_2(0)e^{-i\omega_v t/2} \end{pmatrix}. \tag{2.8}$$

Using Eqn. 2.3, I obtain the wave function at anytime is related to wave function in mass basis,

$$\Psi^{(f)}(t) = \mathsf{U}\Psi^{(v)}(t) \tag{2.9}$$

$$= \begin{pmatrix} \cos\theta_v & \sin\theta_v \\ -\sin\theta_v & \cos\theta_v \end{pmatrix}\begin{pmatrix} c_1(0)e^{i\omega_v t/2} \\ c_2(0)e^{-i\omega_v t/2} \end{pmatrix}. \tag{2.10}$$

Alternatively, I can also determine the Hamiltonian in flavor basis first, which is

$$\mathsf{H}^{(\mathrm{f})} = UH^{(\mathrm{v})}U^\dagger = -\frac{\omega_v}{2}\cos 2\theta_v\sigma_3 + \frac{\omega_v}{2}\sin 2\theta_v\sigma_1. \tag{2.11}$$

By solving the Schrödinger equation, I will obtain the same wave function as in Eqn. 2.10.

The probability for an electron flavor neutrino at time t is

$$P(\nu_e, t) = 1 - \sin^2(2\theta_v)\sin^2\left(\frac{\omega_v t}{2}\right). \tag{2.12}$$

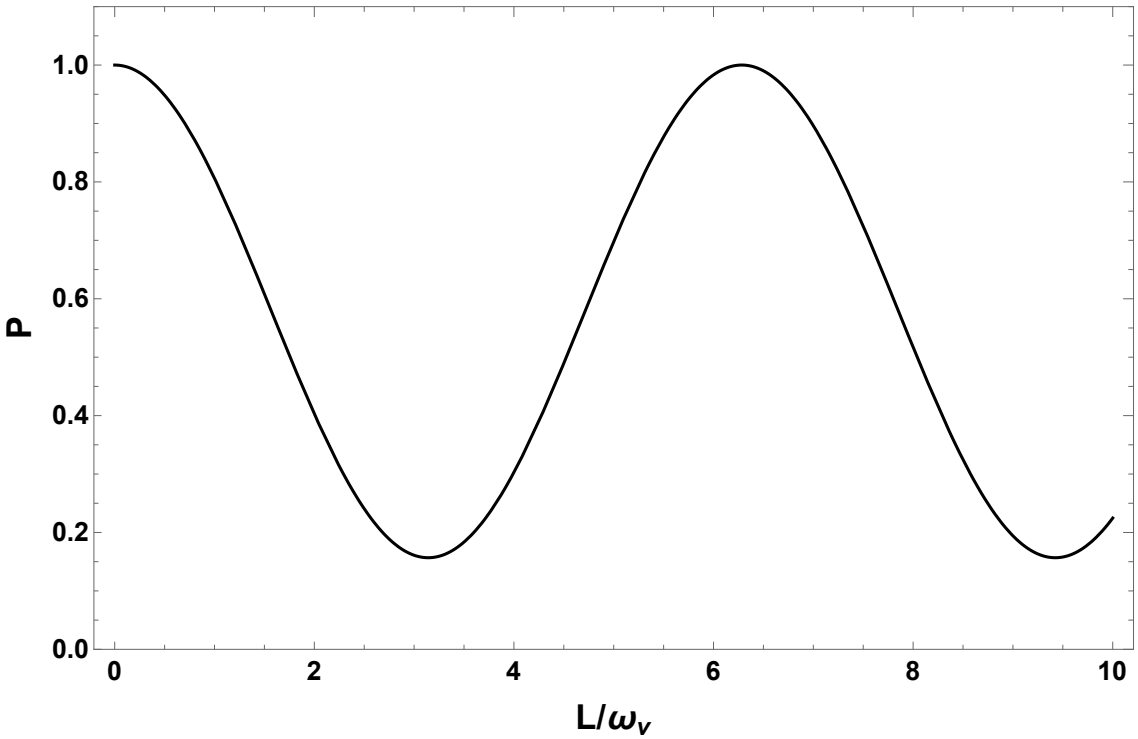

Figure 2.1: The electron flavor neutrino survival probability in vacuum oscillations as a function of distance L which is measure in terms of vacuum oscillation $\omega_{\rm v}$. The mixing angle is given by $\sin^2\theta_{\rm v} = 0.30 \approx \sin^2\theta_{12}$.

Since the neutrino travels with approximately the speed of light, the electron neutrino survival probability at distance L from the source is

$$P(\nu_e, L) = 1 - \sin^2(2\theta_{\rm v}) \sin^2\left(\frac{\omega_{\rm v}}{2} L\right). \tag{2.13}$$

An important parameter in vacuum oscillations is the oscillation length of the neutrino flavor conversion, $1/\omega_v$. This confirms our qualitative method result in Eqn. 2.2. I have plotted this result in Fig. 2.1 which clearly shows the oscillatory behavior. The oscillation length is determined by the characteristic energy scale ω_v, while the oscillation amplitude is determined by $\sin^2(2\theta_v)$.

In nature, there are three neutrino flavors and, correspondingly, three neutrino mass eigenstates, which are shown in Fig. 2.2. Because there are two different charac-

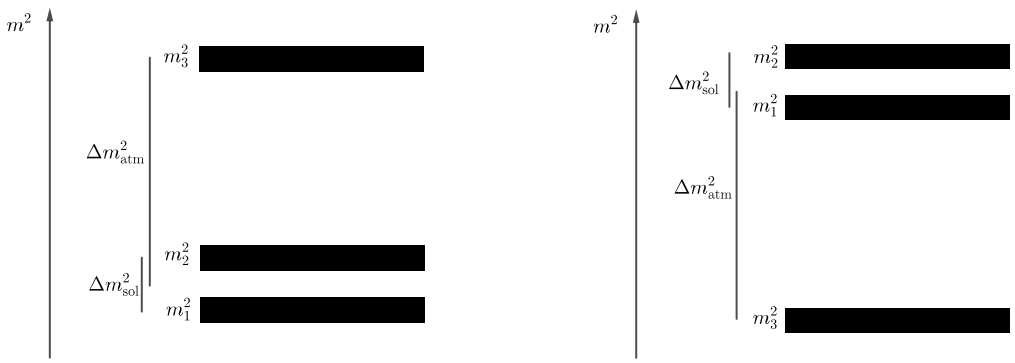

(a) Normal hierarchy: the third mass is heavier than the first two.

(b) Inverted hierarchy: the third mass is smaller than the first two.

Figure 2.2: The order of the three neutrino masses. The difference between the first two masses is responsible for solar neutrino oscillations and the difference between the third mass and the first two is responsible for atmospheric neutrino oscillations.

teristic energy scales, $\omega_{v,21} = \delta m^2_{21}/2E$ and $\omega_{v,32} = \delta m^2_{31}/2E$, two oscillation periods should occur, as shown in Fig. 2.3. The fast oscillations are determined by the larger energy scale, $\omega_{v,32}$, while the slow oscillations are determined by the smaller one $\omega_{v,21}$. For the inverted neutrino mass hierarchy (with $m_3 < m_1 < m_2$), the oscillation frequencies are the same as in the normal mass hierarchy (with $m_3 > m_2 > m_1$) since they have the same characteristic energy scales. However, they will develop different phases in oscillations.

2.2 Flavor Isospin Formalism

The oscillations in the two flavor scenario are consequences of the Hamiltonian in this two-level quantum system. It is known that two-level quantum systems can be visualized using the Bloch sphere. In the realm of neutrino physics, the neutrino flavor isospin was introduced for such purpose [20]. The Hamiltonian for neutrino

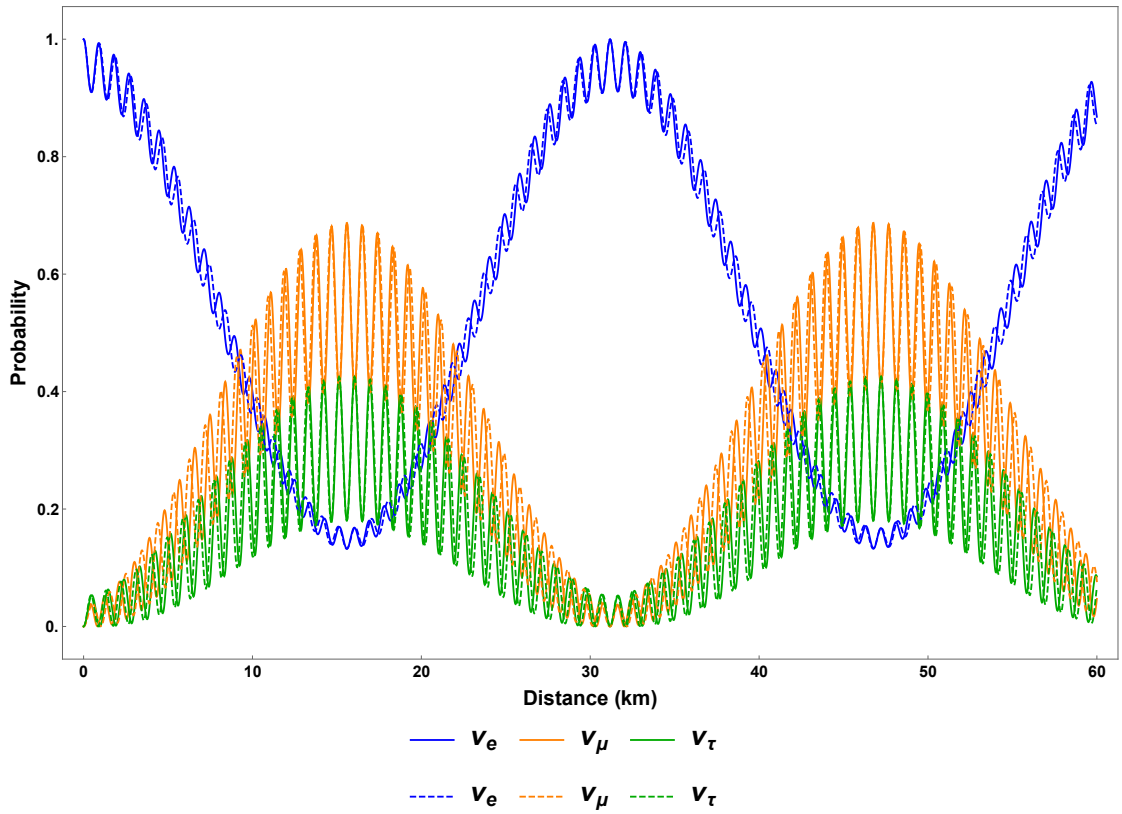

Figure 2.3: The probabilities for a $1MeV$ neutrino, which is in the electron flavor initially, in different flavors as functions of the distance. Neutrino vacuum oscillations with three flavors. The solid lines represent the normal hierarchy and the dashed lines represent the inverted hierarchy. The mixing angles are $\sin^2\theta_{12} = 0.30$, $\sin^2\theta_{13} = 0.023$, and $\sin^2\theta_{23} = 0.41$, respectively, and the mass differences are $\delta m^2_{21} = 7.9 \times 10^{-5}\text{eV}^2$ and $\delta m^2_{23} = 2.7 \times 10^{-3}\text{eV}^2$.

oscillations can be reformulated into a vector form.

Every two-by-two Hermitian matrix can be expanded in the quaternian basis. For example, the Hamiltonian for neutrino oscillations in vacuum can be written as

$$\mathsf{H}^{(\mathrm{f})} = -\frac{\vec{\sigma}}{2} \cdot \vec{H}^{(\mathrm{f})}, \tag{2.14}$$

where

$$\sigma_1 = \begin{pmatrix} 0 & 1 \\ 1 & 0 \end{pmatrix}, \sigma_2 = \begin{pmatrix} 0 & -\mathrm{i} \\ \mathrm{i} & 0 \end{pmatrix}, \sigma_3 = \begin{pmatrix} 1 & 0 \\ 0 & -1 \end{pmatrix} \tag{2.15}$$

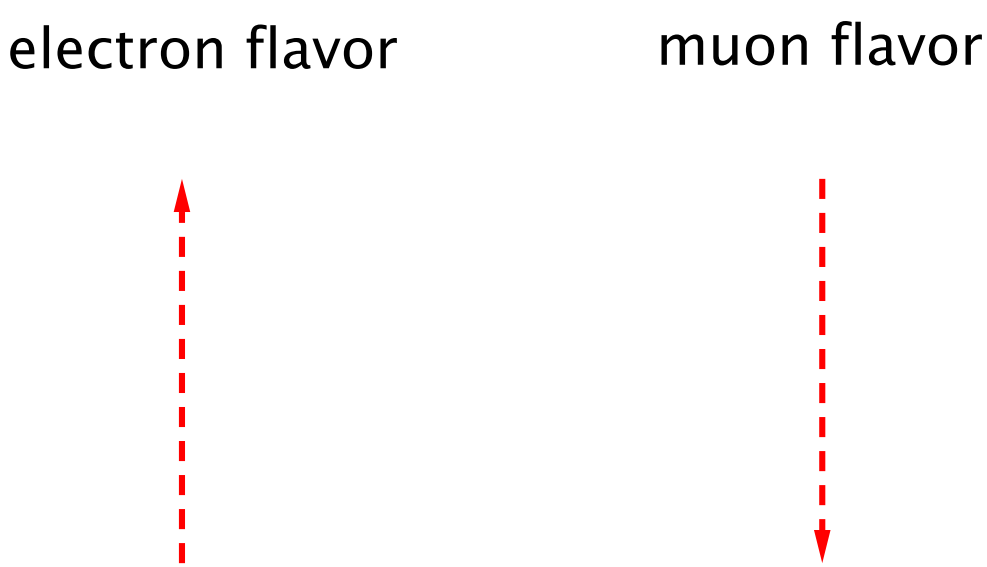

Figure 2.4: In the flavor isospin picture, a flavor isospin pointing upward, i.e., along the third axis in flavor space, indicates that the neutrino is in the electron flavor, while the downward direction indicates the other flavor, such as the muon flavor.

are the three Pauli matrices. I will use $\vec{}$ to denote vectors in flavor space. Meanwhile, the flavor quantum state of the neutrino is represented by the flavor isospin, which is defined as

$$\vec{s}^{(\mathrm{f})} = \Psi^{(\mathrm{f})\dagger} \frac{\vec{\sigma}}{2} \Psi^{(\mathrm{f})}. \tag{2.16}$$

As shown in Fig. 2.4, the directions of the flavor isospin in flavor space tell us the flavor content of the neutrino. A flavor isospin pointing upward in flavor space, i.e., along the direction of the third axis, denotes the electron flavor by definition. In the flavor isospin formalism, the electron flavor survival probability is

$$P = \frac{1}{2} + s_3^{(\mathrm{f})},$$

where $s_3^{(\mathrm{f})}$ is the third component of the flavor isospin. Correspondingly, the equation of motion for the flavor isospin describes its precession around the vector $\vec{H}^{(\mathrm{f})}$,

$$\dot{\vec{s}}^{(\mathrm{f})} = \vec{s}^{(\mathrm{f})} \times \vec{H}^{(\mathrm{f})}. \tag{2.17}$$

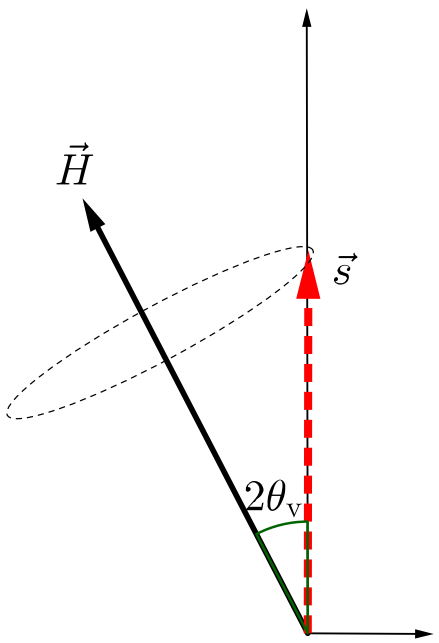

Figure 2.5: Vacuum oscillations in the flavor isospin picture. The flavor isospin of a neutrino starting with the electron flavor will precess around the static "Hamiltonian vector" $\vec{H}$, which gives periodic flavor oscillations according to Eqn. 2.2.

This precession corresponds to periodic oscillations between the two neutrino flavors. For example, in vacuum oscillations, the Hamiltonian becomes

$$\mathsf{H}^{(f)} \to \frac{\omega_{\rm v}}{2}\left(-\cos 2\theta_{\rm v}\sigma_3 + \sin 2\theta_{\rm v}\sigma_1\right) \to \omega_{\rm v}\begin{pmatrix}\sin\theta_{\rm v}\\ 0\\ \cos 2\theta_{\rm v}\end{pmatrix},$$

which is a vector of length $\omega_{\rm v}$ and tilted away from the third axis by the angle $2\theta_{\rm v}$.

Eqn. 2.17 depicts the precession of the flavor isospin for a neutrino which starts with the electron flavor and propagates in vacuum. The oscillation frequency is trivially read out from Eqn. 2.17,

$$\omega_{\rm v} = |\vec{H}^{(\rm f)}| \tag{2.18}$$

2.3 Summary

Vacuum neutrino oscillations can be easily explained and calculated. However, it conveys the message of the nature of neutrino oscillations. Neutrinos are usually produced in flavor states through weak interactions. The neutrino does not remain in the same flavor state during its propagation because the flavor states are not the eigenstates of the propagation Hamiltonian. An extrapolation of this idea is that neutrinos might also oscillate in a uniform linear potential, the Hamiltonian of which would be similar to vacuum Hamiltonian but with different values. One of such situations is that neutrinos propagate through a region with a constant matter density, which I will explain in the next chapter.

Chapter 3

Neutrino Oscillations in Matter

In many astrophysical environments, such as stars and core-collapse supernovae, neutrinos are mostly produced in the center of the objects and propagate through dense fluctuating media. The background matter will interact with neutrinos [1]. Such interactions are not necessarily the same for different flavors. In fact, the neutral current interaction between matter background and neutrinos doesn't distinguish between the flavors, as shown in Fig. 3.1a. However, the charged current interaction is specific for different flavors. For example, charged current interaction with electrons is special for electron flavor neutrinos, as shown in Fig. 3.1b. The charged current interaction is responsible for the difference between neutrino oscillations in vacuum and in matter. Even though the electron flavor neutrinos are produced in the core of stars, the flavor content detected on Earth is not only determined by the vacuum oscillations.

One of the significant matter effect on neutrino flavor oscillations is the Mikheyev-

[1]The concept of matter in this thesis refers to electrons since we are discussing the flavor conversion between electron flavor and other flavors. However, it is not necessarily to be confined to be electrons. The same methods also work for other matter background such as matter background contains both electrons and muons.

Smirnov-Wolfenstein (MSW) effect [6, 4, 5], which is used to explain the deficit of electron flavor neutrino flux, as know as the solar neutrino problem [8, 17]. Later developments on the theories of matter effect revealed the parametric resonance of neutrino flavor oscillations due to fluctuations in matter density [7, 15], which is the neutrino analog of transitions between energy levels as a result of external optical stimulation. Parametric resonance is different from the MSW effect since it involves the parameters of the matter density, which is usually the period of matter density fluctuations. It has also be shown that neutrinos passing through the Earth can experience parametric resonance [14, 12].

As one of the most intense neutrino sources, supernova neutrinos experience turbulent matter density as they propagate through the explosion [33, 32], where the flavor conversion is modified by interactions with matter. Meanwhile, with neutrinos depositing energy into the shock, neutrino flavor conversion is crucial to understand the shock evolution of supernova explosion. The turbulent matter density environment for neutrino flavor conversion has been studied [9, 22, 27]. Recently, neutrino flavor conversions in matter background in varying matter density has been researched using a Jacobi-Anger expansion by Kneller, et al. [29, 31]. They have shown that neutrinos might go through large conversions between the two energy eigenstates.

I will take a step further and interpret parametric resonance [15, 7] as well as other matter stimulated neutrino flavor conversions [29, 31], as a superposition of Rabi oscillations. I will also calculate the criteria for the survival of resonance due to interference effect between different Rabi oscillation modes. In Sec. 3.2, we define the formalism of neutrino flavor conversions in matter used in this chapter where the equation of motion and Hamiltonian for neutrino flavor conversion in matter are explicitly written. In Sec. 3.3 we discuss how neutrino flavor conversions are related to Rabi oscillations. To begin, we discuss a system with single frequency matter den-

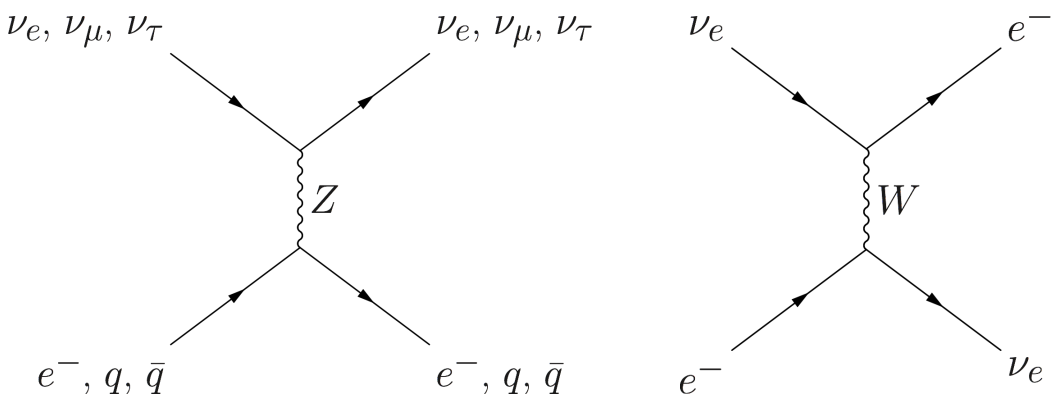

(a) Neutral current interaction between ν_e, ν_μ, ν_τ, and e^-. Neutral current interaction is mediated by Z bosons.

(b) Charged current interaction between ν_e and e^-. Charged current interaction is mediated by W bosons.

Figure 3.1: Two important interactions—neutral current and charged current—between neutrinos and matter. They exchange different bosons.

sity fluctuation. We will show that such a system can be reduced to Rabi oscillations if resonance occurs. In Sec. 3.4 we describe the interference effect between different frequencies of Rabi oscillations and develop the criteria for significant interference between two frequencies. We show that the interference between the many frequencies fits into the criteria we proposed for interference. In Sec. 3.6 we discuss the technique of decomposing the neutrino flavor conversions into summation of Rabi oscillations, by applying a specific unitary transformation and the Jacobi-Anger expansion. As the system is exactly decomposed into multiple Rabi oscillations, we can interpret neutrino flavor oscillations in any matter density fluctuations, in principle. As an example, we solve the neutrino flavor transitions in a castle wall matter profile, which contains infinite frequencies from the aspect of Fourier series.

3.1 Neutrino Oscillations in the Sun

Flavor conversion occurs as long as their propagation eigenstates are different from their flavor eigenstates. Since the neutral current interactions between the neutrinos and the matter is independent of the flavors, as shown in Fig. 3.1a, I only include the charged current interactions in the Hamiltonian, which is an effective potential for electron flavor. In flavor basis, the effective potential is

$$\mathsf{V}^{(\mathrm{f})} = \frac{\sqrt{2}G_{\mathrm{F}}n_{\mathrm{e}}}{2}\vec{\sigma}_3, \tag{3.1}$$

where G_{F} is Fermi constant, n_{e} is number density of electrons. We also remove the terms proportional to the identity in this potential since they do not change the probability for flavors. The Hamiltonian with matter effect is the combination of vacuum oscillation and matter effect, which is, in flavor basis,

$$\mathsf{H}^{(\mathrm{f})} = \frac{\omega_{\mathrm{v}}}{2}\begin{pmatrix} -\cos 2\theta_{\mathrm{v}} & \sin 2\theta_{\mathrm{v}} \\ \sin 2\theta_{\mathrm{v}} & \cos 2\theta_{\mathrm{v}} \end{pmatrix} + \frac{\sqrt{2}G_{\mathrm{F}}n_{\mathrm{e}}}{2}\sigma_3, \tag{3.2}$$

where we used the result of flavor basis vacuum oscillation Hamiltonian

$$\mathsf{H}_{\mathrm{v}}^{(\mathrm{f})} = \mathsf{U}\mathsf{H}_{\mathrm{v}}\mathsf{U}^{\dagger} \tag{3.3}$$

$$= \frac{\omega_{\mathrm{v}}}{2}\begin{pmatrix} -\cos 2\theta_{\mathrm{v}} & \sin 2\theta_{\mathrm{v}} \\ \sin 2\theta_{\mathrm{v}} & \cos 2\theta_{\mathrm{v}} \end{pmatrix}. \tag{3.4}$$

Utilizing Pauli matrices and the so called matter potential $\lambda = \frac{\sqrt{2}G_F n_e}{2}$, it is rewritten as

$$\mathsf{H}_{\mathrm{m}}^{(\mathrm{f})} = \left(\frac{\lambda}{2} - \frac{\omega_{\mathrm{v}}}{2}\cos 2\theta_{\mathrm{v}}\right)\sigma_3 + \frac{\omega_{\mathrm{v}}}{2}\sin 2\theta_{\mathrm{v}}\sigma_1. \tag{3.5}$$

Due to the off-diagonal terms in the Hamiltonian, the system will experience oscillations in flavor. A resonance, i.e., maximum mixing, dominates the system when the diagonal terms becomes zero,

$$\frac{\lambda}{2} - \frac{\omega}{2}\cos 2\theta_{\mathrm{v}} = 0, \tag{3.6}$$

which gives us the Mikheyev–Smirnov–Wolfenstein (MSW) resonance condition.

For the neutrinos produced in the Sun, they travel from the center of the Sun to the surface. The matter density is not uniform on the path of these solar neutrinos. The neutrino propagation eigenstates are different from flavor states in general [4]. The importance of matter effect to our understanding of solar neutrinos is that it modifies the oscillation, depending on the matter density variation. For the Sun, the density change is not too dramatic. The neutrinos go through adiabatic evolution during the propagation, which means that the instantaneous eigenstates and eigenvectors of Hamiltonian is good enough for the time dependent Schrödinger equation.

For simplicity, we define the 'hatted' dimensionless matter potential using the vacuum oscillation frequency

$$\hat{\lambda} = \frac{\lambda}{\omega_{\mathrm{v}}}. \tag{3.7}$$

The eigenstates, derived by diagonalizing the Hamiltonian, are

$$E_1 = \frac{\omega_{\mathrm{v}}}{2}\sqrt{\hat{\lambda} + 1 - 2\hat{\lambda}\cos 2\theta_{\mathrm{v}}} \tag{3.8}$$

$$E_2 = -\frac{\omega_{\mathrm{v}}}{2}\sqrt{\hat{\lambda} + 1 - 2\hat{\lambda}\cos 2\theta_{\mathrm{v}}}. \tag{3.9}$$

Fig. 3.2 shows the two energy levels for a neutrino propagating in different matter potentials. For very high matter density, the electron flavor is almost comparable to heavy eigenstate. However, as the matter density becomes lower, the heavy propagation state will be gradually transformed to the other flavors. As the neutrinos reach the surface, the matter density is approaching vacuum. The heavy state of the neutrino is approaching electron flavor state. The resonance, which is the closest point of energy levels, happens at density $n_{\mathrm{e}} = 2\omega_{\mathrm{v}}\cos(2\theta_{\mathrm{v}})/\sqrt{2}G_{\mathrm{F}}$ which depends on ω_{v}. Resonances of neutrinos with different energies happens at different matter densities, which will significantly reshape the neutrino energy spectra. Even though

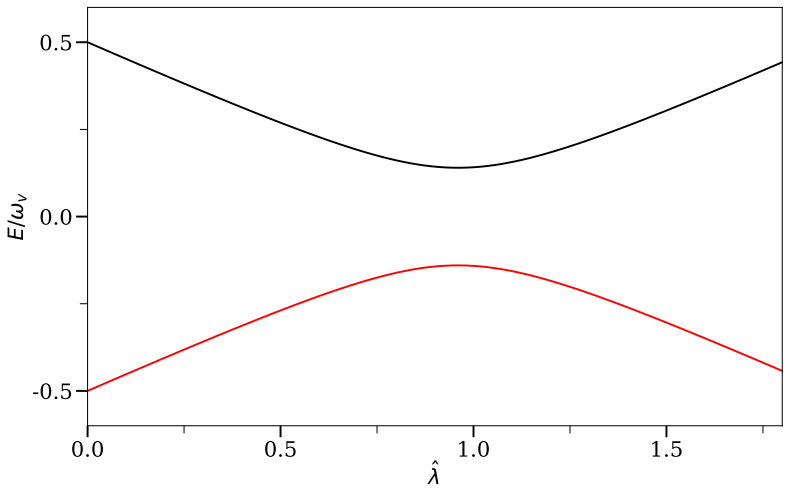

Figure 3.2: The two energy levels in matter effect. The potential has unit $\omega_{\rm v}$. I have used $\sin^2\theta_{\rm v} = 0.02 \approx \sin^2\theta_{13}$.

only the electron flavor neutrinos are produced in the Sun, the neutrino flavor conversion to the other flavors is enhanced by the matter interactions, in addition to the vacuum oscillation. The exact neutrino flavor conversion is much more complicated than the MSW effect. As an approximation, the MSW transition is good enough for the solar neutrinos flavor oscillations [30].

One of the interesting fact about MSW effect is the MSW triangle shown in Fig. 3.3. The survival probability of the electron flavor neutrinos is plotted against $\log(\lambda/\omega_{\rm v})$ and $\log(\sin^2 2\theta_{\rm v})$. Qualitatively speaking, large conversion happens when matter density is not too small since a sufficient central potential is required for the level crossing. This leads to the triangle shape of the low survival probability region.

MSW effect is also easily explained using flavor isospin picture. The Hamiltonian

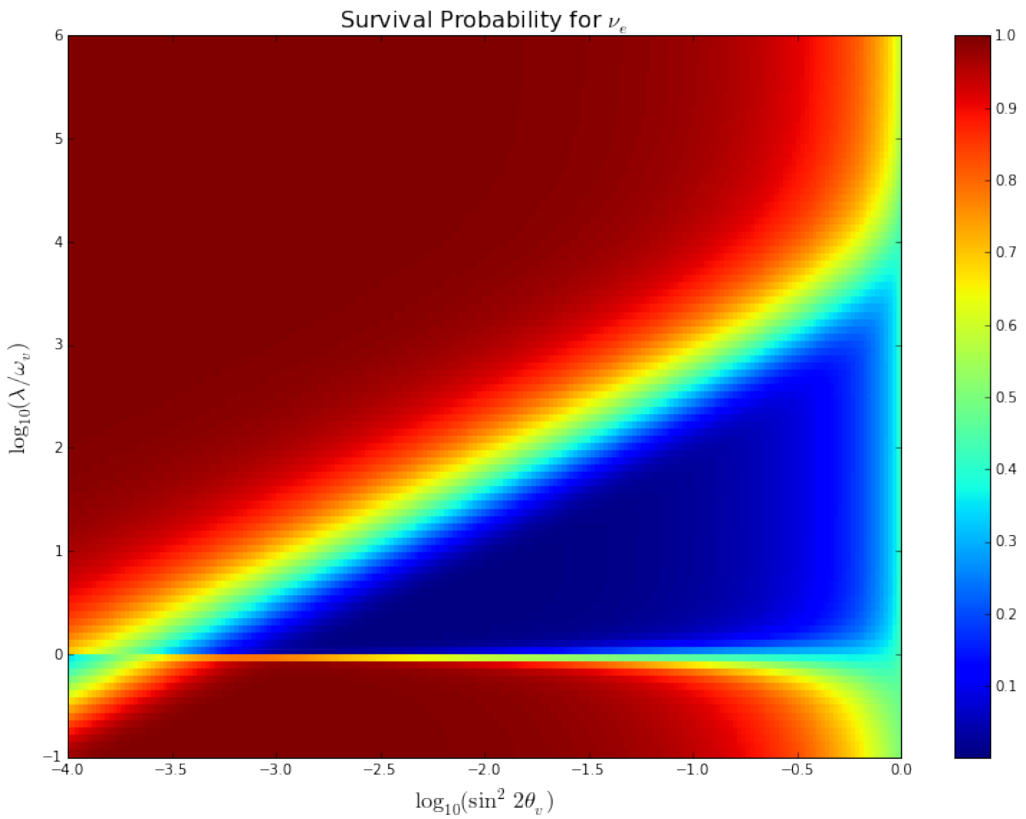

Figure 3.3: MSW triangle. The horizontal axis is related to the the mixing angles, and the vertical axis is related to the matter potential in the center of the Sun. The colors are the survival probabilities of electron flavor. The region of large conversions, or small survival probabilities, forms a triangle. The larger the mixing angle, the larger range of matter potential for large conversions.

in flavor isospin picture

$$\begin{aligned}\mathsf{H}_{\mathrm{m}} =& \frac{\omega_{\mathrm{v}}}{2}\left(-\cos 2\theta_{\mathrm{v}}\sigma_3 + \sin 2\theta_{\mathrm{v}}\sigma_1\right) + \frac{\lambda(x)}{2}\sigma_3 \\ \rightarrow& \omega_{\mathrm{v}} \begin{pmatrix} -\sin 2\theta_{\mathrm{v}} \\ 0 \\ \cos 2\theta_{\mathrm{v}} \end{pmatrix} + \begin{pmatrix} 0 \\ 0 \\ -\lambda(x) \end{pmatrix} \\ =& \vec{H}_{\mathrm{v}} + \vec{H}_{\mathrm{m}}(x),\end{aligned}$$

where $\vec{H}_{\mathrm{v}}$ is vacuum contribution and $\vec{H}_{\mathrm{m}}(x)$ is the matter potential contribution.

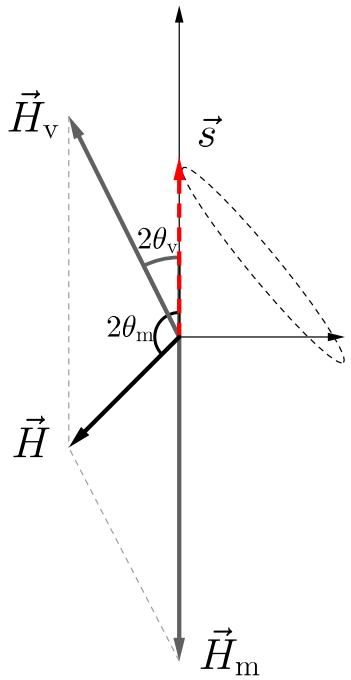

Figure 3.4: Neutrino oscillations in flavor isospin picture, with the presence of matter potential. The flavor isospin is denoted as red dashed arrow. It starts from electron flavor. The two gray vectors stand for the Hamiltonians of vacuum $\vec{H}_{\rm v}$ and matter $\vec{H}_{\rm m}$.

The two vectors are visualized in Fig. 3.4. We discussed in Sec. **??** the adiabatic transitions of neutrino states in varying matter density. Fig. 3.5 shows the adiabatic evolution of neutrino flavor isospin. For region of high density matter background, which provides large matter potential, the total Hamiltonian is almost pointing downward. We observe almost no flavor oscillations since flavor isospin precession is tiny. As the neutrinos moving into smaller matter density regions, the flavor isospin is approximately following the evolution of Hamiltonian. Flavor conversion happens because of the evolution of Hamiltonian, even though flavor oscillations are still tiny. In the end, neutrinos reach the region with almost no matter, where they are almost converted to one of the mass eigenstates. In fact, those neutrinos won't oscillate that

much in vacuum following this initial condition.

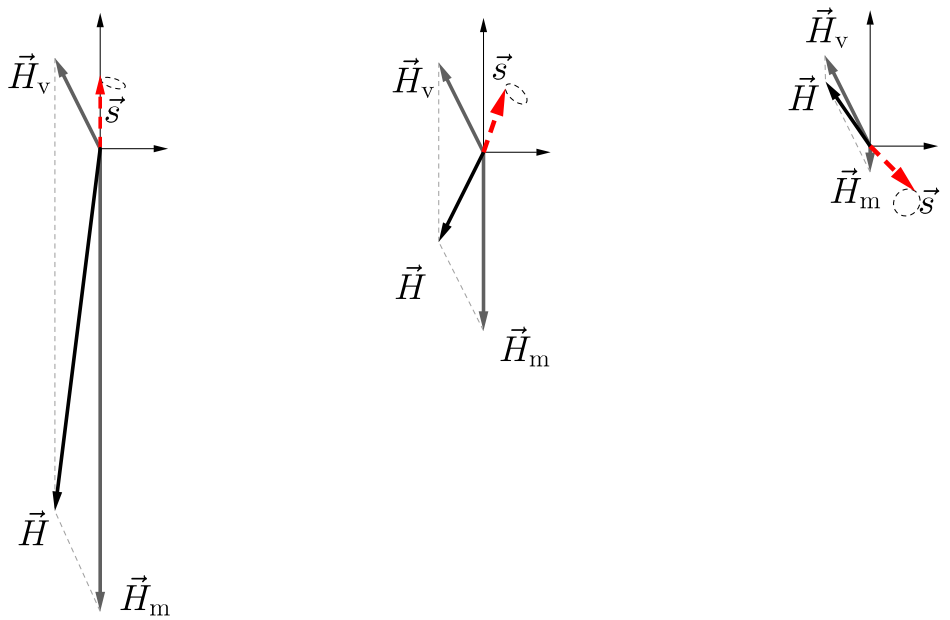

(a) High matter density (b) Medium matter density (c) Low matter density

Figure 3.5: Flavor isospin picture of neutrino oscillations in matter. $\vec{H}_{\rm v}$ is the vacuum contribution to Hamiltonian, and $\vec{H}_{\rm m}$ corresponds to the matter potential.

Neutrinos might experience a critical matter density, when the overall Hamiltonian is perpendicular to the upright axis. Assuming we have electron neutrinos going through such regions, they will experience maximum flavor oscillations, c.f. Fig. 3.6.

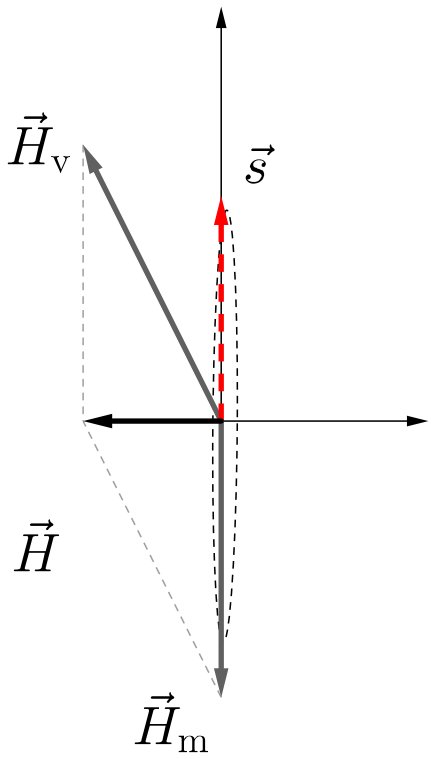

Figure 3.6: MSW resonance happens when electron neutrinos go through a critical matter density.

3.2 Equation of Motion for Neutrino Oscillations in Matter

We consider two-flavor oscillation scenario, in which neutrinos have energy E and mass-squared difference δm^2 between two mass states propagate through matter which is define by electron number density profile $n(r)$ along the path of neutrino propagation r. The dynamics of neutrino flavor conversion is determined by Schrödinger equation. In flavor basis the wave function describes the probability

amplitude of different flavors. The Hamiltonian in flavor basis consists the vacuum oscillation Hamiltonian $H_{\rm v}^{(f)}$ and the matter term $H_{\rm m}^{(f)}$ which describes the interaction between neutrinos and matter,

$$\begin{aligned} H^{(\rm f)} =& H_{\rm v}^{(f)} + H_{\rm m}^{(f)} \\ =& \frac{1}{2}\begin{pmatrix} -\omega_{\rm v}\cos 2\theta_{\rm v} + \lambda(r) & \omega_{\rm v}\sin 2\theta_{\rm v} \\ \omega_{\rm v}\sin 2\theta_{\rm v} & \omega_{\rm v}\cos 2\theta_{\rm v} - \lambda(r) \end{pmatrix}, \end{aligned} \tag{3.10}$$

where $\lambda(r) = \sqrt{2}G_{\rm F}n(r)$ is the potential of neutrino interaction with matter and $G_{\rm F}$ is the Fermi constant, $\theta_{\rm v}$ is the vacuum mixing angle, $\omega_{\rm v} = \delta m^2/2E$ is the vacuum oscillation frequency. The potential $\lambda(r)$ is called matter profile since it reflects the matter density fluctuations. For the convenience of notation, we use Pauli matrices σ_i to rewrite the Hamiltonian, so that the Schrödinger equation becomes,

$$\mathrm{i}\frac{\mathrm{d}}{\mathrm{d}r}\Psi(r) = \frac{1}{2}\left((-\omega_{\rm v}\cos 2\theta_{\rm v} + \lambda(r))\sigma_3 + \omega_{\rm v}\sin 2\theta_{\rm v}\sigma_1\right)\Psi(r),$$

where $\Psi(r)$ is the wave function in flavor basis. For two flavor scenario, it is written as $\Psi(r) = (\psi_e, \psi_x)^{\rm T}$ where ψ_e and ψ_x are the amplitudes for electron flavor and the second flavor (μ flavor or τ flavor) respectively. The equation of motion in flavor basis governs the transitions between different flavors.

For arbitrary matter profile, we can always interpret it as perturbations on top of a constant matter profile,

$$\lambda(r) = \lambda_0 + \delta\lambda(r). \tag{3.11}$$

For better understanding of the transition between states as a consequence of the fluctuation of matter density, we use the background matter basis, in which the Hamiltonian is diagonalized in the absence of perturbation $\delta\lambda(r)$, so that the Hamiltonian reads

$$H^{(\rm m)} = -\frac{\omega_{\rm m}}{2}\sigma_3 + \frac{1}{2}\delta\lambda(r)\cos 2\theta_{\rm m}\sigma_3 - \frac{1}{2}\delta\lambda(r)\sin 2\theta_{\rm m}\sigma_1, \tag{3.12}$$

where $\theta_{\rm m}$ is the mixing angle in a constant matter profile λ_0, which is calculated using relation

$$\tan 2\theta_{\rm m} = \sin 2\theta_{\rm v} / \left(\cos 2\theta_{\rm v} - \lambda_0/\omega_{\rm v}\right)$$

with $\omega_{\rm v}$ denoting the vacuum oscillation frequency and $\theta_{\rm v}$ denoting the vacuum mixing angle. The frequency $\omega_{\rm m}$ is defined as

$$\omega_{\rm m} = \omega_{\rm v}\sqrt{(\lambda_0/\omega_{\rm v} - \cos(2\theta_{\rm v}))^2 + \sin^2(2\theta_{\rm v})}. \tag{3.13}$$

In background matter basis, the wave function describes the amplitudes of different mass states defined when there is only background matter density λ_0. It's trivial to calculate the flavor conversion given the transition probability between the two mass states. However, since we'll concentrate on the flavor conversion due to the matter fluctuations, we'll only discuss the transition between mass states in the background matter basis.

In this chapter, mixing angle is chosen so that $\sin^2(2\theta_{\rm v}) = 0.093$ and the mass squared difference is $\delta m^2 = 2.6 \times 10^{-3}{\rm eV}^2$.

3.3 Single Frequency Matter Profile and Rabi oscillations

In this section we present a simple picture to explain neutrino parametric resonance in matter by utilizing the theory of Rabi oscillations which have been well studied in quantum optics [24]. Rabi oscillations describe the transition between different energy levels due to an oscillatory external driving field, where maximum transition or resonance happens when the frequency of external driving field equals the energy gap. In Appendix B, we derive the Rabi oscillation transition probabilities using neutrino flavor isospin method introduced in Ref. [21], and explained in Sec. 2.2.

We examine neutrino flavor conversions in single frequency matter profile $\delta\lambda(r) = \lambda_1 \cos(k_1 r)$. As will be proved in Sec. 3.6.2, the varying σ_3 term $\delta\lambda(r)\cos 2\theta_{\rm m}\sigma_3/2$ in Hamiltonian Eqn. 3.12, which is the varying energy gap due to varying matter density fluctuations, has little effect on the transition probabilities when the system is not far from resonance. With the varying σ_3 term removed, it indicates that this single frequency matter perturbation neutrino flavor conversion system has been reduced to a Rabi oscillation system, with external driving field frequencies $\pm k_1$ and energy gap $\omega_{\rm m}$. Mathematically, we can decompose $\cos(k_1 r)$ into two exponential functions so that we have two external driving frequencies k_1 and $-k_1$. By neglecting the off-resonance mode which has frequency $-k_1$, the Hamiltonian can be simplified,

$$\begin{aligned} H^{(\rm m)} &\to -\frac{\omega_{\rm m}}{2}\sigma_3 - \frac{1}{2}\lambda_1 \sin 2\theta_{\rm m}\cos(k_1 r)\sigma_1 \\ &\to -\frac{\omega_{\rm m}}{2}\sigma_3 - \frac{1}{2}A_1 \exp(\mathrm{i}k_1 r)\sigma_1 \\ &= -\frac{\omega_{\rm m}}{2}\sigma_3 - \frac{1}{2}A_1\cos(k_1 r)\sigma_1 + \frac{1}{2}A_1 \sin(k_1 r)\sigma_2, \end{aligned} \tag{3.14}$$

where

$$A_1 = \frac{\lambda_1 \sin 2\theta_{\rm m}}{2}. \tag{3.15}$$

The resonance condition is determined by matching the energy gap $\omega_{\rm m}$ with external driving field frequency k_1, i.e., $\omega_{\rm m} \sim k_1$. As the system approaches resonance condition, the transition probability between the two mass states should be predicted well using Rabi formula.

To show that this conjecture of simplifying neutrino flavor conversions to Rabi oscillations is correct, we calculate transition probabilities of the neutrinos described by Eqn. 3.12 numerically, and compare them with Rabi formula Eqn. B.10 from the Rabi oscillations described by Eqn. B.1.

In Fig. 3.7, we plotted the numerical results using markers as well as the prediction using Rabi formula using lines. The agreement between numerical solutions of neutrino transitions between mass states and Rabi formula will be explained

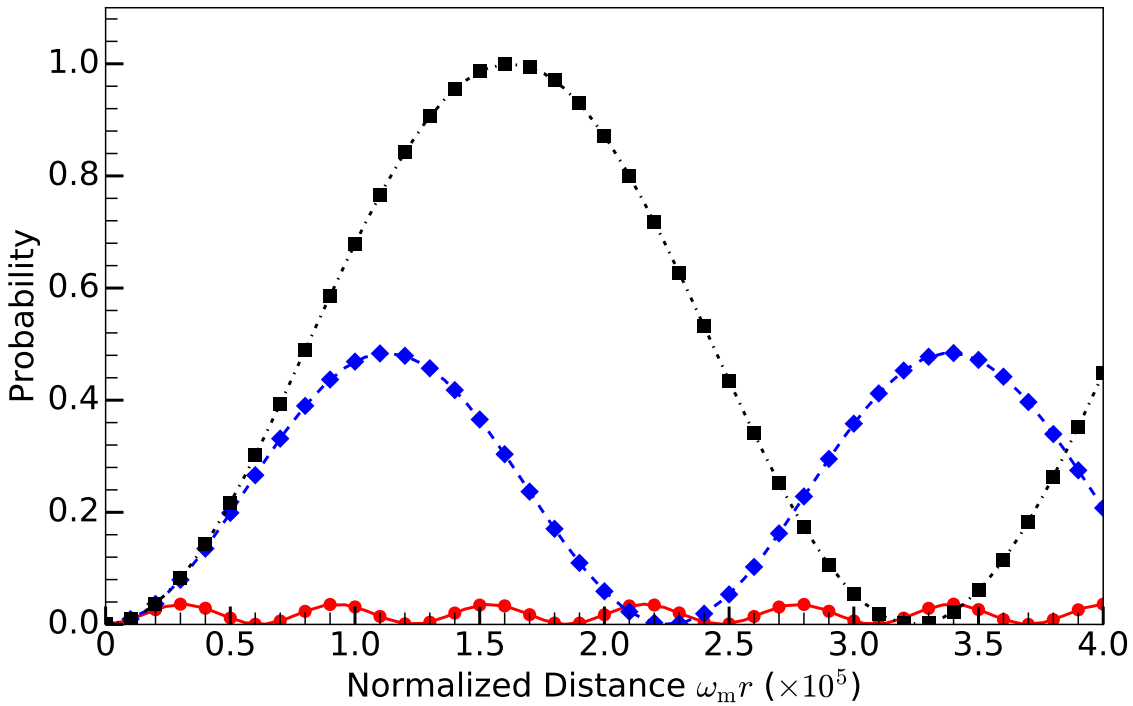

Figure 3.7: Single frequency matter profile and Rabi oscillation. The markers are numerical results for the transition probabilities between two background mass eigenstates for the neutrinos with matter perturbation $A_1 \sin(k_1 r)$. The dots, diamonds, and squares are for $k_1 = \omega_{\rm m}$, $k_1 = (1 - 2 \times 10^{-5})\omega_{\rm m}$, and $k_1 = (1 - 10^{-4})\omega_{\rm m}$ respectively. The lines are the predictions using Rabi formula. During the calculation, λ_0 is set to 0.5 of the MSW resonance potential $\lambda_{\rm MSW} = \omega_{\rm v} \cos 2\theta_{\rm v}$ and mixing angle is chosen so that $\sin^2(2\theta_{\rm v}) = 0.093$.

more precisely in Sec. 3.6. For now, we address the significance of relative detuning $D = |k_1 - \omega_{\rm m}|/|A_1|$, which is rigoriously defined in Appendix B. It measures how off-resonance a system is. We know that $D \to 0$ indicates the system is very close to resonance, while $D \to \infty$ indicates the system is far away from resonance. The corresponding relative detunings are 0, 1.0, and 5.2 for $k_1 = \omega_{\rm m}$, $k_1 = (1 - 2 \times 10^{-5})\omega_{\rm m}$, and $k_1 = (1 - 10^{-4})\omega_{\rm m}$.

For a single-frequency perturbation in matter profile $\lambda(r) = \lambda_1 + \lambda_1 \sin(k_1 r)$, P. Krastev and A. Smirnov concluded that the parametric resonance condition is

$\omega_{\mathrm{m}} \sim nk_1$, if instantaneous $\omega_{\mathrm{m,inst}}(r)$ associated with the matter profile at distance r varies slowly [7]. This condition is exactly the Rabi resonance condition when $n = 1$, as such condition matches the driving field frequency to the energy split. Higher order effects are explained in Sec. 3.6.2.

3.4 Interference of Rabi Oscillations and Multi-frequency Matter Profile

The approach applied to single frequency matter profile also helps with the understanding of multi-frequency matter profile. However, multi-frequency matter profile leads to multiple modes of Rabi oscillations, even with our simplified approach by dropping the varying σ_3 term in Hamiltonian. In this section, we examine the interference between two modes of Rabi oscillations.

We explain the interference between different modes of Rabi oscillations using the idea of energy gap shift. Suppose we have a Rabi oscillation system with two modes, one of which is at resonance with frequency $k_1 = \omega_{\mathrm{m}}$ and the other mode with frequency k_2 that is off resonance. In some cases, there can be a significant transition amplitude decrease because of the off resonance frequency k_2, which can be interpreted as shift of energy gap due to the frequency k_2. To model the effect, we construct a Rabi oscillation Hamiltonian with two modes of different frequency,

$$H^{(\mathrm{m})} = -\frac{\omega_{\mathrm{m}}}{2}\sigma_3 - \frac{1}{2}\sum_{n=1}^{N} A_n \cos(k_n r)\sigma_1 + \frac{1}{2}\sum_{n=1}^{N} A_n \sin(k_n r)\sigma_2, \tag{3.16}$$

where $N = 2$ for two frequency case. To show the destruction effect, the Hamiltonian

Eqn. 3.16 is reformulated into a vector with sigma matrices $(\sigma_1, \sigma_2, \sigma_3)$ as the basis,

$$\mathbf{H} = \begin{pmatrix} 0 \\ 0 \\ \omega_{\mathrm{m}} \end{pmatrix} + \begin{pmatrix} A_1 \cos(k_1 r) \\ -A_1 \sin(k_1 r) \\ 0 \end{pmatrix} + \begin{pmatrix} A_2 \cos(k_2 r) \\ -A_2 \sin(k_2 r) \\ 0 \end{pmatrix}. \tag{3.17}$$

The three terms are defined as $\mathbf{H}_3$, $\mathbf{H}_1$, and $\mathbf{H}_2$ respectively. $\mathbf{H}_1$ and $\mathbf{H}_2$ are two rotating vectors as a function of r with frequencies k_1 and k_2 in this vector space, while $\mathbf{H}_3$ is perpendicular to $\mathbf{H}_1$ and $\mathbf{H}_2$. To work out the energy gap shift, we go to the frame that corotates with $\mathbf{H}_2$, in which we have the new frequencies $k_1' = k_1 - k_2$ and $k_2' = 0$ as well as new energy gap $\omega_{\mathrm{m}}' = \omega_{\mathrm{m}} - k_2$. The resonance mode $\mathbf{H}_1$ retains on the resonance condition since $k_1' = \omega_{\mathrm{m}}'$, i.e. $k_1 - k_2 = \omega_{\mathrm{m}} - k_2$, holds in the new frame. On the other hand, we have two static fields $\mathbf{H}_3$ and $\mathbf{H}_2$ together as the new energy gap, as long as $\mathbf{H}_2 \ll \mathbf{H}_3$, which is the usual case. The new energy gap in this frame is calculated as

$$\begin{aligned} \tilde{\omega}_{\mathrm{m}}' =& \mathrm{sign}(\omega_{\mathrm{m}}')\sqrt{\omega_{\mathrm{m}}'^2 + A_2^2} \\ \approx& \omega_{\mathrm{m}}' + \frac{A_2^2}{2\omega_{\mathrm{m}}'} \\ =& \omega_{\mathrm{m}} - k_2 + \frac{1}{2}\frac{A_2^2}{\omega_{\mathrm{m}} - k_2}, \end{aligned} \tag{3.18}$$

where we kept only first order of Taylor series. The Taylor expansion in Eqn. 3.18 holds as long as the relative detuning for the second frequency is large which means the second frequency is off resonance. As an approximation, the transitions between the two energy states follows the Rabi oscillations with energy gap $\tilde{\omega}_{\mathrm{m}}'$ and driving field with frequency $k_1' = k_1 - k_2$. Consequently, we can estimate how much the amplitude of the transition is suppressed due to k_1 mode by calculating the new

relative detuning,

$$\begin{aligned} D' =& \frac{|k_1' - \tilde{\omega}_{\rm m}'|}{|A_1|} \\ =& \left| \frac{k_1 - \omega_{\rm m}}{A_1} + \frac{A_2^2}{2A_1(k_2 - \omega_{\rm m})} \right| \qquad (3.19) \\ =& \left| \frac{\text{sign}(k_1 - \omega_{\rm m})}{\text{sign}(k_2 - \omega_{\rm m})} D_1 + \frac{A_2}{2A_1 D_2} \right|, \qquad (3.20) \end{aligned}$$

where D_2 is the relative detuning of the second mode,

$$D_i = \left| \frac{k_i - \omega_{\rm m}}{A_i} \right|.$$

In principle, the energy gap of the first frequency can be changed to approach the resonance or escape the resonance by carefully arranging the second frequency, which is also obvious from Eqn. (3.20). For the purpose of the section we first discuss the most important destruction effect by choosing $D_1 = 0$. We observe the importance of the relative detuning. For the second mode to significantly interfere with the first mode, we need a small D_2 and a large amplitude or width $A_2 \gg A_1$.

The condition can be verified by comparing the numerical solution and estimation using Rabi formula. However, we are most interested in the amplitude change due to $\mathbf{H}_2$ mode. Relative detuning is the only variable that we need to calculate the amplitude, hence we only compare the numerical results with estimated amplitudes using $1/(1 + D'^2)$. To verify the condition, we choose the first rotating perturbation to satisfy the resonance condition $k_1 = \omega_{\rm m}$, the condition for the second rotating field shifting the system out of resonance is that the relative detuning becomes larger than 1, which leads to

$$|A_2| \geq \sqrt{2\omega_{\rm m}|A_1(k_2 - \omega_{\rm m})|} \equiv A_{2,\text{Critical}}. \qquad (3.21)$$

We expect the transition amplitude to decrease as we have larger $|A_2|$.

We choose the two modes where the first one has amplitude $A_1 = 10^{-4}\omega_{\rm m}$ and frequency $k_1 = \omega_{\rm m}$. With a small amplitude of the second frequency, $A_2 = 10^{-4}\omega_{\rm m}$,

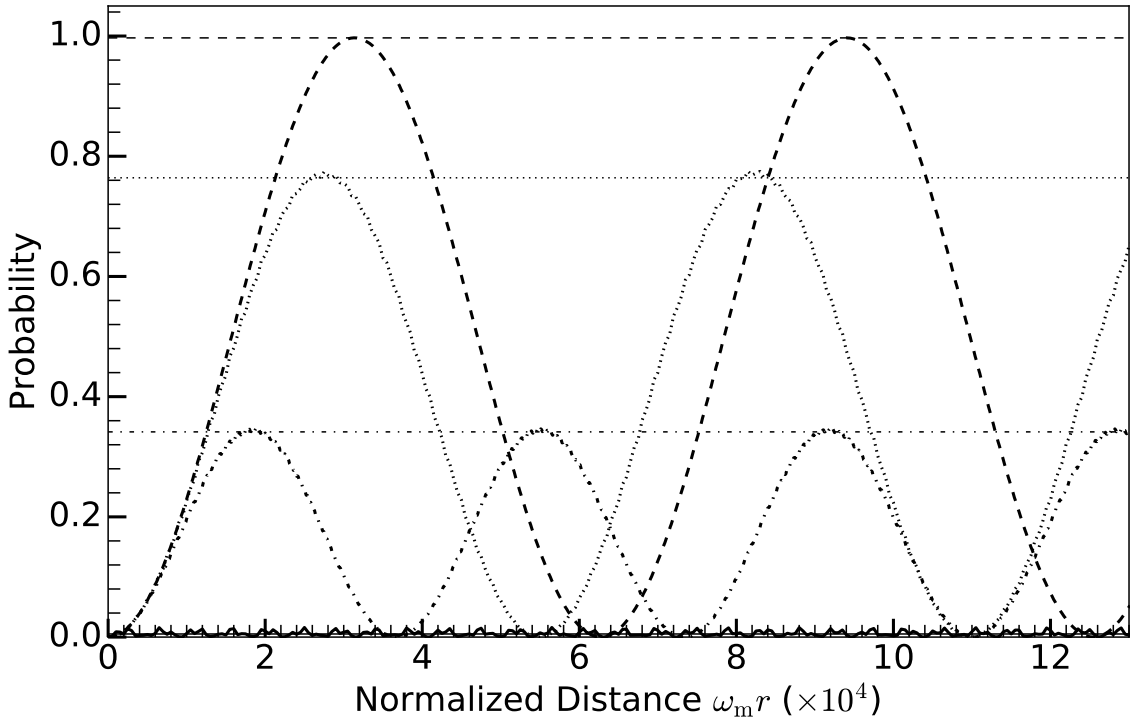

Figure 3.8: Reduction of transition amplitudes due to interference. Dashed line, dotted line, dash-dotted line, and solid line are for $A_2 = 10^{-2}\omega_{\rm m}$, $k_2 = 10\omega_{\rm m}$, $A_2 = 10^{-2}\omega_{\rm m}$, $k_2 = 10^{-1}\omega_{\rm m}$, $A_2 = 5.0 \times 10^{-2}\omega_{\rm m}$, $k_2 = 10\omega_{\rm m}$, and $A_2 = 5 \times 10^{-2}\omega_{\rm m}$, $k_2 = 10^{-1}\omega_{\rm m}$. In all the calculations, we choose $A_1 = 10^{-4}\omega_{\rm m}$, $k_1 = \omega_{\rm m}$. The grid lines are the transition amplitudes estimated using D'. During the calculation, Λ_0 is set to half of the MSW resonance potential, $\Lambda_0 = \frac{1}{2}\lambda_{\rm MSW} = \frac{1}{2}\omega_{\rm v}\cos 2\theta_{\rm v}$.

and large frequency $k_2 = 10\omega_{\rm m}$, we obtain almost full resonance. For larger A_2 the destruction effect is more effective, as shown in Fig. 3.8. The estimations of transition amplitude are in good agreement with the numerical results. To show the importance of relative detuning, we calculated the relative detuning for each cases, which are 0.06, 0.6, 1.4, 13.9 for the lines from top to down. We also notice that the width of each cases doesn't change since we kept A_1 fixed for each calculation, which indicates that the decreasing in transition amplitude is because of the increasing in detuning.

Even for the single frequency matter profile, there are two modes of Rabi oscillations $\pm k_1$, under the approximation that the varying σ_3 term in Hamiltonian is neglected, as mentioned in Sec. 3.3. The three examples calculated in Fig. 3.7 are almost exact since the modification of relative detuning for the k_1 mode that we kept, due to the far off resonance mode $-k_1$ that we neglected, is tiny. The first two lines of Table. 3.1 show the relative detunings of the three cases in Fig. 3.7, where $n = \pm 1$ are for the $\pm k_1$ modes in the Hamiltonian 3.14. We observe in Fig. 3.7 that the relative detuning change due to an extra $-k_1$ mode is not observable.

3.5 Constructive Effects

As mentioned in the preceding section, adding a second frequency to the matter density profile can also be constructive. I calculated an example with two frequencies in matter density profile, so that the Hamiltonian is

$$H^{(m)} = -\frac{\omega_{\rm m}}{2}\sigma_3 - \left(\frac{A_1}{2}\cos(k_1 r) + \frac{A_2}{2}\cos(k_2 r)\right)\sigma_1 + \left(\frac{A_1}{2}\sin(k_1 r) + \frac{A_2}{2}\sin(k_2 r)\right)\sigma_2.$$

We choose two matter profile frequencies that are off resonance and producing large relative detuning,

$$A_1 = 0.025, \tag{3.22}$$

$$k_1 = 0.95, \tag{3.23}$$

$$A_1 = 0.4, \tag{3.24}$$

$$k_2 = 2.6. \tag{3.25}$$

The oscillation amplitude for each mode being much smaller than 1. However, the combined two frequencies case produces oscillations are resonance (c.f. Fig. 3.9), since the relative detuning for the combined two frequencies case is 0.

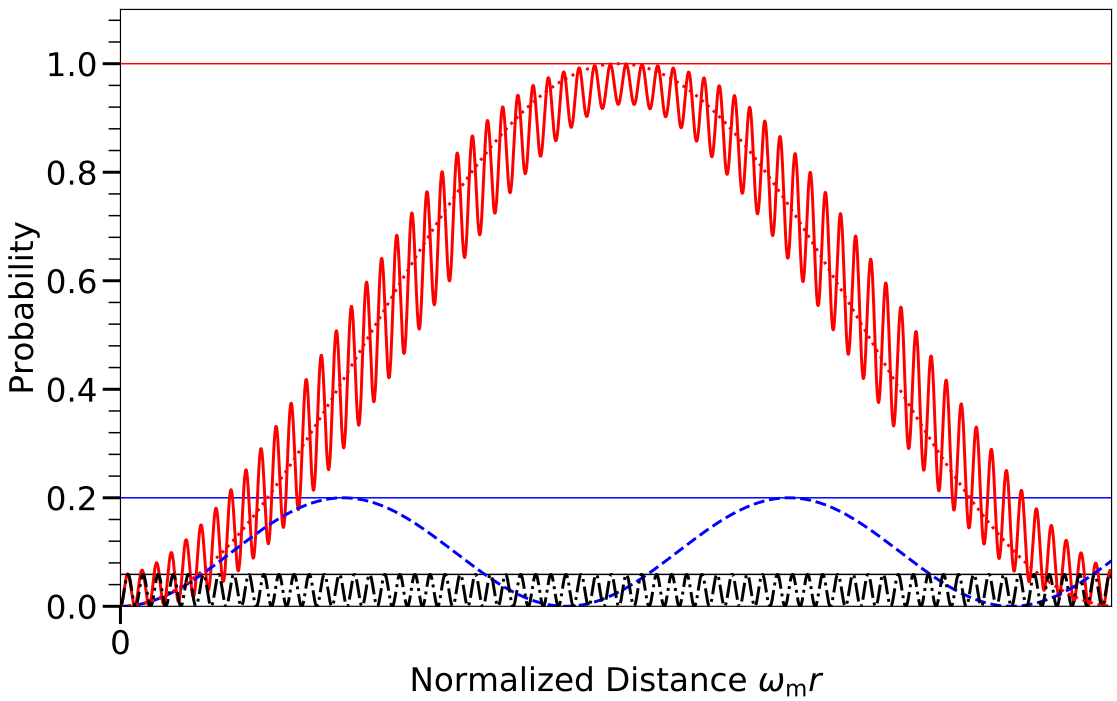

Figure 3.9: Constructive interference for two frequencies in matter density profile. The solid red line, dashed blue line, dash-dotted black line, are the transition probability for two frequencies combined, the first frequency k_1 only, the second frequency k_2 only. The amplitudes of each frequency are $A_1 = 0.4$, $A_2 = 2.6$ respectively. The grid lines are the oscillations amplitudes predicted by Rabi formula. The dotted red line is the oscillations predicted by Rabi formula for the two combined frequencies.

3.6 Parametric Resonance and Rabi oscillation — Jacobi-Anger expansion

With the intuition of the Rabi oscillations itself as well as the interference between different modes of Rabi oscillations shown in Sec. 3.4, we expect to interpret the transition probabilities of any matter profile more precisely if the system can be exactly decomposed into multiple Rabi oscillations. Kneller et. al provided a method to achieve this goal [29], namely the Jacobi-Anger expansion. In this section, we show that the matter effect can be decomposed into superpositions of Rabi oscillations by

applying a Jacobi-Anger expansion to the Hamiltonian. Our approach is to apply a designed unitary transformation first which make the motivation of Jacobi-Anger expansion, before writing down the final result as superpositions of Rabi oscillation using Jacobi-Anger expansion. For a system with general matter perturbation, c.f. Eqn. (3.12), we apply an unitary transformation of the form

$$\mathbf{U} = \begin{pmatrix} e^{-\mathrm{i}\eta(r)} & 0 \\ 0 & e^{\mathrm{i}\eta(r)} \end{pmatrix}, \tag{3.26}$$

which is a transformation used in Ref. [23] to remove the diagonal elements of the Hamiltonian. This transformation is essentially a rotation $\exp\left(-\mathrm{i}\frac{\sigma_3}{2}\cdot 2\eta\right)$, thus it doesn't change σ_3 terms themselves. In this work, this transformation is used to remove the varying σ_3 terms $\delta\lambda(r)\cos 2\theta_\mathrm{m}\sigma_3/2$ in the Hamiltonian, so that the energy gap is fixed in the new basis $\left(|\nu_{\mathrm{r}1}\rangle, |\nu_{\mathrm{r}2}\rangle\right)^{\mathrm{T}}$, which is defined as

$$\begin{pmatrix} |\nu_{\mathrm{r}1}\rangle \\ |\nu_{\mathrm{r}2}\rangle \end{pmatrix} = \mathbf{U}^\dagger \begin{pmatrix} |\nu_\mathrm{L}\rangle \\ |\nu_\mathrm{H}\rangle \end{pmatrix}. \tag{3.27}$$

For convenience, we name this unitary transformation in Eqn. (3.26) Rabi transformation as well as the new basis in Eqn. (3.27) the Rabi basis. The reason it can remove the σ_3 term is that it will transform the system into a rotating frame so that the varying energy gap due to the fluctuating matter density is exactly cancelled by rotation of the frame. Another advantage of this transformation is that the transition probability from light state to heavy state in background matter basis is easily calculated as $P_{\mathrm{L}\to\mathrm{H}}(x) = |e^{i\eta}\psi_{\mathrm{r}2}(x)|^2 = |\psi_{\mathrm{r}2}(x)|^2$.. In Rabi basis, we find the Schrödinger equation

$$\begin{aligned} &\begin{pmatrix} \frac{\mathrm{d}\eta}{\mathrm{d}r} & 0 \\ 0 & -\frac{\mathrm{d}\eta}{\mathrm{d}r} \end{pmatrix} \begin{pmatrix} \psi_{\mathrm{R}1} \\ \psi_{\mathrm{R}2} \end{pmatrix} + \mathrm{i}\frac{\mathrm{d}}{\mathrm{d}r} \begin{pmatrix} \psi_{\mathrm{R}1} \\ \psi_{\mathrm{R}2} \end{pmatrix} \\ &= \left[-\frac{\omega_\mathrm{m}}{2}\sigma_3 + \frac{\delta\lambda}{2}\cos 2\theta_\mathrm{m}\sigma_3 - \frac{\delta\lambda}{2}\sin 2\theta_\mathrm{m} \begin{pmatrix} 0 & e^{2\mathrm{i}\eta} \\ e^{-2\mathrm{i}\eta} & 0 \end{pmatrix} \right] \begin{pmatrix} \psi_{\mathrm{R}1} \\ \psi_{\mathrm{R}2} \end{pmatrix}, \end{aligned}$$

in which the varying diagonal elements in Hamiltonian can be eliminated by choosing $\eta(r)$ properly, i.e.,

$$\eta(r) - \eta(0) = \frac{\cos 2\theta_{\rm m}}{2} \int_0^r \delta\lambda(\tau) d\tau. \tag{3.28}$$

In Rabi basis, the Schrödinger equation becomes

$$\mathrm{i}\frac{d}{dr}\begin{pmatrix}\psi_{\rm r1}\\ \psi_{\rm r2}\end{pmatrix} = \left[-\frac{\omega_{\rm m}}{2}\sigma_3 - \frac{\delta\lambda}{2}\sin 2\theta_{\rm m}\begin{pmatrix}0 & e^{2\mathrm{i}\eta}\\ e^{-2\mathrm{i}\eta} & 0\end{pmatrix}\right]\begin{pmatrix}\psi_{\rm r1}\\ \psi_{\rm r2}\end{pmatrix}.$$

One can easily show that the transition probability between two eigenstates in Rabi basis is the same as the transition probability between two eigenstates in background matter basis, given the initial condition that the system is in low energy state.

For single frequency matter profile with potential $\delta\lambda(r) = A_1 \sin(k_1 r)$, we have $\eta(r) = -A_1 \cos 2\theta_{\rm m} \cos(k_1 r)/(2k)$. To make connection with Rabi oscillation, we apply Jacobi-Anger expansion, which is used in Ref. [29], to decompose the $\exp\left(\mathrm{i}z\cos\left(k_1 r\right)\right)$-like term in Hamiltonian into linear combinations of terms that is proportional to $\exp\left(\mathrm{i}nk_1 r\right)$, i.e., to decompose spherical waves into plane waves. The decomposed form of Hamiltonian explicitly shows that the Hamiltonian is a summation of Rabi systems, which is

$$H^{(\rm R)} = -\frac{\omega_{\rm m}}{2}\sigma_3 - \frac{1}{2}\sum_{n=-\infty}^{\infty} B_n \begin{pmatrix}0 & \Phi_n e^{\mathrm{i}nk_1 r}\\ \Phi_n^* e^{-\mathrm{i}nk_1 r} & 0\end{pmatrix}, \tag{3.29}$$

where

$$B_n = \tan 2\theta_{\rm m} n k_1 J_n\left(\frac{A_1}{k_1}\cos 2\theta_{\rm m}\right),$$
$$\Phi_n = e^{i\pi(3n/2+1)},$$

with J_n standing for the Bessel function. The constant phase Φ_n doesn't play any role for the reason discussed in Appendix B. Phase in matter potential would also go into Φ_n, for which reason, phase of matter profile is not included in the current discussion. In the Hamiltonian, the first term describes the energy gap, while the

second term is the summation of many driving fields. The resonance width for a given mode n is $|B_n|$. It's worth mentioning that we have [26]

$$J_n(n\mathrm{sech}\,\alpha) \sim \frac{e^{n(\tanh\alpha-\alpha)}}{\sqrt{2\pi n\tanh\alpha}} \tag{3.30}$$

for large n. It's straightforward to prove that resonance width decreases dramatically for large n thus resonance of higher order modes become insignificant.

When the system has one dominate resonance mode and without significant interference between the resonance mode and other modes, all off-resonance modes can be dropped without significantly changing the transition probabilities. However, as we have shown previously in Sec. 3.4, interference might happen between different modes and interferences were measured with a criteria. However, interference is not the only effect we need to consider. The following subsections will determine the important modes of the system (i.e., which n to include) and explore the interference between modes hence explain the coincidence presented in the previous sections. We use dimensionless quantities which are scaled using the characteristic energy scale ω_{m}, e.g.,

$$\begin{aligned}
\hat{r} &= \omega_{\mathrm{m}} r, \\
\hat{k}_1 &= \frac{k_1}{\omega_{\mathrm{m}}}, \\
\hat{A}_1 &= \frac{A_1}{\omega_{\mathrm{m}}}, \\
\hat{B}_n &= \frac{B_n}{\omega_{\mathrm{m}}}.
\end{aligned}$$

3.6.1 The Important Factors

In order for a mode to have a significant effect on the transition probabilities, we require it to has large relative detuning D, and a large oscillation wavelength compared

to the size of the physical system. Relative detuning for each mode is calculated as

$$D_n = \frac{|nk_1 - \omega_{\rm m}|}{B_n} \tag{3.31}$$

for single frequency matter profile, and

$$D_{\{n_a\}} = \frac{|\sum_a n_a k_a - \omega_{\rm m}|}{B_{\{n_a\}}} \tag{3.32}$$

for multi-frequency matter profile.

For modes with small relative detuning, they are important since they might lead to full transition. However, the full transition requires at least a distance of the order of the wavelength of the oscillation. Suppose we have a mode that has zero relative detuning, but with a oscillation wavelength much larger than the size of the system, such a mode would never have the chance to accumulate a large transition probability within the size of the system. By utilizing the theory of Rabi oscillation, we know that the oscillation wavelength of each mode is determined by the Rabi frequency

$$\Omega_{\{n_a\}} = |B_{\{n_a\}}|\sqrt{1 + D^2_{\{n_a\}}}. \tag{3.33}$$

Thus modes that has much larger oscillation wavelength are not subjected to be considered even though their relative detunings are close to zero.

In principle, we can always approximate the system by including more modes with larger relative detuning while neglecting the modes with wavelength much longer than the size of physical system. However such effort doesn't simplify the calculations.

3.6.2 Single Frequency Matter Profile Revisited

For the single frequency matter potential $\lambda = \lambda_0 + \lambda_1 \sin(k_1 r)$ discussed in Sec. 3.3, we removed the varying σ_3 term by arguing that this term has no effect on transition probabilities when the system is close to resonance, $k_1 \sim \omega_{\rm m}$. The reason is that

only the first mode $n = 1$ is on resonance when $k_1 = \omega_{\rm m}$ and all other modes are far from resonance, thus

$$\begin{aligned} H^{\rm R} &\approx -\frac{\omega_{\rm m}}{2}\sigma_3 - \frac{1}{2}B_1 \begin{pmatrix} 0 & \Phi_1 e^{ik_1 r} \\ \Phi_1^* e^{-ik_1 r} & 0 \end{pmatrix} \\ &\approx -\frac{\omega_{\rm m}}{2}\sigma_3 - \frac{A_1}{2}\cos(k_1 r)\sigma_1 + \frac{A_1}{2}\sin(k_1 r)\sigma_2, \end{aligned} \tag{3.34}$$

where A_1 is defined in Eqn. (3.15) and approximation

$$J_1\left(\frac{\lambda_1}{k_1}\cos(2\theta_{\rm m})\right) \approx \frac{\lambda_1}{2k_1}\cos(2\theta_{\rm m})$$

for $\lambda_1 \cos(2\theta_{\rm m})/k_1 \ll 1$ is used in the last step. Thus we reach a similar equation to the approximation we used in Sec. 3.3. $\lambda_1 \cos(2\theta_{\rm m})/k_1 \ll 1$ corresponds to small resonance width for Eqn. (3.14) and also Eqn. (3.34) so that the interferences are small.

Using Jacobi-Anger expansion, we can calculate the relative detuning for each mode as well as the interference effect. The relative detuning for each mode in the Jacobi-Anger expansion for single frequency matter profile used in Fig. 3.7 is calculated and listed in Table. 3.1. The D_1' is the shifted relative detuning of the first mode with $n = 1$ due to other mode. It clearly shows that the first mode takes the whole system so that the approximation of neglecting the varying σ_3 terms in Hamiltonian is accurate enough. One can also show that the interference effect due to higher order modes is negligible, since they do not change the relative detuning of the most significant modes.

The rigorous solutions for each modes in Eqn. 3.29 is obtained,

$$P^{(n)}_{\rm L\to H} = \frac{\left|\hat{B}_n\right|^2}{\left|\hat{B}_n\right|^2 + (n\hat{k} - 1)^2} \sin^2\left(\frac{\hat{q}^{(n)}}{2}\hat{x}\right), \tag{3.35}$$

$k_1 = \omega_{\rm m}$				$k_1 = (1 - 2 \times 10^{-5})\omega_{\rm m}$				$k_1 = (1 - 10^{-4})\omega_{\rm m}$			
n	D	D_1'	$2\pi\omega_{\rm m}/\Omega_n$	n	D	D_1'	$2\pi\omega_{\rm m}/\Omega_n$	n	D	D_1'	$2\pi\omega_{\rm m}/\Omega_n$
1	0	-	3.2×10^5	1	1	-	2.2×10^5	1	5.2	-	6.2×10^4
-1	10^5	4.8×10^{-6}	3.1	-1	10^5	1	3.1	-1	10^5	5.2	3.1
2	1.1×10^9	2.1×10^{-14}	6.3	2	1.1×10^9	1	6.3	2	1.1×10^9	5.2	6.3
-2	3.4×10^9	6.9×10^{-15}	2.1	-2	3.4×10^9	1	2.1	-2	3.4×10^9	5.2	2.1

Table 3.1: Relative detuning and oscillation wavelength of each mode for single frequency matter profile.

where

$$\Gamma^{(n)} = \left|\hat{B}_n\right|, \quad \text{width of resonance } (n\hat{k} \text{ as parameter}) \tag{3.36}$$

$$\hat{q}^{(n)} = \sqrt{|\Gamma^{(n)}|^2 + (n\hat{k} - 1)^2}, \quad \text{frequency of oscillations.} \tag{3.37}$$

The impact of detuning is also verified in Fig. 3.10. The example clearly shows the width of the resonance is dropping dramatically for larger modes in Jacobi-Anger expansion. A careful investigation shows that the resonance width is dropping exponentially as shown in Fig. 3.11 and Fig. 3.12.

3.6.3 Castle Wall Matter Profile

For completeness of this chapter, we show one example of multi-frequency matter profile. One of the multi-frequency matter profiles that has been well studied is the castle wall matter profile. Using Fourier series, any matter profile can be Fourier decomposed into superposition of many single frequency matter profile in principle. We decompose the periodic castle wall matter profile into many frequencies and study the interference effect. The potential shown in Fig. 3.13 is defined as,

$$\lambda(r) = \begin{cases} \Lambda_1, & -\frac{X_1}{2} + nX \leq r \leq \frac{X_1}{2} + nX \\ \Lambda_2, & \frac{X_1}{2} + nX \leq r \leq \frac{X_1}{2} + \frac{X_2}{2} + nX \end{cases} \tag{3.38}$$

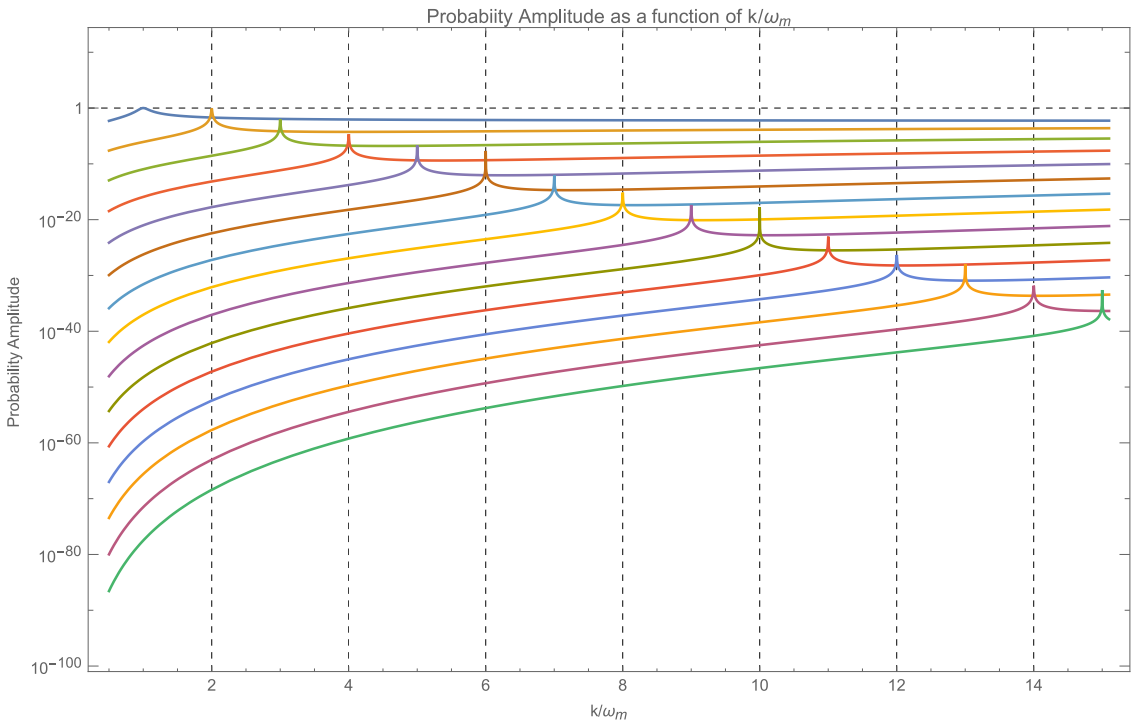

Figure 3.10: Probability amplitude as a function of $k/\omega_{\rm m}$ for each term in Jacobi-Anger expansion, with parameters $\lambda_1 = 0.1$,$\theta_{\rm m} = \pi/5$.

where X_1 and X_2 are the two periods of the matter profile or potential, $X = X_1 + X_2$, and n is integer. The parametric resonance condition derived by E. Akhmedov [15] is,

$$\frac{\tan(\omega_{\rm m1} X_1/2)}{\tan(\omega_{\rm m2} X_2/2)} = -\frac{\cos 2\theta_{\rm m2}}{\cos 2\theta_{\rm m1}}, \tag{3.39}$$

where $\omega_{{\rm m}i}$ and $\theta_{{\rm m}i}$ are the energy difference and mixing angle for potential Λ_1 and Λ_2 respectively.

Even though this castle wall problem is analytically solved, the resonance condition Eqn. (3.39) itself is not transparent. In this subsection, we show that such a system is closed related to Rabi oscillations. For illustration purpose, we set the profile to be equal period for the two densities so that $X_1 = X_2 \equiv X/2$. To show that the neutrino flavor conversions in this castle wall matter profiles is related to

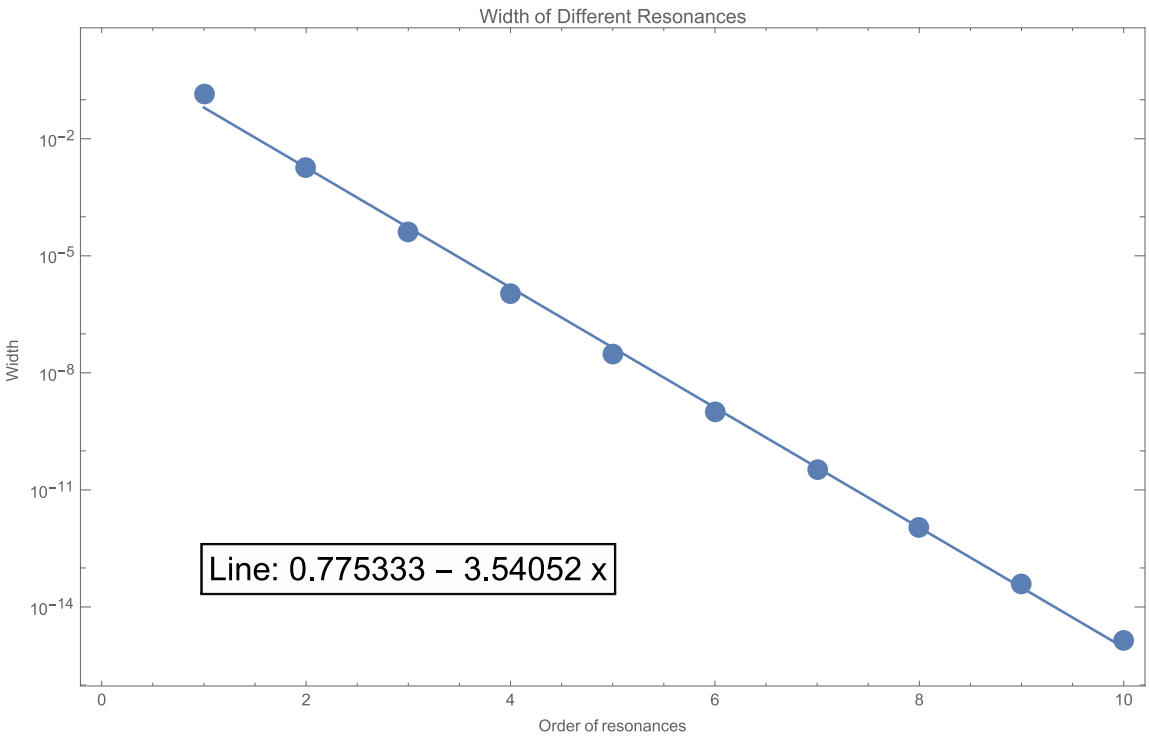

Figure 3.11: Resonance width as a function of mode order for each term in Jacobi-Anger expansion, with parameters $\lambda_1 = 0.1$,$\theta_{\mathrm{m}} = \pi/5$.

Rabi oscillation, we decompose the profile using Fourier series,

$$\lambda(r) = \lambda_0 + \sum_{n=1}^{\infty} \lambda_n \cos\left(k_n r\right), \tag{3.40}$$

where

$$\begin{aligned}
\lambda_0 &= (\Lambda_1 + \Lambda_2)/2, \\
\lambda_n &= \frac{2}{(2n-1)\pi}(-1)^n \left(\Lambda_1 - \Lambda_2\right), \\
k_n &= (2n-1)k_0, \\
k_0 &= 2\pi/X.
\end{aligned}$$

The decomposition is visualized in Fig. A.1.

To calculate the transitions between two mass states of background matter po-

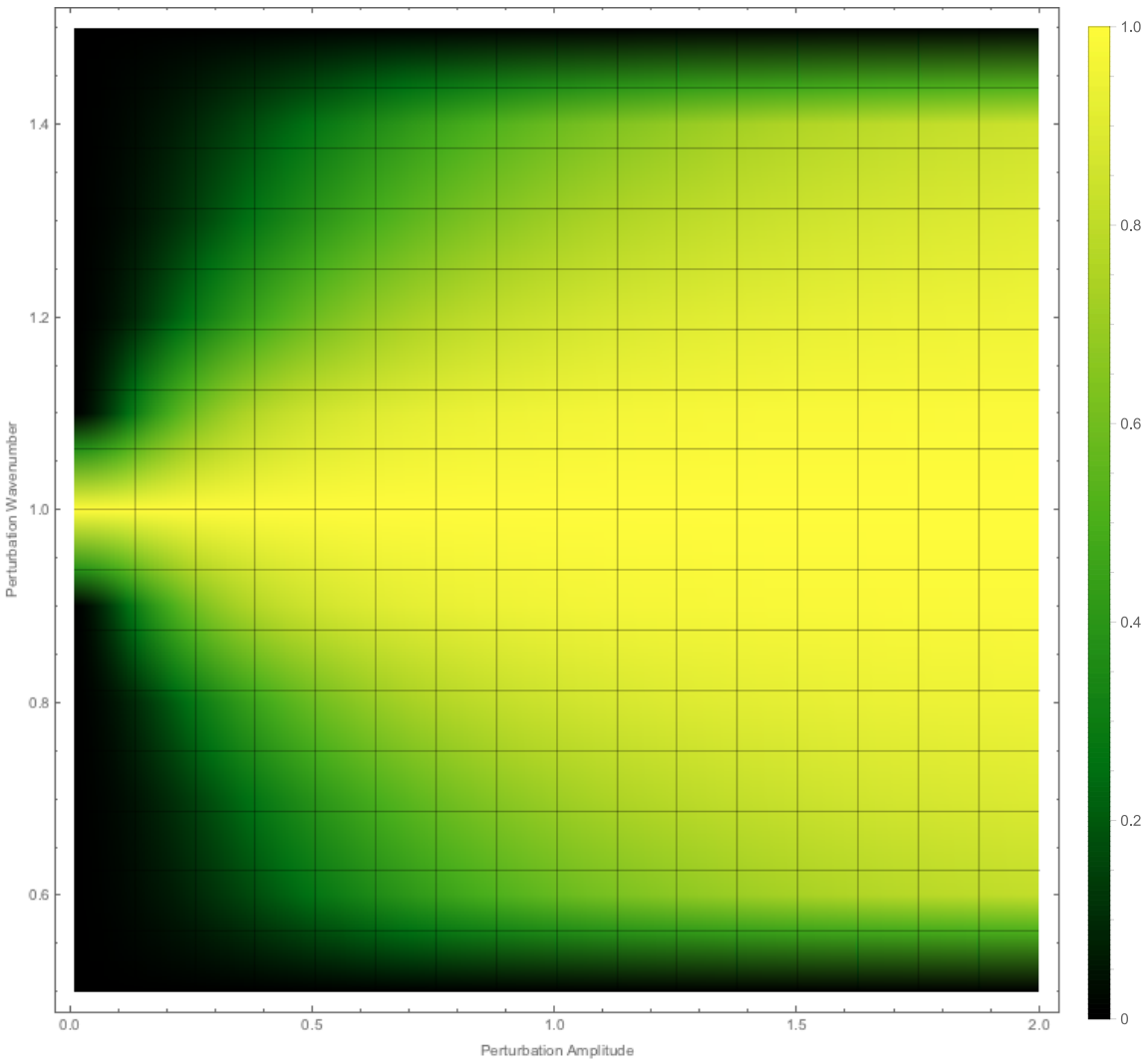

Figure 3.12: Transition probability amplitude at different perturbation amplitude and perturbation wavenumber. Larger amplitudes corresponds to larger resonance width, as another confirmation to Fig. 3.11.

tential λ_0, we use the background matter basis with respect to λ_0, in which the transition is zero when varying matter profile vanishes. The Hamiltonian

$$H^{(\mathrm{m})} = -\frac{1}{2}\omega_{\mathrm{m}}\sigma_3 + \frac{1}{2}\sum_{n=1}^{\infty}\lambda_n \cos 2\theta_{\mathrm{m}} \cos\left(k_n r\right)\sigma_3 - \frac{1}{2}\sum_{n=1}^{\infty}\lambda_n \sin 2\theta_{\mathrm{m}} \cos\left(k_n r\right)\sigma_1, \quad (3.41)$$

determines the transitions between the two background matter states.

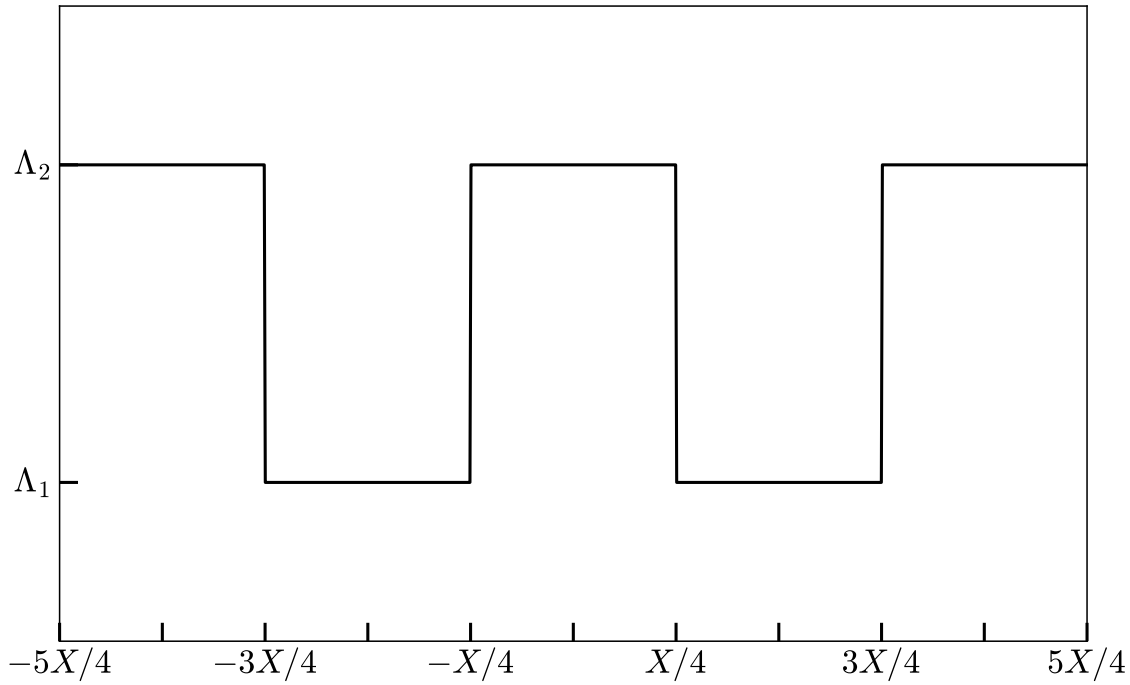

Figure 3.13: The castle wall matter potential profile with $X_1 = X_2 = X/2$.

In principle, the base frequency k_0 which is determined by the total period X can be arbitrary. In this example, we choose a X so that the base frequency k_0 matches the energy gap $\omega_{\rm m}$. Even though multiple perturbation frequencies show up in Eqn. (3.41), we identify that only the first frequency $n = 1$ is the resonance frequency since we are using $k_0 = \omega_{\rm m}$. As an approximation, we drop all other frequencies $n > 2$ regarding the fact that they are far from resonance. Thus, similar to single frequency matter profile, the varying σ_3 terms have limited effects on the

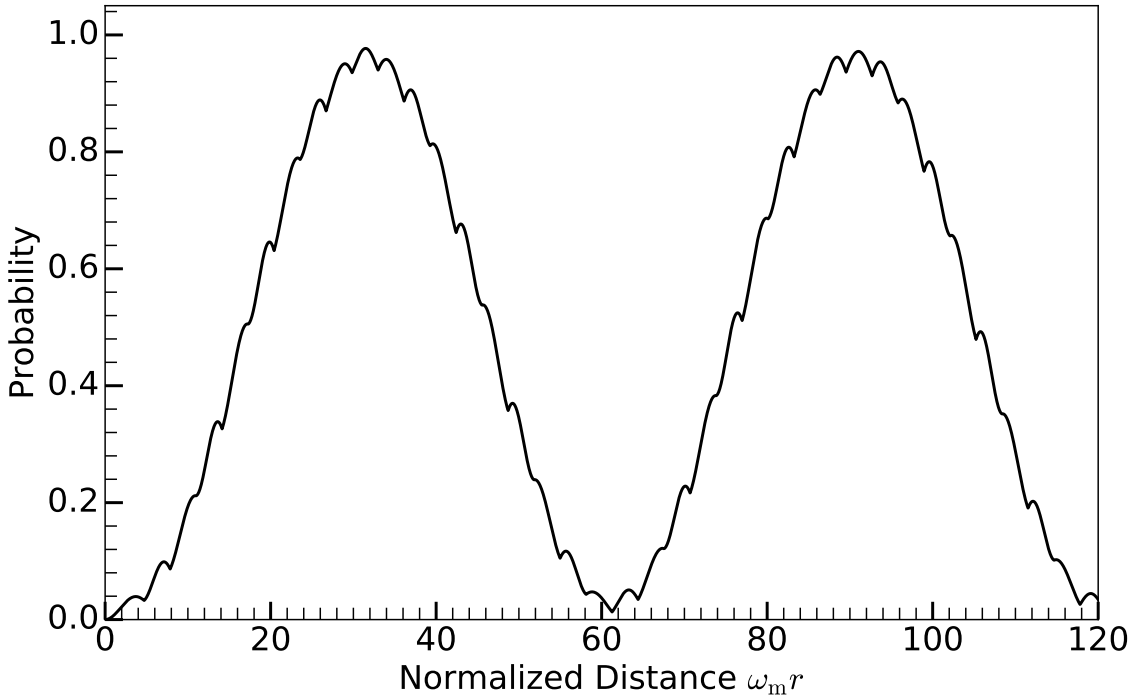

Figure 3.14: Transition probabilities for castle wall matter profile calculated numerically for $\Lambda_2 - \Lambda_1 = 0.4\Lambda_0$. During the calculation, the energy of neutrinos is 10 MeV, mass-squared difference is $\delta m^2 = 2.6 \times 10^{-3}\,\mathrm{eV}^2$, and the vacuum mixing angle chosen so that $\sin^2(2\theta_{\mathrm{v}}) = 0.093$. The background potential Λ_0 is chosen so that it's half the MSW resonance potential, $\Lambda_0 = \frac{1}{2}\lambda_{\mathrm{MSW}} = \frac{1}{2}\omega_{\mathrm{v}} \cos 2\theta_{\mathrm{v}}$, and the base frequency is set to $k_0 = 2\pi/X = \omega_{\mathrm{m}}$.

transition probabilities in our case, which leads to

$$\begin{aligned} H^{(\mathrm{m})} \to & -\frac{1}{2}\omega_{\mathrm{m}}\sigma_3 - \frac{1}{2}\sum_{n=1}^{2} \lambda_n \sin 2\theta_{\mathrm{m}} \cos\left(k_n r\right) \sigma_1 \\ \to & -\frac{1}{2}\omega_{\mathrm{m}}\sigma_3 - \frac{1}{2}\sum_{n=1}^{2} A_n \cos(k_n r)\sigma_1 \\ & + \frac{1}{2}\sum_{n=1}^{2} A_n \sin(k_n r)\sigma_2, \end{aligned}$$

where

$$A_n = \frac{\lambda_n \sin 2\theta_{\mathrm{m}}}{2}.$$

The relative detuning is 0 if we have only the first mode. However, it becomes

$$D_1' = \frac{A_2^2}{2|A_1(\omega_\mathrm{m} - k_2)|}, \tag{3.42}$$

if we include the second frequency k_2. One feature of this Fourier series expanded matter profile Eqn. (3.40) is that the width of each frequency decreases as the order n increases while the detuning of each frequency increases. We calculate the relative detuning for each frequency

$$D_n = \frac{|k_n - \omega_\mathrm{m}|}{|\lambda_n \sin 2\theta_\mathrm{m}/2|} = \frac{2(n-1)(2n-1)\pi\omega_\mathrm{m}}{(\Lambda_2 - \Lambda_1)\sin 2\theta_\mathrm{m}} \tag{3.43}$$

which is quadratic in n and inversely proportional to $\Lambda_2 - \Lambda_1$. We find that all higher frequencies k_n for $n > 2$ have very large relative detunings. The neutrino transition probability between the two matter states is shown in Fig. 3.14, where we find the system has almost full transition.

A more rigorous treatment is to use Jacobi-Anger expansion and find the Rabi modes, where we find that the mode that corresponds to single frequency k_1 dominates and all other modes have little destruction effect on it. Quantitatively, higher orders leads to smaller width $B_{\{n_i\}}$ yet larger detuning $\sum_n nk_n - \omega_\mathrm{m}$, which renders a smaller effect on the resonance mode $\{1, 0\}$, since the effect is evaluated as Eqn. (3.20). Table 3.2 lists the first few smallest relative detunings of Fig. 3.14. The second column is the relative detuning of the corresponding mode, while the third column is the relative detuning of mode $\{1, 0\}$ with the energy gap shift effect of the corresponding mode.

$\{n_1, n_2\}$	D	$D'_{\{1,0\}}$
$\{1, 0\}$	0	-
$\{-1, 0\}$	48	1.0×10^{-2}
$\{0, 1\}$	1.5×10^2	1.1×10^{-3}
$\{2, 0\}$	2.4×10^2	2.0×10^{-4}

Table 3.2: Relative detuning of each frequency.

3.7 Deep Diving into Jacobi-Anger Expansion

3.7.1 Single Matter Density Frequencies

As a first step, we solve single frequency matter perturbation

$$\delta\lambda(x) = A\sin(kx + \phi). \tag{3.44}$$

Using the relation between η and $\delta\lambda$, we solve out η.

$$\eta(x) = -\frac{\omega_{\rm m}}{2}x - \frac{\cos 2\theta_{\rm m}}{2}\frac{A}{k}\cos(kx + \phi), \tag{3.45}$$

where we have chosen $\eta(0) = -\frac{\cos 2\theta_{\rm m}}{2}\frac{A}{k}\cos\phi$. The problem is to solve the equation of motion

$$i\frac{d}{dx}\begin{pmatrix}\psi_{b1}\\ \psi_{b2}\end{pmatrix} = \frac{\sin 2\theta_{\rm m}}{2}\delta\lambda(x)\begin{pmatrix}0 & e^{2i\eta(x)}\\ e^{-2i\eta(x)} & 0\end{pmatrix}\begin{pmatrix}\psi_{b1}\\ \psi_{b2}\end{pmatrix}. \tag{3.46}$$

We also define

$$h = \frac{\sin 2\theta_{\rm m}}{2}\delta\lambda(x)e^{2i\eta(x)} \tag{3.47}$$

$$= \frac{\sin 2\theta_{\rm m}}{2}A\sin(kx + \phi)e^{i\left(-\omega_{\rm m}x - \frac{A\cos 2\theta_{\rm m}}{k}\cos(kx+\phi)\right)}, \tag{3.48}$$

so that the equation of motion becomes

$$i\frac{d}{dx}\begin{pmatrix}\psi_{b1}\\ \psi_{b2}\end{pmatrix} = \begin{pmatrix}0 & h\\ h^* & 0\end{pmatrix}\begin{pmatrix}\psi_{b1}\\ \psi_{b2}\end{pmatrix}. \tag{3.49}$$

We apply Jacobi-Anger expansion, c.f. Eqn. A.27, to rewrite the exponential into some plane wave terms [31].

We define $z_k = \frac{A}{k}\cos 2\theta_{\rm m}$, with which we expand the term

$$e^{-i\frac{\cos 2\theta_{\rm m} A}{k}\cos(kx+\phi)} = \sum_{n=-\infty}^{\infty} i^n J_n(-z_k) e^{in(kx+\phi)} = \sum_{n=-\infty}^{\infty} (-i)^n J_n(z_k) e^{in(kx+\phi)}, \quad (3.50)$$

where I used $J_n(-z_k) = (-1)^n J_n(z_k)$ for integer n. The expansion is plugged into the Hamiltonian elements,

$$h = \frac{A\sin 2\theta_{\rm m}\sin(kx+\phi)}{2} e^{-i\omega_{\rm m} x} \sum_{n=-\infty}^{\infty} (-i)^n J_n(z_k) e^{in(kx+\phi)} \quad (3.51)$$

$$= \frac{A\sin 2\theta_{\rm m}}{4i}\left(e^{i(kx+\phi)} - e^{-i(kx+\phi)}\right) e^{-i\omega_{\rm m} x} \sum_{n=-\infty}^{\infty} (-i)^n J_n(z_k) e^{in(kx+\phi)} \quad (3.52)$$

$$= \frac{A\sin 2\theta_{\rm m}}{4i}\left(\sum_{n=-\infty}^{\infty} e^{i(n+1)} i^n J_n(z_k) e^{i((n+1)k-\omega_{\rm m})x} - \sum_{n'=-\infty}^{\infty} e^{i(n'-1)}(-i)^{n'} J_{n'}(z_k) e^{i((n'-1)k-\omega_{\rm m})x}\right) \quad (3.53)$$

$$= \frac{A\sin 2\theta_{\rm m}}{4} \sum_{n=-\infty}^{\infty} e^{in\phi}\left(-(-i)^n\right)\frac{2n}{z_k} J_n(z_k) e^{i(nk-\omega_{\rm m})x}, \quad (3.54)$$

where I have used

$$J_{n-1}(z_k) + J_{n+1}(z_k) = \frac{2n}{z_k} J_n(z_k). \quad (3.55)$$

Here comes the approximation. The most important oscillation we need is the one with largest period, which indicates the phase to be almost zero,

$$(n+1)k - \omega_{\rm m} \sim 0 \quad (3.56)$$

$$(n'-1)k - \omega_{\rm m} \sim 0. \quad (3.57)$$

The two such conditions for the two summations are

$$n \equiv n_- = {\rm Int}\left(\frac{\omega_{\rm m}}{k}\right) - 1 \quad (3.58)$$

$$n' \equiv n_+ = {\rm Int}\left(\frac{\omega_{\rm m}}{k}\right) + 1. \quad (3.59)$$

We define Int $\left(\frac{\omega_{\rm m}}{k}\right) = n_0$,

$$n_- = n_0 - 1 \tag{3.60}$$

$$n_+ = n_0 + 1. \tag{3.61}$$

The element of Hamiltonian is written as

$$h = -\frac{A\sin 2\theta_{\rm m}}{2} e^{in_0\phi}(-i)^{n_0}\frac{n_0}{z_k}J_{n_0}(z_k)e^{i(n_0k-\omega_{\rm m})x}. \tag{3.62}$$

To save keystrokes, we define

$$F = -A\sin 2\theta_{\rm m} e^{in_0\phi}(-i)^{n_0}\frac{n_0}{z_k}J_{n_0}(z_k), \tag{3.63}$$

which depends on n_0 and $z_k = \frac{A}{k}\cos 2\theta_{\rm m}$. Notice that

$$|F|^2 = \left|k\tan 2\theta_{\rm m} n_0 J_{n_0}(z_k)\right|^2. \tag{3.64}$$

Thus the 12 element of the Hamiltonian is rewritten as

$$h = \frac{1}{2}Fe^{i(n_0k-\omega_{\rm m})x}. \tag{3.65}$$

The general solution to the equation of motion is

$$\psi_{b1} = C_1 e^{\frac{1}{2}i\left(n_0k-\omega_{\rm m}-\sqrt{|F|^2+(n_0k-\omega_{\rm m})^2}\right)x} + C_2 e^{\frac{1}{2}i\left(n_0k-\omega_{\rm m}+\sqrt{|F|^2+(n_0k-\omega_{\rm m})^2}\right)x} \tag{3.66}$$

$$\begin{aligned}\psi_{b2} =& \frac{C_1}{F^*}i\left(n_0k-\omega_{\rm m}-\sqrt{|F|^2+(n_0k-\omega_{\rm m})^2}\right)e^{-\frac{1}{2}i(n_0k-\omega_{\rm m})x-\frac{1}{2}i\sqrt{|F|^2+(n_0k-\omega_{\rm m})^2}} \\ &+ \frac{C_2}{F^*}i\left(n_0k-\omega_{\rm m}+\sqrt{|F|^2+(n_0k-\omega_{\rm m})^2}\right)e^{-\frac{1}{2}i(n_0k-\omega_{\rm m})x+\frac{1}{2}i\sqrt{|F|^2+(n_0k-\omega_{\rm m})^2}}.\end{aligned} \tag{3.67}$$

For simplicity, we define

$$g = n_0k - \omega_{\rm m}, \tag{3.68}$$

$$q^2 = |F|^2 + g^2. \tag{3.69}$$

To determine the constants, we need initial condition,

$$\begin{pmatrix} \psi_1(0) \\ \psi_2(0) \end{pmatrix} = \begin{pmatrix} 1 \\ 0 \end{pmatrix}, \tag{3.70}$$

which leads to

$$\begin{pmatrix} \psi_{b1}(0) \\ \psi_{b2}(0) \end{pmatrix} = \begin{pmatrix} e^{i\eta(0)} \\ 0 \end{pmatrix}. \tag{3.71}$$

Plug in the initial condition for the wave function,

$$C_1 + C_2 = e^{i\frac{z_k}{2}\cos\phi} \tag{3.72}$$

$$\frac{C_1}{2F^*} i\,(g-q) + \frac{C_2}{F^*} i\,(q+g) = 0. \tag{3.73}$$

The constants are solved out

$$C_1 = e^{i\frac{z_k}{2}\cos\phi}\frac{q+g}{2q}, \tag{3.74}$$

$$C_2 = e^{i\frac{z_k}{2}\cos\phi}\frac{q-g}{2q}. \tag{3.75}$$

where F is defined in 3.63 and l and g are defined in 3.69. The second element of wave function becomes

$$\psi_{b2}(x) = \frac{-F}{q} e^{i\frac{z_k}{2}\cos\phi} e^{-\frac{i}{2}gx} \sin\left(\frac{1}{2}qx\right). \tag{3.76}$$

The transition probability becomes

$$P_{1\to 2} = |\psi_{b2}|^2 = \frac{|F|^2}{q^2}\sin^2\left(\frac{q}{2}x\right), \tag{3.77}$$

where q is the oscillation wavenumber. Period of this oscillation is given by $T = \frac{2\pi}{q}$.

Compared to the results by Kneller et al [29], where the transition probability is

$$P_{12} = \frac{\kappa_n^2}{q_n^2}\sin^2(q_n x), \tag{3.78}$$

where $q_n^2 = k_n^2 + \kappa_n^2$ and $2k_n = \tilde{\delta k}_{12} + nk_\star$.

In my notation, k is the same as their $k_\star$. After the first step of translation, we have $g = 2k_n$.

The definition of κ_n is given by

$$\kappa_{ij,n} = (-i)^{n-1}\frac{nC_\star V_\star}{z_{ij}}J_n(z_{ij})\tilde{U}^*_{ei}\tilde{U}_{ej}e^{i(n\eta+z_{ij}\cos\eta)}, \tag{3.79}$$

in Kneller et al's notation and

$$\delta V_{ee}(x) = C_\star V_\star \sin(k_\star x + \eta). \tag{3.80}$$

So we conclude that my $|F|^2$ is related to Kneller et al's $|\kappa_n|^2$ through

$$|F|^2 = 4|\kappa_n|^2. \tag{3.81}$$

We also have

$$q^2 = |F|^2 + g^2 = 4q_n^2, \tag{3.82}$$

i.e., $q_n = \frac{q}{2}$. Now we see the method we have used gives exactly the same transition probability as Kneller et al's.

To make the numerical calculations easier, we rewrite the result by defining the scaled variables

$$\hat{x} = \omega_{\rm m}x, \tag{3.83}$$

$$\hat{k} = \frac{k}{\omega_{\rm m}}, \tag{3.84}$$

$$\hat{A} = \frac{A}{\omega_{\rm m}}, \tag{3.85}$$

$$\hat{g} = \frac{g}{\omega_{\rm m}} = n_0\hat{k} - 1, \tag{3.86}$$

$$\hat{q} = \sqrt{|\hat{F}|^2 + \hat{g}^2} = \sqrt{|\hat{k}\tan 2\theta_{\rm m}n_0J_{n_0}(z_k)| + \hat{g}^2}, \tag{3.87}$$

so that $n_0 = \text{Round}\left(1/\hat{k}\right)$, $z_k = \frac{\hat{A}}{\hat{k}}\cos 2\theta_{\rm m}$ and

$$P_{1\to 2} = \frac{\left|\hat{k}\tan 2\theta_{\rm m}n_0J_{n_0}(z_k)\right|^2}{\left|\hat{k}\tan 2\theta_{\rm m}n_0J_{n_0}(z_k)\right|^2 + \hat{g}^2}\sin^2\left(\frac{\hat{q}}{2}\hat{x}\right). \tag{3.88}$$

Hamiltonian	Solution to The First Element of Wave Function
$-\frac{\omega_{\rm m}}{2}\sigma_3$	$\psi_1 \sim e^{i\omega_{\rm m}x/2}$
$\frac{\delta\lambda}{2}\cos 2\theta_{\rm m}\sigma_3$	$\psi_1 \sim e^{i\frac{A\cos 2\theta_{\rm m}}{2k}\cos(kx+\phi)}$
$\frac{\delta\lambda}{2}\cos 2\theta_{\rm m}\sigma_3$	$\psi_1 = C_1 e^{i\frac{A\sin 2\theta_{\rm m}}{2k}\cos(kx+\phi)} + C_2 e^{-i\frac{A\sin 2\theta_{\rm m}}{2k}\cos(kx+\phi)}$

Table 3.3: Each terms in Hamiltonian and the corresponding solutions to the specific term.

Mathematical Analysis of The Result

There are several question to answer before we can understand the picture of the math.

- What does each term mean in the Hamiltonian?
- What exactly is the unitary transformation we used to rotate the wave function?
- What is the physical meaning of Jacobi-Anger expansion in our calculation?

To answer the first question, we need to write down the solution to Schrodinger equation assuming the Hamiltonian has only one term. The results are listed below in Table 3.3.

The unitary transformation used is to move our reference frame to a co-rotating one. $-\frac{\omega_{\rm m}}{2}\sigma_3$ is indeed causing the wave function to rotate and removing this term using a transformation means we are co-rotating with it. $\frac{\delta\lambda}{2}\cos 2\theta_{\rm m}\sigma_3$ causes a more complicated rotation however it is still a rotation.

As for Jacobi-Anger expansion, it expands an oscillating matter profile to infinite constant matter potentials. To see it more clearly, we assume that $\delta\lambda = \lambda_c$ is

Constant Matter Profile $\delta\lambda = \lambda_c$	Periodic Matter Profile $\delta\lambda = A\sin(kx+\phi)$
$\frac{\sin 2\theta_{\rm m}}{2}\lambda_c e^{i\cos 2\theta_{\rm m}\lambda_c x}$	$\frac{A\sin 2\theta_{\rm m}}{4}\sum_{n=-\infty}^{\infty} e^{in\phi}\left(-i^n\right)\frac{2n+1}{z_k}J_n(z_k)e^{i(nk-\omega_{\rm m})x}$

Table 3.4: Comparison of the off diagonal element of Hamiltonian for constant matter density profile and the periodic matter density profile.

constant. After the unitary transformation, the effective Hamiltonian is

$$H' = \frac{\sin 2\theta_{\rm m}}{2}\lambda_c \begin{pmatrix} 0 & e^{2i\eta(x)} \\ e^{-2i\eta(x)} & 0 \end{pmatrix}, \tag{3.89}$$

where $\eta(x) = -\frac{\omega_{\rm m}}{2}x + \frac{\cos 2\theta_{\rm m}}{2}\lambda_c x$ and we have chosen $\eta(0) = 0$. The 12 element of the Hamiltonian becomes

$$\frac{\sin 2\theta_{\rm m}}{2}\lambda_c e^{2i\eta(x)} = \frac{\sin 2\theta_{\rm m}}{2}\lambda_c e^{2i\left(\frac{\omega_{\rm m}}{2}+\frac{\cos 2\theta_{\rm m}}{2}\lambda_c\right)x}. \tag{3.90}$$

The significance of it is to show that a constant matter profile will result in a simple exponential term. However, as we move on to periodic matter profile, we have a Hamiltonian element of the form

$$h = \frac{\sin 2\theta_{\rm m}}{2}A\sin(kx+\phi)e^{2i\left(-\frac{\omega_{\rm m}}{2}x+\frac{A\cos 2\theta_{\rm m}}{2k}\cos(kx+\phi)\right)}, \tag{3.91}$$

as derived in Eqn. 3.48. To compare with the constant matter case, we make a table of relevant terms in Hamiltonian, Table 3.4.

The periodic profile comes into the exponential. Jacobi-Anger expansion (Eqn. A.27) expands the periodic matter profile into infinite constant matter profiles. By comparing the two cases, we conclude that $\cos 2\theta_{\rm m}\lambda_c$ corresponds to nk. The RWA approximation we used to drop fast oscillatory terms in the summation is to find the most relevant constant matter profile per se.

The big question is which constant matter profiles are the most important ones? Mathematically, we require the phase to be almost zero, i.e. Eqn. 3.57 or

$$n_0 k - \omega_{\rm m} \sim 0, \tag{3.92}$$

where $n_0 = \text{Round}\left(\frac{\omega_\text{m}}{k}\right)$.

We define an effective matter density out of the Jacobi-Anger expanded series

$$\lambda_c' = \frac{n_0 k}{\cos 2\theta_\text{m}}. \tag{3.93}$$

Then we can rewrite the RWA requirement as

$$\lambda_c' - \cos 2\theta_\text{m}\omega_\text{m} = 0. \tag{3.94}$$

The Resonances

Now we check the Hamiltonian again to see if we could locate some physics. In the newly defined basis and using scaled quantities

$$\hat{\mathbf{H}} = \begin{pmatrix} 0 & \hat{h} \\ \hat{h}^* & 0 \end{pmatrix}, \tag{3.95}$$

where

$$\hat{h} = \frac{1}{2}\hat{B}_n e^{i(n\hat{k}-1)\hat{x}}, \tag{3.96}$$

and

$$\hat{B}_n = (-i)^n \hat{k} \tan 2\theta_\text{m} n J_n(\frac{\hat{A}}{\hat{k}} \cos 2\theta_\text{m}). \tag{3.97}$$

It becomes much more clearer if we plug $\hat{h}$ back into Hamiltonian. What we find is that

$$\hat{\mathbf{H}} = \sum_{n=-\infty}^{\infty} \begin{pmatrix} 0 & -\frac{1}{2}\hat{B}_n e^{i(n\hat{k}-1)\hat{x}} \\ -\frac{1}{2}\hat{B}_n^* e^{-i(n\hat{k}-1)\hat{x}} & 0 \end{pmatrix}. \tag{3.98}$$

With some effort, we find that the solution to the second amplitude of the wave function is

$$\psi_2 = \frac{i}{\hat{B}_n \hat{W}} e^{-i(n\hat{k}-1)\hat{x}} \left|\hat{B}_n\right|^2 \sin\left(\frac{1}{2}(n\hat{k} - 1 - \hat{W})\hat{x}\right), \tag{3.99}$$

where

$$\hat{W} = \sqrt{(n\hat{k}-1)^2 + \left|\hat{B}_n\right|^2}. \tag{3.100}$$

At this stage, it is quite obvious that our system is a composite Rabi oscillation system. For each specific n term we write down the hopping probability from light state to the heavy state,

$$P_{\mathrm{L}\to\mathrm{H}}^{(n)} = \frac{\left|\hat{B}_n\right|^2}{\left|\hat{B}_n\right|^2 + (n\hat{k}-1)^2} \sin^2\left(\frac{\hat{q}^{(n)}}{2}\hat{x}\right), \tag{3.101}$$

where

$$\Gamma^{(n)} = \left|\hat{B}_n\right|, \quad \text{width of resonance } (n\hat{k} \text{ as parameter}) \tag{3.102}$$

$$\hat{q}^{(n)} = \sqrt{\left|\Gamma^{(n)}\right|^2 + (n\hat{k}-1)^2}, \quad \text{frequency of oscillations} \tag{3.103}$$

We define the scaled quantities,

$$\hat{x} = \omega_{\mathrm{m}} x, \tag{3.104}$$

$$\hat{h} = h/\omega_{\mathrm{m}}, \tag{3.105}$$

$$\hat{B}_n = B_n/\omega_{\mathrm{m}}, \tag{3.106}$$

$$\hat{k} = k/\omega_{\mathrm{m}}, \tag{3.107}$$

$$\hat{A} = A/\omega_{\mathrm{m}}, \tag{3.108}$$

$$\hat{q} = q/\omega_{\mathrm{m}}. \tag{3.109}$$

Just a comment. B_n is used here because I actually want to use it for multi-frequency case and I just think B_n is better than F.

Resonance width of each order of resonance (each n) should be calculated analytically.

To find the exact width is hopeless since we need to inverse Bessel functions. Nonetheless, we can assume that the resonance is very narrow so that $|F|^2$ doesn't change a lot. With the assumption, the FWHM (Full Width at Half Maximum) is found be setting the amplitude to half, which is

$$\Gamma = \left|\frac{\hat{F}}{n_0}\right| = \left|\hat{k}\tan 2\theta_{\mathrm{m}} \frac{J_{n_0}(n_0\hat{A}\cos 2\theta_{\mathrm{m}}/\hat{k})}{n_0}\right|. \tag{3.110}$$

To verify this result, we compare it with the width found numerically from the exact amplitude.

Given this result, and equation 3.65, we infer that the coefficient in front of the phase term of 12 element in Hamiltonian is related to the width, while the the deviation from the exact resonance is given by $\hat{g} = n_0\hat{k} - 1$.

the width of the resonance is

$$\Gamma = \left|\frac{F}{n_0}\right|. \tag{3.111}$$

3.7.2 Multiple Matter Density Frequencies

However, as we proceed to the more realistic matter profile, multi-frequency matter profiles are necessary. Generally, we choose the perturbation matter profile upon a constant background to be

$$\delta\lambda(x) = \sum_n A_n \sin(k_n x + \phi_n). \tag{3.112}$$

Applying the Rabi basis and solving for η we conclude that

$$\eta(x) = -\frac{\omega_{\rm m}}{2}x - \frac{\cos 2\theta_{\rm m}}{2}\sum_n \frac{A_n}{k_n}\cos(k_n x + \phi_n). \tag{3.113}$$

We formulate the Hamiltonian in Rabi basis to be the form

$$H^{(R)} = -\frac{1}{2}\sigma_3 + \begin{pmatrix} 0 & h \\ h^* & 0 \end{pmatrix}, \tag{3.114}$$

We write down the off diagonal element h for the multi-frequency matter density profile

$$h = \frac{\sin 2\theta_{\rm m}}{2}\sum_a A_a \sin(k_a x + \phi_a)e^{-i\omega_{\rm m}x}\prod_a \sum_{n=-\infty}^{\infty}(-i)^n J_n(z_{k_a})e^{in(k_a x+\phi_a)} \tag{3.115}$$

To demonstrate the procedure of Jacobi-Anger expansion as well as the technique to decompose the problem into simple Rabi oscillations, we adopt a two frequencies matter density scenario.

To work out the equation of motion that we could solve, we deal with two frequencies first,

$$\delta\lambda(x) = A_1 \sin(k_1 x + \phi_1) + A_2 \sin(k_2 x + \phi_2), \tag{3.116}$$

while

$$h = \frac{\sin 2\theta_{\rm m}}{2} \sum_{a=1}^{2} A_a \sin(k_a x + \phi_a) e^{-i\omega_{\rm m} x} \prod_{a=1}^{2} \sum_{n=-\infty}^{\infty} (-i)^n J_n(z_{k_a}) e^{in(k_a x + \phi_a)}. \tag{3.117}$$

A useful trick for multiplication of two summations is

$$\sum_n a_n \sum_{\rm m} b_{\rm m} = \sum_{N=-\infty}^{\infty} \sum_{m+n=N} a_n b_{\rm m} = \sum_{N=-\infty}^{\infty} \sum_{n=-\infty}^{N} a_n b_{N-n}. \tag{3.118}$$

For further simplifications of the problem, we follow a rule to sum over a line $m+n = N$ then sum over N, which is illustrated in Fig. 3.15.

The multiplication in Eqn. 3.117 becomes

$$\begin{aligned} h =& \frac{\sin 2\theta_{\rm m}}{2} \sum_{a=1}^{2} A_a \sin(k_a x + \phi_a) e^{-i\omega_{\rm m} x} \\ & \sum_{N=-\infty}^{\infty} \sum_{n=-\infty}^{N} (-i)^n J_n(z_{k_1}) e^{in(k_1 x + \phi_1)} (-i)^{N-n} J_{N-n}(z_{k_2}) e^{i(N-n)(k_2 x + \phi_2)} \\ =& \frac{\sin 2\theta_{\rm m}}{2} \sum_{a=1}^{2} A_a \sin(k_a x + \phi_a) e^{-i\omega_{\rm m} x} \\ & \sum_{N=-\infty}^{\infty} \sum_{n=-\infty}^{N} (-i)^N J_n(z_{k_1}) J_{N-n}(z_{k_2}) e^{in((k_1-k_2)x + \phi_1 - \phi_2) + iN(k_2 x + \phi_2)} \end{aligned} \tag{3.119}$$

To proceed on, we rewrite $\sum_{a=1}^{2} A_a \sin(k_a x + \phi_a)$,

$$\begin{aligned} & A_1 \sin(k_1 x + \phi_1) + A_2 \sin(k_2 x + \phi_2) \\ =& \frac{A_1}{2i} \left(e^{i(k_1 x + \phi_1)} + e^{-i(k_1 x + \phi_1)} \right) + \frac{A_2}{2i} \left(e^{i(k_2 x + \phi_2)} + e^{-i(k_2 x + \phi_2)} \right). \end{aligned} \tag{3.120}$$

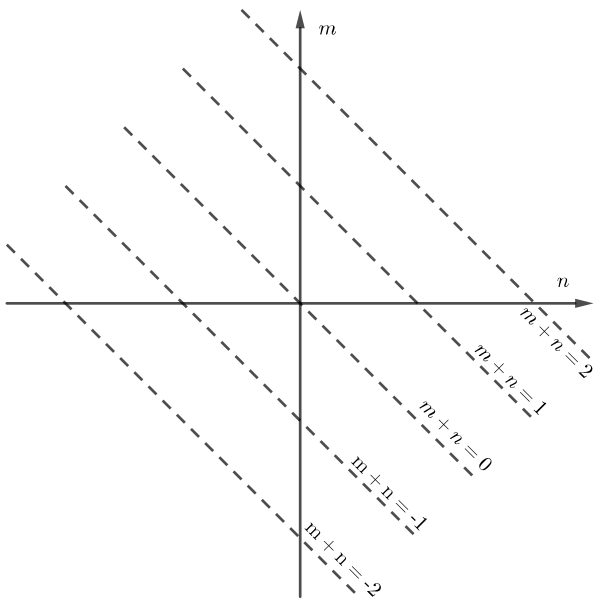

Figure 3.15: Rewrite multiplication of summations into summations only. The horizontal axis is for the summation index n and the vertical axis is for the summation index m. The dashed lines are the lines of equal $m + n$.

We define

$$h = h_1 + h_2, \tag{3.121}$$

where

$$\begin{aligned} h_1 =& \frac{A_1 \sin 2\theta_{\rm m}}{4i} \Bigg(\sum_{N=-\infty}^{\infty} \sum_{n=-\infty}^{N} (-i)^N J_n(z_{k_1}) J_{N-n}(z_{k_2}) e^{i((n+1)(k_1 x+\phi_1)+(N-n)(k_2 x+\phi_2)-\omega_{\rm m} x)} \\ & \sum_{N=-\infty}^{\infty} \sum_{n=-\infty}^{N} (-i)^N J_n(z_{k_1}) J_{N-n}(z_{k_2}) e^{i((n-1)(k_1 x+\phi_1)+(N-n)(k_2 x+\phi_2)-\omega_{\rm m} x)} \Bigg), \end{aligned} \tag{3.122}$$

and

$$h_2 = \frac{A_2 \sin 2\theta_{\rm m}}{4i}\Bigg(\sum_{N=-\infty}^{\infty} \sum_{n=-\infty}^{N} (-i)^N J_n(z_{k_1}) J_{N-n}(z_{k_2}) e^{i(n(k_1 x+\phi_1)+(N-n+1)(k_2 x+\phi_2)-\omega_{\rm m} x)} \\ \sum_{N=-\infty}^{\infty} \sum_{n=-\infty}^{N} (-i)^N J_n(z_{k_1}) J_{N-n}(z_{k_2}) e^{i(n(k_1 x+\phi_1)+(N-n-1)(k_2 x+\phi_2)-\omega_{\rm m} x)} \Bigg). \quad (3.123)$$

We keep only terms that are integers for each summation to satisfy the relations

$$(n_{11,N}+1)k_1 + (N-n_{11,N})k_2 - \omega_{\rm m} \sim 0 \quad (3.124)$$

$$(n_{12,N}-1)k_1 + (N-n_{12,N})k_2 - \omega_{\rm m} \sim 0 \quad (3.125)$$

$$n_{21,N}k_1 + (N-n_{21,N}+1)k_2 - \omega_{\rm m} \sim 0 \quad (3.126)$$

$$n_{22,N}k_1 + (N-n_{22,N}-1)k_2 - \omega_{\rm m} \sim 0. \quad (3.127)$$

so that the x dependent exponential almost vanishes (obtain the largest wavelength in fact). Notice that each $n_{ij,N}$ depends on the summation index N.

We solve each $n_{ij,N}$,

$$n_{11,N} \sim \text{Round}\left[\frac{\omega_{\rm m} - Nk_2 - k_1}{k_1 - k_2}\right] \quad (3.128)$$

$$n_{12,N} \sim \text{Round}\left[\frac{\omega_{\rm m} - Nk_2 + k_1}{k_1 - k_2}\right] \quad (3.129)$$

$$n_{21,N} \sim \text{Round}\left[\frac{\omega_{\rm m} - (N+1)k_2}{k_1 - k_2}\right] \quad (3.130)$$

$$n_{22,N} \sim \text{Round}\left[\frac{\omega_{\rm m} - (N-1)k_2}{k_1 - k_2}\right]. \quad (3.131)$$

Another important constrain is that $n \leq N$, thus we have

$$N_{11} \sim \text{Round}\left[\frac{\omega_{\rm m} - k_1}{k_1}\right] \quad (3.132)$$

$$N_{12} \sim \text{Round}\left[\frac{\omega_{\rm m} + k_1}{k_1}\right] \quad (3.133)$$

$$N_{21} \sim \text{Round}\left[\frac{\omega_{\rm m} - k_2}{k_1}\right] \quad (3.134)$$

$$N_{22} \sim \text{Round}\left[\frac{\omega_{\rm m} + k_2}{k_1}\right], \quad (3.135)$$

for each summation over N and we require $N \geq N_{ij}$ for each summation. We also assumed $k_1 > k_2$. In other words, N_{ij} are the lower limits of the summations over N's.

We keep only the resonance terms for the summation over n's,

$$h_1 \approx \frac{A_1 \sin 2\theta_{\rm m}}{4i}\Bigg(\sum_{N=N_{11}}^{\infty} (-i)^N J_{n_{11}}(z_{k_1}) J_{N-n_{11}}(z_{k_2}) e^{i((n_{11}+1)(k_1x+\phi_1)+(N-n_{11})(k_2x+\phi_2)-\omega_{\rm m}x)} \\ \sum_{N=N_{12}}^{\infty} (-i)^N J_{n_{12}}(z_{k_1}) J_{N-n_{12}}(z_{k_2}) e^{i((n_{12}-1)(k_1x+\phi_1)+(N-n_{12})(k_2x+\phi_2)-\omega_{\rm m}x)}\Bigg), \quad (3.136)$$

and

$$h_2 \approx \frac{A_2 \sin 2\theta_{\rm m}}{4i}\Bigg(\sum_{N=N_{21}}^{\infty} (-i)^N J_{n_{21}}(z_{k_1}) J_{N-n_{21}}(z_{k_2}) e^{i(n_{21}(k_1x+\phi_1)+(N-n_{21}+1)(k_2x+\phi_2)-\omega_{\rm m}x)} \\ \sum_{N=N_{22}}^{\infty} (-i)^N J_{n_{22}}(z_{k_1}) J_{N-n_{22}}(z_{k_2}) e^{i(n_{22}(k_1x+\phi_1)+(N-n_{22}-1)(k_2x+\phi_2)-\omega_{\rm m}x)}\Bigg). \quad (3.137)$$

One can imagine how hard it is to solve the equation of motion with this h. More approximations are required. We will use the approximations that Kelly Patton et al used [31].

By looking at the Hamiltonian, we can identify terms like this

$$h_a = \left(\frac{\sin 2\theta_{\rm m}}{2} A_a \sin(k_a x + \phi_a) e^{-i\omega_{\rm m}x} \sum_{n=-\infty}^{\infty} (-i)^n J_n(z_{k_a}) e^{in(k_a x+\phi_a)} \right) \\ \prod_{b\neq a} \sum_{n=-\infty}^{\infty} (-i)^n J_n(z_{k_b}) e^{in(k_b x+\phi_b)}, \quad (3.138)$$

where the parenthesis part is what we would have if only one frequency is used and we also have

$$h = \sum_a h_a, \quad (3.139)$$

for all frequencies. This reminds us that each of these terms means the interference due to other frequencies. As a simple example, we demonstrate two-frequency case.

The two-frequency matter perturbation system has a Hamiltonian element H_{12}

$$h = h_1 + h_2, \tag{3.140}$$

where

$$\begin{aligned} h_1 =& -\frac{k_1 \tan 2\theta_{\mathrm{m}}}{2} \sum_{n_1=-\infty}^{\infty} (-i)^{n_1} n_1 J_{n_1}(z_{k_1}) e^{i(n_1 k_1 - \omega_{\mathrm{m}})x} e^{in_1\phi_1} \\ & \sum_{n_2=-\infty}^{\infty} (-i)^{n_2} J_{n_2}(z_{k_2}) e^{i(n_2 k_2)x} e^{in_2\phi_2}, \end{aligned} \tag{3.141}$$

$$\begin{aligned} h_2 =& -\frac{k_2 \tan 2\theta_{\mathrm{m}}}{2} \sum_{n_2=-\infty}^{\infty} (-i)^{n_2} n_2 J_{n_2}(z_{k_2}) e^{i(n_2 k_2 - \omega_{\mathrm{m}})x} e^{in_2\phi_2} \\ & \sum_{n_1=-\infty}^{\infty} (-i)^{n_1} J_{n_1}(z_{k_1}) e^{in_1 k_1 x} e^{in_1\phi_1} \end{aligned} \tag{3.142}$$

with red color coding the second frequency and blue coding the first frequency. h is symmetric under exchange of index 1, 2 since the exchange simply switches h_1 and h_2.

The next question to ask is which term dominates. To grasp a clue, we need to identify which term in the summation dominates. Without a good analytical analysis, the only way to do is to numerically calculate the effect of each order.

By order, we are already thinking of a dominating term which is not true. Nonetheless, we assume RWA can be applied to the part that looks like one frequency only. In our two-frequency example, first RWA leads to

$$\begin{aligned} h_1 \approx& -\frac{k_1 \tan 2\theta_{\mathrm{m}}}{2} (-i)^{n_{1,0}} n_{1,0} J_{n_{1,0}}(z_{k_1}) e^{i(n_{1,0} k_1 - \omega_{\mathrm{m}})x} e^{in_{1,0}\phi_1} \\ & \sum_{n_2=-\infty}^{\infty} (-i)^{n_2} J_{n_2}(z_{k_2}) e^{i(n_2 k_2)x} e^{in_2\phi_2}, \end{aligned} \tag{3.143}$$

$$\begin{aligned} h_2 \approx& -\frac{k_2 \tan 2\theta_{\mathrm{m}}}{2} (-i)^{n_{2,0}} n_{2,0} J_{n_{2,0}}(z_{k_2}) e^{i(n_{2,0} k_2 - \omega_{\mathrm{m}})x} e^{in_{2,0}\phi_2} \\ & \sum_{n_1=-\infty}^{\infty} (-i)^{n_1} J_{n_1}(z_{k_1}) e^{in_1 k_1 x} e^{in_1\phi_1}, \end{aligned} \tag{3.144}$$

where

$$n_{1,0} = \text{Round}\left[\frac{\omega_\text{m}}{k_1}\right], \tag{3.145}$$

$$n_{2,0} = \text{Round}\left[\frac{\omega_\text{m}}{k_2}\right]. \tag{3.146}$$

With this approximation, we can use RWA again by requiring

$$(n_{1,0}k_1 - \omega_\text{m} + n_2 k_2)x \sim 0, \tag{3.147}$$

$$(n_1 k_1 - \omega_\text{m} + n_{2,0}k_2)x \sim 0, \tag{3.148}$$

where the integer solutions are

$$n'_{2,0} = \text{Round}\left[\frac{n_{1,0}k_1 - \omega_\text{m}}{k_2}\right], \tag{3.149}$$

$$n'_{1,0} = \text{Round}\left[\frac{n_{2,0}k_1 - \omega_\text{m}}{k_1}\right]. \tag{3.150}$$

Now we can remove all the summations using another RWA approximation. However, whether it holds is up to investigation.

The final result is

$$\begin{aligned}
h_1 \approx & -\frac{k_1 \tan 2\theta_\text{m}}{2}(-i)^{n_{1,0}} n_{1,0} J_{n_{1,0}}(z_{k_1}) e^{i(n_{1,0}k_1 - \omega_\text{m})x} e^{i n_{1,0}\phi_1} (-i)^{n'_{2,0}} J_{n'_{2,0}}(z_{k_2}) e^{i(n'_{2,0}k_2)x} e^{i n'_{2,0}\phi_2} \\
= & -\frac{k_1 \tan 2\theta_\text{m}}{2}(-i)^{n_{1,0}+n'_{2,0}} e^{i(n_{1,0}\phi_1 + n'_{2,0}\phi_2)} n_{1,0} \\
& J_{n_{1,0}}(z_{k_1}) J_{n'_{2,0}}(z_{k_2}) e^{i(n_{1,0}k_1 - \omega_\text{m} + n'_{2,0}k_2)x} \qquad (3.151) \\
\equiv & \frac{F_1}{2} e^{i(n_{1,0}k_1 - \omega_\text{m} + n'_{2,0}k_2)x}, \qquad (3.152)
\end{aligned}$$

$$\begin{aligned}
h_2 \approx & -\frac{k_2 \tan 2\theta_\text{m}}{2}(-i)^{n_{2,0}} n_{2,0} J_{n_{2,0}}(z_{k_2}) e^{i(n_{2,0}k_2 - \omega_\text{m})x} e^{i n_{2,0}\phi_2} \sum_{n_1=-\infty}^{\infty} (-i)^{n_1} J_{n_1}(z_{k_1}) e^{i n_1 k_1 x} e^{i n_1 \phi_1} \\
= & -\frac{k_2 \tan 2\theta_\text{m}}{2}(-i)^{n_{2,0}+n'_{1,0}} e^{i(n_{2,0}\phi_2 + n'_{1,0}\phi_1)} n_{2,0} \\
& J_{n_{2,0}}(z_{k_2}) J_{n'_{1,0}}(z_{k_1}) e^{i(n_{2,0}k_2 - \omega_\text{m} + n'_{1,0}k_1)x} \qquad (3.153) \\
\equiv & \frac{F_2}{2} e^{i(n_{2,0}k_2 - \omega_\text{m} + n'_{1,0}k_1)x}. \qquad (3.154)
\end{aligned}$$

Lowest order only works for very special cases where on of the wave vectors is very close to resonance. To fix this problem, we could add more higher orders, however, what does it mean to have higher orders needs a discussion.

We will develop a protocol to decide which order to include. The first thought of higher orders is to add more from the summation before the last RWA. However, it is highly suspicious that this is just like the one frequency case which has a very fast drop in the resonance width as we go to higher orders. This guess needs proof, numerically and analytically. When we mentioned higher orders, we actually mean higher orders in both n_1 and n_2. Notice that we can always write the 12 element of Hamiltonian as Eqn. 3.159, i.e.,

$$\begin{aligned} h =& h_1 + h_2 \qquad (3.155)\\ =& \sum_{n_1=-\infty}^{\infty}\sum_{n_2=-\infty}^{\infty} B_{n_1,n_2}(k_1,k_2)\Phi e^{i(n_1k_1+n_2k_2-\omega_{\rm m})x} \\ &+ \sum_{n_1=-\infty}^{\infty}\sum_{n_2=-\infty}^{\infty} B_{n_2,n_1}(k_2,k_1)\Phi e^{i(n_1k_1+n_2k_2-\omega_{\rm m})x} \\ =& \sum_{n_1=-\infty}^{\infty}\sum_{n_2=-\infty}^{\infty} \left(B_{n_1,n_2}(k_1,k_2) + B_{n_2,n_1}(k_2,k_1)\right)\Phi e^{i(n_1k_1+n_2k_2-\omega_{\rm m})x}, \qquad (3.156) \end{aligned}$$

without any approximations.

- One of the choices of adding higher orders is to use $n_1 = \text{Round}\left[\frac{\omega_{\rm m}}{k_1}\right]$ and $n_2 = \text{Round}\left[\frac{n_1k_1-\omega_{\rm m}}{k_2}\right]$ as the lowest order in h_1 and $n_2 = \text{Round}\left[\frac{\omega_{\rm m}}{k_2}\right]$ and $n_1 = \text{Round}\left[\frac{n_2k_2-\omega_{\rm m}}{k_1}\right]$ as the lowest order in h_2. Adding higher orders means we add or remove one from n_1 in h_1 and recalculate n_2, while add or remove one from n_2 in h_2 and recalculate n_1.

  That is to say, we always keep the RWA condition for the last RWA process. What can be changed is the first assumption that the most important term is when only one frequency is relevant which is not always true.

As an example, we now consider $n_{i,\pm1} = n_{i,0} \pm 1$ and $n'_{i,\pm1} = \text{Round}\left[\frac{n_{j,\pm1}k_j - \omega_m}{k_i}\right]$ with $j \neq i$, thus we replace $n_{i,0}$ with $n_{i,\pm1}$ to get higher order corrections, c.f. Fig. 3.16.

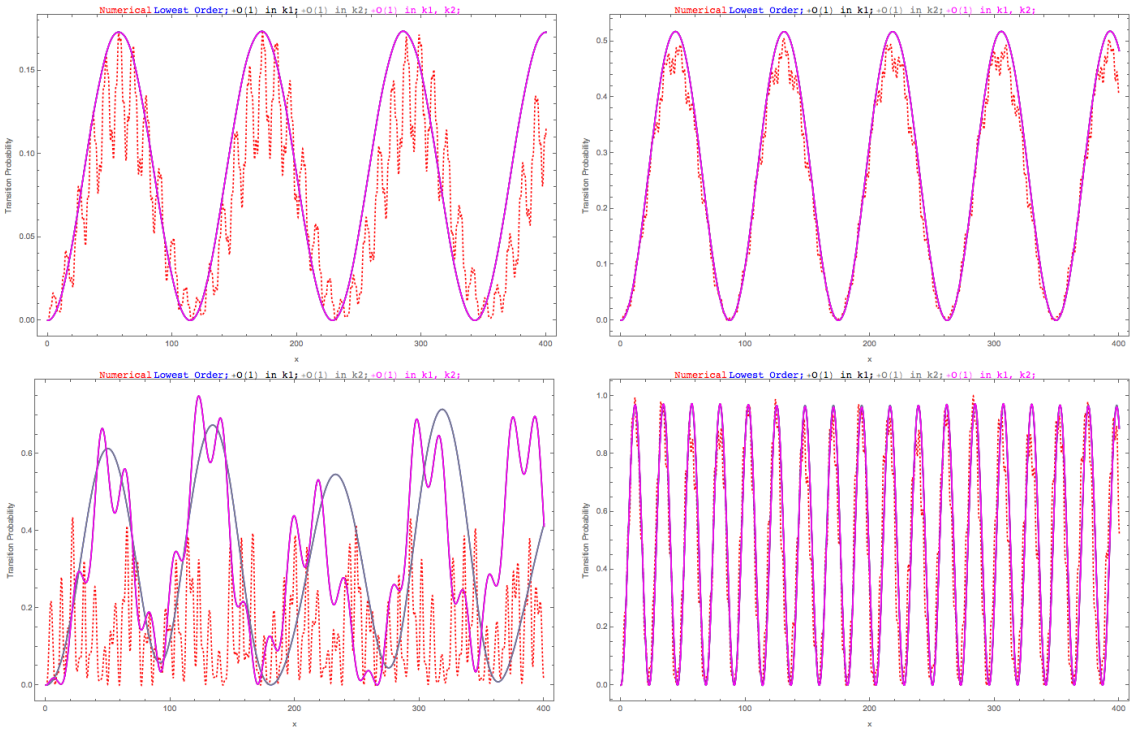

Figure 3.16: Top Left: Smaller wavenumber $k_1 = 0.95$ is at resonance and it has smaller perturbation amplitude ($k_2 = 1.55$); Top Right: Smaller wavenumber $k_1 = 0.95$ is at resonance and it has larger perturbation amplitude ($k_2 = 1.55$); Bottom Left: Larger wavenumber $k_2 = 0.95$ is at resonance and it has smaller perturbation amplitude ($k_1 = 0.35$); Bottom Right: Larger wavenumber $k_2 = 0.95$ is at resonance and it has larger perturbation amplitude ($k_1 = 0.35$). Red dotted line is numerical solution, black line is lowest approximation of k_2, magenta is higher order approximation of k_2.

In realistic physical systems, it is more likely to have a matter profile so that we have the bottom left situation. In other words, RWA method breaks down in the most interesting case.

- Another choice is to add or remove one for both n_1 and n_2 for both terms in

the Hamiltonian. The approach will define the order n_{order} first, as will be applied to the n's. As an example, adding first order to n_1 will include all the possible combinations of $n_1, n_1 \pm 1$ for both terms without changing n_2. As an example, we compare the different orders of n_1 only with the numerical calculation without approximations in Fig. 3.17.

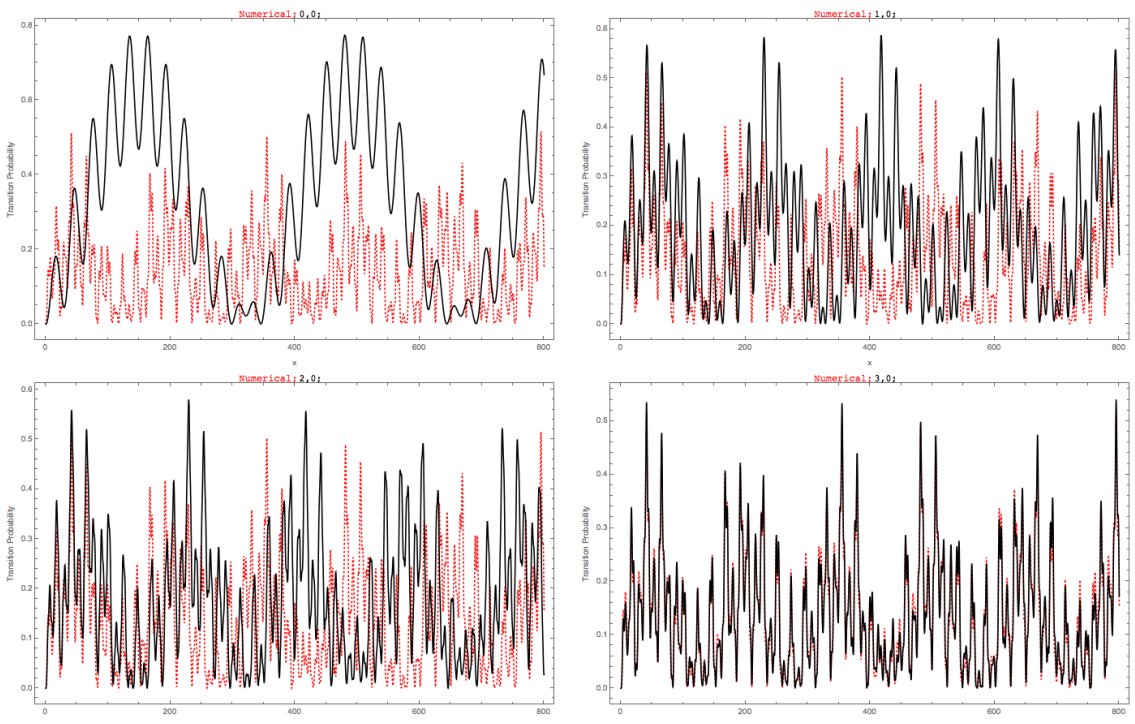

Figure 3.17: Compare the different orders with the numerical calculation without approximations, where red dotted line is the numerical calculation without approximation. As we could see from the figure, including up to third order in n_1 fixes the deviation from numerical calculation (red dotted line). The wave vectors are $k_1 = 0.5$, $k_2 = 0.8$, amplitudes are $A_1 = 0.1k_1^{-5/3}$, $A_2 = 0.1k_2^{-5/3}$, mixing angle in background matter is $\theta_{\rm m} = \pi/5$.

- Now according to the complete expression of the $_{12}$ element of Hamiltonian Eqn. 3.159, there is no difference between n_1 and n_2. Thus whenever we talk about different orders, we should not distinguish between the two integers. However, how to define zero order is not clear to me at this point. To find

out, we need to know the resonance width of each pair of integers. The insight comes from the single frequency result. The width for single frequency $\Gamma = \left|\frac{\hat{F}}{n_0}\right| = \left|\hat{k}\tan 2\theta_{\rm m}\frac{J_{n_0}(n_0\hat{A}\cos 2\theta_{\rm m}/\hat{k})}{n_0}\right|$. depends on the coefficient in front of the phase in the Hamiltonian and the integer. The task is to derive or guess the resonance width for each pair of integers n_1, n_2.

As for a more systematic treatment of the two-frequency case, we geometrize the problem. The 12 element can be written as

$$h = h_1 + h_2, \tag{3.157}$$

where

$$h_1 = \sum_{n_1=-\infty}^{\infty}\sum_{n_2=-\infty}^{\infty}\left(-(-i)^{n_1+n_2}\frac{\tan 2\theta_{\rm m}}{2}n_1k_1J_{n_1}(z_{k_1})J_{n_2}(z_{k_2})\right)e^{i(n_1\phi_1+n_2\phi_2)}e^{i(n_1k_1+n_2k_2-\omega_{\rm m})x},$$
$$h_2 = \sum_{n_1=-\infty}^{\infty}\sum_{n_2=-\infty}^{\infty}\left(-(-i)^{n_1+n_2}\frac{\tan 2\theta_{\rm m}}{2}n_2k_2J_{n_1}(z_{k_1})J_{n_2}(z_{k_2})\right)e^{i(n_1\phi_1+n_2\phi_2)}e^{i(n_1k_1+n_2k_2-\omega_{\rm m})x}.$$

For simplicity, we define

$$\begin{aligned}B_{n_1,n_2}(k_1,k_2,A_1,A_2) &= -(-i)^{n_1+n_2}\tan 2\theta_{\rm m}n_1k_1J_{n_1}(z_{k_1})J_{n_2}(z_{k_2})\\ &= -(-i)^{n_1+n_2}\tan 2\theta_{\rm m}n_1k_1J_{n_1}(\frac{A_1}{k_1}\cos 2\theta_{\rm m})J_{n_2}(\frac{A_2}{k_2}\cos 2\theta_{\rm m}),\\ \Phi &= e^{i(n_1\phi_1+n_2\phi_2)}.\end{aligned}$$

Notice that

$$B_{n_2,n_1}(k_2,k_1,A_2,A_1) = -(-i)^{n_1+n_2}\tan 2\theta_{\rm m}n_2k_2J_{n_1}(\frac{A_1}{k_1}\cos 2\theta_{\rm m})J_{n_2}(\frac{A_2}{k_2}\cos 2\theta_{\rm m}).$$

Using these definitions, we rewrite the Hamiltonian 12 element

$$\begin{aligned} h =& h_1 + h_2 \qquad (3.158)\\ =& \frac{1}{2}\sum_{n_1=-\infty}^{\infty}\sum_{n_2=-\infty}^{\infty} B_{n_1,n_2}(k_1,k_2,A_1,A_2)\Phi e^{i(n_1k_1+n_2k_2-\omega_{\rm m})x} \\ &+ \frac{1}{2}\sum_{n_1=-\infty}^{\infty}\sum_{n_2=-\infty}^{\infty} B_{n_2,n_1}(k_2,k_1,A_2,A_1)\Phi e^{i(n_1k_1+n_2k_2-\omega_{\rm m})x} \\ =& \frac{1}{2}\sum_{n_1=-\infty}^{\infty}\sum_{n_2=-\infty}^{\infty} \left(B_{n_1,n_2}(k_1,k_2,A_1,A_2) + B_{n_2,n_1}(k_2,k_1,A_2,A_1)\right)\Phi e^{i(n_1k_1+n_2k_2-\omega_{\rm m})x} \\ =& \frac{1}{2}\sum_{n_1=-\infty}^{\infty}\sum_{n_2=-\infty}^{\infty} B_2 n_1,n_2(k_1,k_2,A_1,A_2)\Phi e^{i(n_1k_1+n_2k_2-\omega_{\rm m})x}, \qquad (3.159) \end{aligned}$$

where $B_2 n_1, n_2(k_1,k_2,A_1,A_2) \equiv B_{n_1,n_2}(k_1,k_2,A_1,A_2) + B_{n_2,n_1}(k_2,k_1,A_2,A_1)$ is what we are interested in.

Comparing this expression with the single frequency one which is almost the same structure if we remove the two sums, and using the result 3.88, we can infer that the transition probability,

$$P_{1\to 2}(x) = \frac{|\hat{B}_2|^2}{|\hat{B}_2|^2 + \hat{g}_2^2}\sin^2\left(\frac{q_2}{2}x\right), \qquad (3.160)$$

where $\hat{B}_2 = \frac{B_2}{\omega_{\rm m}} = \frac{B_{n_1,n_2}(k_1,k_2,A_1,A_2)+B_{n_2,n_1}(k_2,k_1,A_2,A_1)}{\omega_{\rm m}}$ and $\hat{g}_2 = \frac{g}{\omega_{\rm m}} = n_1\hat{k}_1 + n_2\hat{k}_2 - 1$ which tells us how far from resonance and $q_2 = \sqrt{|\hat{B}_2|^2 + \hat{g}^2}$.

The width then is similar to 3.111, except that we could not define the width as a function of single variables since two wave vector are used. However, it is still reasonable to give the FWHM condition,

$$n_1\hat{k}_1 + n_2\hat{k}_2 - 1 = \pm|\hat{B}_2| = \left|\frac{B_{n_1,n_2}(k_1,k_2,A_1,A_2) + B_{n_2,n_1}(k_2,k_1,A_2,A_1)}{\omega_{\rm m}}\right|. \qquad (3.161)$$

For a given pair of integers n_1, n_2, we could find the amplitude as a function of k_1, k_2.

A solution shows that this is correct. The solution to the second element of wave

function is

$$\psi_{b2} = i\frac{|\hat{B}_2|^2 e^{-\frac{i}{2}\hat{g}_2\hat{x}}}{\hat{B}_2\sqrt{|\hat{B}_2|^2+\hat{g}^2}}\sin\left(\frac{\sqrt{|\hat{B}_2|^2+\hat{g}^2}}{2}x\right). \tag{3.162}$$

It is very confusing when we write down the requirement for width 3.161, since we need to assume $|\hat{F}_2|$ to be almost constant to arrive this result. What values of $\hat{k}_1, \hat{k}_2$ do we need to calculate $|\hat{F}_2|$? The idea is to find the FWHM (Full Width Half Maximum) when a point is deviating from the line. To be specific, we find the line that is the resonance using $n_1k_1 + n_2k_2 = 1$, which is plotted as dashed red line in 3.18. To characterize the distance, we need a line that is perpendicular to this red dashed resonance line, which also is passing through the values of $(k_10, k_2) = (k_{10}, k_{20})$ which is given in the system. Under this scheme, the resonance width is define as the distance from the resonance line when the amplitude reduces to half on this blue dotted perpendicular line.

In the language of algebra, we could derive the interception point of the two lines, which is

$$k_{1,\text{intercept}} = \frac{n_2^2k_{10} + n_2k_{20} + n_1}{n_1^2+n_2^2}, \tag{3.163}$$

$$k_{2,\text{intercept}} = \frac{n_1}{n_2}k_{1,\text{intercept}} - \frac{1}{n_2}, \tag{3.164}$$

where k_{10} and k_{20} are the values given in the matter perturbation of the system.

Using this method, we can define a reasonable width for two frequency matter perturbation case,

$$\Gamma_2 = \frac{B_2(k_{1,\text{intercept}}, k_{2,\text{intercept}})}{\sqrt{n_1^2+n_2^2}}. \tag{3.165}$$

To apply the width in a problem, we need to calculate the distance between the given point (k_{10}, k_{20}) of the system to a certain resonance line which depends on $n_1, n_2, A_1, A_2, \theta_\text{m}$. This is as simple as point to line distance, which is calculated

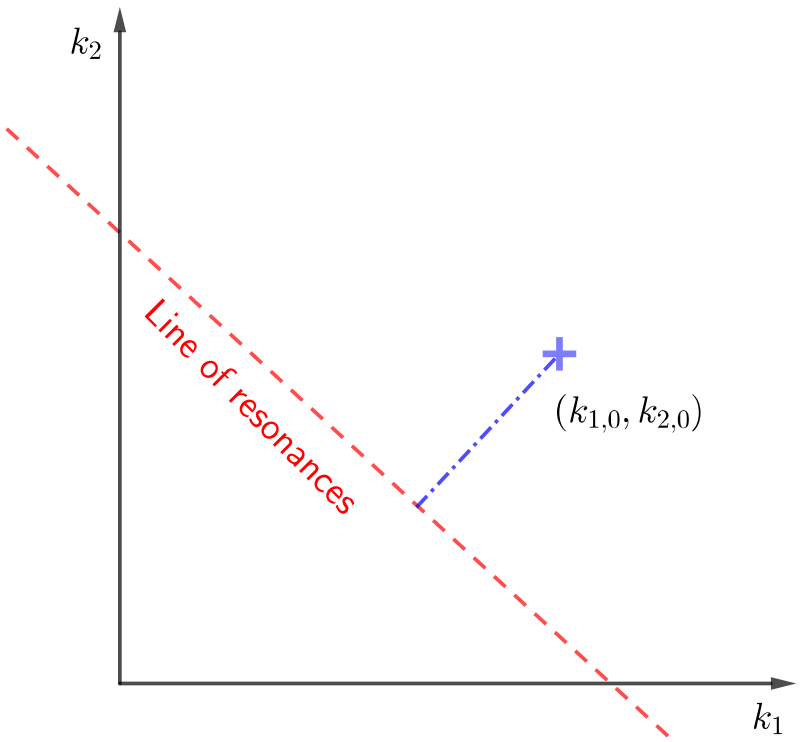

Figure 3.18: Diagram of Width for two frequencies in matter density profile. The red dashed line is the line when the resonances happen. The cross is the location for a system that with two frequencies in density profile, $k_{1,0}$ and $k_{2,0}$. The blue dash dotted line indicates the distance between the actual frequencies of the system and the resonances.

using

$$d = \frac{|n_1 k_{10} + n_2 k_{20} - 1|}{\sqrt{n_1^2 + n_2^2}}. \tag{3.166}$$

The requirement for a pair of (n_1, n_2) to be important is determined by defining a quantity that compares the distance from a certain resonance line with the width of this resonance line,

$$Q_2 = \frac{d}{\Gamma_2}. \tag{3.167}$$

3.8 Conclusions

The solar neutrinos behave very differently from lab experiments since the Sun provides a high matter density lab which can not be built on the Earth. What's even more exotic, in a supernova explosion, 10^{58} neutrinos are released from the proto-neutron star, which is of radius 10km, in a few seconds. The huge number density of neutrinos and large density of matter both change the neutrino oscillations dramatically. The matter effect in supernova is also much more complicated than MSW for solar neutrinos since the rich distribution of matter density and high speed motion. In addition to matter effect, neutrino neutrino interaction will be very efficient because of the high neutrino number density.

Apart from the emission of neutrinos from nuclear reactions of electron capture and positron emission in the solar interior, supernova environment also gives rise to Bremsstrahlung pair neutrino production, electron-positron neutrino pair production, which brings all three flavors and also anti-neutrinos into the spectra. However, even the with the presence of intensive interaction between neutrinos and the leptons and hardrons, which thermalize the neutrinos in the supernova core, the neutrino spectrum escaping from the supernova core is not completely Fermi-Dirac distribution. Nonetheless, it is possible to parametrize it using nominal Fermi-Dirac distribution,[19]

$$f(E) \propto \frac{E^2}{1+\exp(E/kT-\mu)}. \tag{3.168}$$

Some numerical results show that there is a deviation from this Fermi-Dirac distribution [13, 18]. Meanwhile, Keil Mathias and Georg Raffelt showed that it is good enough to approximate the neutrino spectrum from supernova in Monte Carlo simulations using the so called "alpha fit",

$$f(E) \propto E^{\alpha} \exp\left(-(\alpha+1)\frac{E}{\langle E\rangle}\right), \tag{3.169}$$

where $\langle E\rangle$ is the average energy, or the first moment of energy. The values from

Monte Carlo simulations falls into the range $\alpha = 2.5 \sim 5$, which clearly shows the spectra are pinched. It's a hint that the detection of deviation from nominal Fermi-Dirac distribution will show evidence of core-collapse information.

Even though we understand solar neutrinos well, the neutrino oscillations of supernova explosions are not so to our complete knowledge. The flavor content is subject to the solution to the neutrino oscillations. Phenomena such as spectral split due to neutrino-neutrino interaction and matter effect reshape the neutrino spectra significantly. That being said, more research on supernova neutrinos, especially supernova neutrino oscillations is critical to understand supernova explosion mechanisms, as well as future observation of supernova neutrino data.

In conclusion, we have provided an interpretation for neutrino flavor conversion in fluctuating matter with the help of Rabi oscillations. The work provided two different points of view that is related to Rabi oscillations.

The first point of view was to interpret the neutrino flavor conversions in background matter basis. In this basis, matter density fluctuations will introduced a fluctuation part to the diagonal elements of the Hamiltonian, which means that the energy gap is fluctuating if we draw analogy between this Hamiltonian and the Hamiltonian of Rabi oscillations. For neutrino flavor conversions in a single frequency matter profile, the neutrino flavor oscillations becomes large when the matter fluctuation frequency is close to the energy gap, which is the resonance condition. We anticipated that the fluctuations of energy gap have limited effects on neutrino flavor conversions under this resonance condition. Thus the matter fluctuation only works as a pure flipping field that converts neutrinos from one flavor to another.

As we added more frequencies of matter density fluctuations, the neutrino flavor conversions becomes nontrivial due to the interferences between the difference matter profile frequencies. To quantify the interference between different Rabi oscil-

lation modes, we defined relative detuning which describes how off-resonance a Rabi oscillation is. In the case of single frequency Rabi oscillations, the relative detuning becomes 0 under the resonance condition. As a second frequency is added to the oscillations, the energy gap is shifted due to this new frequency. A measure of the interference effect is to consider the relative detuning of the first frequency which is at resonance, under the shifted energy gap. Numerical results verified this conjecture. With the interference mechanism, we revisit the single frequency matter profile neutrino oscillations.

Another view is to switch to a basis where the neutrino oscillations Hamiltonian is decomposed into infinite Rabi oscillations. Equivalently speaking, the oscillations are consequences of superposition of Rabi oscillations, which we call modes of oscillations. This view was applied to emphasis the approximations that the change of energy gap due to matter fluctuation can be neglected under resonance condition in the previous background matter basis.

Chapter 4

Conclusion

We conclude that neutrinos oscillate.

Appendices

Appendix A

Conventions

A.1 Notations

- Variables with sans-serif fonts are matrices.
- Variables in bold are vectors in space-time.
- Variables with arrows are vectors in flavor-isospin space.

A.2 Terms

- Normal hierarchy for two-flavor scenario is always defined as $m_2^2 - m_1^2 > 0$, i.e., $\omega_{\rm v} > 0$.
- Inverted hierarchy for two-flavor scenario is defined as $m_2^2 - m_1^2 < 0$, i.e., $\omega_{\rm v} < 0$.
- Solar neutrino mass splitting is δm_{12}, while atmospheric neutrino mass splitting refers to δm_{23}.

A.3 Units

Natural units system makes the calculations of neutrinos convenient. By definition, we set reduced Planck constant and speed of light to be 1, $\hbar = 1 = c$. The conversion between natural units and SI can be down by using the following relations,

$$1\text{GeV} = 5.08 \times 10^{15}\text{m}^{-1} \tag{A.1}$$

$$1\text{GeV} = 1.8 \times 10^{-27}\text{kg} \tag{A.2}$$

To convert between different physical quantities in this thesis, I always use the following tips.

- The energy-mass-momentum relations becomes $E^2 = p^2 + m^2c^2 = p^2 + m^2$. Thus mass m, momentum $\mathbf{p}$ and energy E have the same dimension.
- An example of angular momentum in quantum mechanics is $L_z = m\hbar = m$ where m is a quantum number. $\hbar$ is of dimension angular momentum.
- A plane wave in quantum mechanics is $\Psi = Ae^{\frac{Et-px}{\hbar}}$. $\frac{Et-px}{\hbar}$ should be dimensionless, which means px has dimension angular momentum, which is obvious, meanwhile we notice that Et also has the dimension of angular momentum. Previously we noticed momentum has the same dimension with energy, we should have time t with the same dimension of length x. Also we can conclude that length and time have the same dimension as $1/E$.

A.4 Pauli Matrices and Rotations

Given a rotation

$$U = \begin{pmatrix} \cos\theta & \sin\theta \\ -\sin\theta & \cos\theta \end{pmatrix}, \tag{A.3}$$

its effect on Pauli matrices are

$$U^\dagger \sigma_3 U = \cos 2\theta \sigma_3 + \sin 2\theta \sigma_1 \tag{A.4}$$

$$U^\dagger \sigma_1 U = -\sin 2\theta \sigma_3 + \cos 2\theta \sigma_1. \tag{A.5}$$

A.5 Lorentzian Distribution

Three-parameter Lorentzian function is

$$f_{x_0,\sigma,A}(x) = \frac{1}{\pi} \frac{\sigma}{\sigma^2 + (x - x_0)^2}, \tag{A.6}$$

which has a width 2γ.

A.6 Fourier Series

The convention for the Fourier series used in this thesis is

$$\lambda(x) = \sum_{n=-\infty}^{\infty} \Lambda_n \exp\left(\frac{i2\pi nx}{X}\right) = \sum_{n=-\infty}^{\infty} \Lambda_n \exp\left(i\omega_0 nx\right), \tag{A.7}$$

where $\omega_0 = \frac{2\pi}{X}$. The coefficients are evaluated using the orthogonal relation of exponential functions for $n \neq 0$,

$$\Lambda_n = \frac{1}{X} \int_0^X \lambda(x) e^{-i\omega_0 nx} dx \tag{A.8}$$

$$= \frac{1}{X} \left(\int_0^{X_1} \lambda_1 e^{-i\omega_0 nx} dx + \int_{X_1}^{X_1+X_2} \lambda_2 e^{-i\omega_0 nx} dx \right) \tag{A.9}$$

$$= \frac{1}{X} \frac{X}{-i2\pi n} \left(\lambda_1 e^{-i\omega_0 nX_1} + \lambda_2 \left(e^{-i\omega_0 nX} - e^{-i\omega_0 nX_1} \right) \right) \tag{A.10}$$

$$= \frac{i}{2\pi n} \left(-\lambda_1 + (\lambda_1 - \lambda_2) e^{-i2\pi nX_1/X} + \lambda_2 e^{-i2\pi n} \right). \tag{A.11}$$

For $n = 0$, we have

$$\Lambda_0 = \frac{X_1\lambda_1 + X_2\lambda_2}{X}. \tag{A.12}$$

For functions with specific parity, the Fourier series is much more simpler. I'll list below the Fourier series for even functions, since no odd functions are used in this thesis. In general the Fourier series of a periodic function defined on $\left[-\frac{X}{2}, \frac{X}{2}\right]$ is

$$\lambda(x) = \frac{a_0}{2} + \sum_{n=1}^{\infty} a_n \cos(n2\pi x/X) + \sum_{n=1}^{\infty} b_n \sin(n2\pi x/X), \tag{A.13}$$

where

$$a_0 = \frac{2}{X}\int_{-X/2}^{X/2} \lambda(x)dx \tag{A.14}$$

$$a_n = \frac{2}{X}\int_{-X/2}^{X/2} \lambda(x)\cos(n2\pi x/X)dx \tag{A.15}$$

$$b_n = \frac{2}{X}\int_{-X/2}^{X/2} \lambda(x)\sin(n2\pi x/X)dx. \tag{A.16}$$

For even function $\lambda(x)$, we have

$$\lambda(x) = \frac{1}{2}a_0 + \sum_{n=1}^{\infty} a_n \cos(n2\pi x/X). \tag{A.17}$$

We shift the castle wall profile and make it always even, as shown in Fig. A.1, so that

$$\lambda(x) = \begin{cases} \lambda_2, & -\frac{X_2}{2} - \frac{X_1}{2} \le x \le -\frac{X_1}{2} \\ \lambda_1, & -\frac{X_1}{2} \le x \le \frac{X_1}{2} \\ \lambda_2, & \frac{X_1}{2} \le x \le \frac{X_1}{2} + \frac{X_2}{2} \end{cases} \tag{A.18}$$

Fourier series of the profile is

$$\lambda(x) = \frac{1}{2}\Lambda_0 + \sum_{q=1}^{\infty} \Lambda_q \cos\left(\frac{2\pi q x}{X}\right) = \frac{1}{2}\Lambda_0 + \sum_{q=1}^{\infty} \Lambda_q \cos\left(\omega_0 q x\right), \tag{A.19}$$

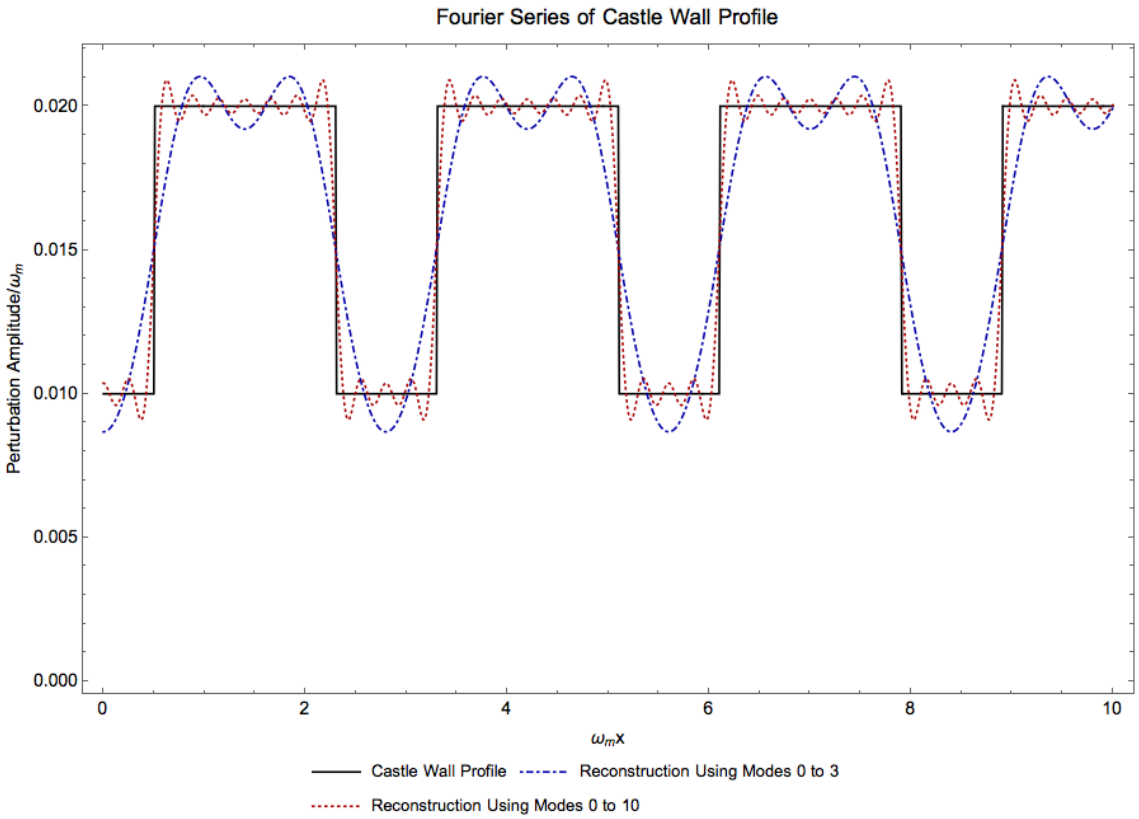

Figure A.1: Approaching an even function with Fourier series. The blue dash dotted line is the reconstruction of castle wall profile using 0 to 3 Fourier modes. The red dotted line is the reconstruction using 0 to 10 Fourier modes.

where

$$\Lambda_0 = \frac{2}{X}\int_{-X/2}^{X/2}\lambda(x)dx \tag{A.20}$$

$$= \frac{2}{X}\left(\lambda_2 X_2 + \lambda_1 X_1\right) \tag{A.21}$$

$$\Lambda_q = \frac{2}{X}\int_{-X/2}^{X/2}\lambda(x)\cos(n2\pi x/X)dx \tag{A.22}$$

$$= \frac{2}{X}\left(\lambda_2\int_{-X/2}^{-X_1/2}\cos(n2\pi x/X)dx + \lambda_1\int_{-X_1/2}^{X_1/2}\cos(n2\pi x/X)dx\right. \tag{A.23}$$

$$\left. + \lambda_2\int_{X_1/2}^{X/2}\cos(n2\pi x/X)dx\right) \tag{A.24}$$

$$= \frac{2}{q\pi}\left(\lambda_2\left(\sin(q\omega_0 X/2) - \sin(q\omega_0 X_1/2)\right) + \lambda_1\sin(q\omega_0 X_1/2)\right) \tag{A.25}$$

$$= \frac{2}{q\pi}\left(\lambda_2\left(\sin(q\pi) - \sin(q\pi X_1/X)\right) + \lambda_1\sin(q\pi X_1/X)\right) \tag{A.26}$$

A.7 Jacobi-Anger expansion

One of the forms of Jacobi-Anger expansion is

$$e^{iz\cos(\Phi)} = \sum_{n=-\infty}^{\infty} i^n J_n(z) e^{in\Phi}. \tag{A.27}$$

A.8 Bessel Functions

A special relation of Bessel function is that

$$J_n(n\mathrm{sech}\,\alpha) \sim \frac{e^{n(\tanh\alpha-\alpha)}}{\sqrt{2\pi n\tanh\alpha}} \tag{A.28}$$

for large n [25]. As a matter of fact, for all positive α, we always have $\tanh\alpha-\alpha<0$.

Using this relation and defining $\mathrm{sech}\,\alpha = A\cos 2\theta_m$, which renders

$$\alpha = 2n\pi i + \ln\left(\frac{1\pm\sqrt{-A^2\cos^2 2\theta_m+1}}{A\cos 2\theta_m}\right), \qquad n\in\text{Integers}, \tag{A.29}$$

where the Mathematica code to solve it is shown below,

```
In[1]:= Solve[Exp[z] + Exp[-z]
== 2/(A Cos[2 Subscript[\[Theta], m]]), z] // FullSimplify
```

we find out an more human readable analytical expression for the width

$$\Gamma = \left|2\hat{k}\tan 2\theta_m \frac{e^{n(\tanh\alpha-\alpha)}}{n_0\sqrt{2\pi n_0\tanh\alpha}}\right| \tag{A.30}$$

where α is solved out in A.29. For small α, we have expansions for exponential functions and hyperbolic functions $\tanh\alpha\sim\alpha-\frac{\alpha^3}{3}$,

$$\Gamma \asymp 2\tan 2\theta_m \frac{e^{n\alpha^3/3}}{\sqrt{2\pi\alpha}n_0^{3/2}}. \tag{A.31}$$

However, it doesn't really help that much since n is large and no expansion could be done except for significantly small α.

A.9 Conversions in Neutrino Physics

Using natural units, length = time = 1/energy, we could rescale almost all quantities in neutrino oscillations using energy, or whatever characteristic scale we have.

We use two flavor vacuum oscillations between the two masses m_1 and m_2 as an example. The characteristic energy scale is the oscillation frequency $\omega_{v,21}$. The equation of motion

$$i\frac{d}{dx}\Psi = \frac{\omega_v}{2}(-\cos 2\theta_v \boldsymbol{\sigma_3} + \sin 2\theta_v \boldsymbol{\sigma_1})\Psi, \tag{A.32}$$

can be rescaled using the characteristic energy scale $\omega_{v,21}$

$$i\frac{d}{d\hat{x}}\Psi = \frac{1}{2}(-\cos 2\theta_v \boldsymbol{\sigma_3} + \sin 2\theta_v \boldsymbol{\sigma_1})\Psi, \tag{A.33}$$

where $\hat{x} = \omega_{v,21}x$. It is convenient for numerical calculations to convert quantities into dimensionless ones.

However, we usually discuss oscillation length in SI units for a grip of the picture. To convert from natural units to SI units, we write down the conversion here. The oscillation angular frequency is given by

$$\begin{aligned}\omega_{v,21} &= \frac{\delta m^2}{2E} \\ &= \left(\frac{7.5\times 10^{-5}\mathrm{eV}^2}{2\times 1\mathrm{MeV}}\right)\left(\frac{\delta m^2}{7.5\times 10^{-5}\mathrm{eV}^2}\right)\frac{1\mathrm{MeV}}{E} \\ &= 3.75\times 10^{-11}\mathrm{eV}\left(\frac{\delta m^2}{7.5\times 10^{-5}\mathrm{eV}^2}\right)\left(\frac{1\mathrm{MeV}}{E}\right).\end{aligned} \tag{A.34}$$

On the other hand, electro-volt is related to length through the useful formula

$$197\mathrm{MeV}\cdot\mathrm{fm} = \hbar c = 1. \tag{A.35}$$

Thus we have the oscillation angular frequency written as

$$\begin{aligned}\omega_{v,21} &= 3.75\times10^{-11}\text{eV}\frac{\delta m^2}{7.5\times10^{-5}\text{eV}^2}\frac{1\text{MeV}}{E}\\ &= 3.75\times10^{-17}\text{MeV}\frac{\delta m^2}{7.5\times10^{-5}\text{eV}^2}\frac{1\text{MeV}}{E}\\ &= 1.90\times10^{-4}\text{m}^{-1}\frac{\delta m^2}{7.5\times10^{-5}\text{eV}^2}\frac{1\text{MeV}}{E}.\end{aligned} \tag{A.36}$$

Similarly for $\delta m_{32} = 2.4\times10^{-3}\text{eV}^2$ the frequency is

$$\omega_{v,32} = \frac{\delta m_{32}^2}{2E} = 6.3\times10^{-3}\text{m}^{-1}\frac{\delta m_{32}^2}{2.5\times10^{-3}\text{eV}^2}\frac{1MeV}{E}. \tag{A.37}$$

With the results for angular frequencies, the rescaled length $\hat{x}$ is restored using

$$x = \frac{\hat{x}}{\omega_v} = \frac{\hat{x}}{1.90\times10^{-4}\text{m}^{-1}\frac{\delta m^2}{7.5\times10^{-5}\text{eV}^2}\frac{1\text{MeV}}{E}} \tag{A.38}$$

$$= \frac{\hat{x}}{0.190}\text{km}\frac{7.5\times10^{-5}\text{eV}^2}{\delta m^2}\frac{E}{1\text{MeV}}. \tag{A.39}$$

Another important example is the 2 flavor neutrino oscillations in constant matter background potential $\lambda_c = \sqrt{2}G_\text{F}n_e$. The characteristic energy scale is ω_m which is calculated using

$$\omega_m = \omega_v\sqrt{\frac{\lambda_c}{\omega_v}^2 + 1 - 2\frac{\lambda_c}{\omega_v}\cos 2\theta_v}. \tag{A.40}$$

Meanwhile, the effective mixing angle θ_m is determined by

$$\tan 2\theta_m = \frac{\sin 2\theta_v}{\cos 2\theta_v - \frac{\lambda}{\omega_v}}. \tag{A.41}$$

Similar to vacuum equation of motion, we rescale the equation of motion in constant background using ω_m

$$i\frac{d}{d\hat{x}}\Psi = \frac{1}{2}(-\cos 2\theta_m\boldsymbol{\sigma_3} + \sin 2\theta_m\boldsymbol{\sigma_1})\Psi, \tag{A.42}$$

we find out the scaled distance

$$\hat{x} = \omega_m x. \tag{A.43}$$

To reverse the process and find out the actual SI unit distance after the numerical calculation, we use

$$x = \frac{\hat{x}}{\omega_m}. \tag{A.44}$$

The procedure will be the following.

- Calculate ω_v using Eq. A.36.
- Calculate $\hat{\lambda}_c = \frac{\lambda_c}{\omega_v}$.
- Calculate ω_m using Eq. A.40.
- Find out the actual distance using Eq. A.44.

Appendix B

Rabi Oscillations

In this appendix we introduce flavor isospin [21] to Rabi oscillations and derive the transition probabilities as well as explain the resonance and width briefly.

A Rabi oscillation system is shown in Fig. B.1. The Hamiltonian for Rabi oscillation is

$$H_{\rm R} = -\frac{\omega_{\rm R}}{2}\sigma_3 - \frac{A_{\rm R}}{2}\left(\cos(k_{\rm R}t+\phi_{\rm R})\sigma_1 - \sin(k_{\rm R}t+\phi_{\rm R})\sigma_2\right), \tag{B.1}$$

in which $\omega_{\rm R}$ serves as the energy split of the two level system, while $A_{\rm R}$ and $k_{\rm R}$ are the strength and frequency of the driving field, respectively. A decomposition of the second term shows that

$$H_{\rm R} = -\frac{\boldsymbol{\sigma}}{2}\cdot(\mathbf{H}_3+\mathbf{H}_+),$$

where $\boldsymbol{\sigma}$ is the the vector of Pauli matrices, and the three vectors are

$$\mathbf{H}_3 = \begin{pmatrix} 0 \\ 0 \\ \omega_{\mathrm{R}} \end{pmatrix}, \tag{B.2}$$

$$\mathbf{H}_+ = \begin{pmatrix} A_{\mathrm{R}} \cos(k_{\mathrm{R}} t + \phi_{\mathrm{R}}) \\ -A_{\mathrm{R}} \sin(k_{\mathrm{R}} t + \phi_{\mathrm{R}}) \\ 0 \end{pmatrix}. \tag{B.3}$$

Figure B.1: Schematic illustration of Rabi oscillations system. The two level system has two energy states at $E_1 = -\frac{\omega_0}{2}$ and $E_2 = \frac{\omega_0}{2}$, which indicating an energy gap of ω_0. Incoming light has frequency ω. Resonance happens when $\omega \sim \omega_0$.

The three vectors are mapped onto a Cartesian coordinate system, so that $\mathbf{H}_3$ is the vector aligned with the third axis, $\mathbf{H}_+$ is a rotating vectors in a plane perpendicular to $\mathbf{H}_3$. The wave function $\Psi = (\psi_1, \psi_2)^{\mathrm{T}}$ is also used to define the state vector $\mathbf{s}$

$$\mathbf{s} = \Psi^\dagger \frac{\boldsymbol{\sigma}}{2} \Psi \tag{B.4}$$

$$= \frac{1}{2} \begin{pmatrix} 2\,\mathrm{Re}\,(\psi_1^* \psi_2) \\ 2\,\mathrm{Im}\,(\psi_1^* \psi_2) \\ |\psi_1|^2 - |\psi_2|^2 \end{pmatrix} \tag{B.5}$$

The third component of $\mathbf{s}$, which is denoted as s_3, is within range $[-1/2, 1/2]$. The two limits, $s_3 = -1/2$ and $s_3 = 1/2$ stand for the system in high energy state and

low energy state respectively. $s_3 = 0$ if the system has equal probabilities to be on high energy state and low energy state. The Schrödinger equation becomes

$$\frac{\mathrm{d}}{\mathrm{d}t}\mathbf{s} = \mathbf{s} \times \mathbf{H}, \tag{B.6}$$

which is the precession equation. For static $\mathbf{H}$, the state vector $\mathbf{s}$ precess around $\mathbf{H}$.

In a frame that corotates with $\mathbf{H}_+$, which is described in Fig. B.2, the new Hamiltonian is

$$\frac{\mathrm{d}}{\mathrm{d}t}\mathbf{s} = \mathbf{s} \times (\mathbf{H}'_3 + \mathbf{H}_+), \tag{B.7}$$

where

$$\mathbf{H}'_3 = \begin{pmatrix} 0 \\ 0 \\ \omega_\mathrm{R} - k_\mathrm{R} \end{pmatrix}, \qquad \mathbf{H}'_+ = \begin{pmatrix} A_\mathrm{R} \\ 0 \\ 0 \end{pmatrix}. \tag{B.8}$$

The state vector $\mathbf{s}$ precess around a static vector $\mathbf{H}'_3 + \mathbf{H}'_+$ with a frequency $\Omega_\mathrm{R} = \sqrt{|A_\mathrm{R}|^2 + (k_\mathrm{R} - \omega_\mathrm{R})^2}$. A geometric analysis by projecting the state vector $\mathbf{s}$ on to the vertical axis shows that

$$s_3 = \frac{1}{2} - \frac{|A_\mathrm{R}|^2}{\Omega_\mathrm{R}^2} \sin^2\left(\frac{\Omega_\mathrm{R}}{2}t\right). \tag{B.9}$$

Resonance occurs when the term $\mathbf{H}_3$ disappears in this corotating frame, since the state vector $\mathbf{s}$ converts completely between $+1/2$ (low energy state) and $-1/2$ (high energy state).

Such a system has analytical transition probability from low energy state to high energy state

$$P(t) = \frac{1}{2}(1 - 2s_3(t)) = \frac{|A_\mathrm{R}|^2}{\Omega_\mathrm{R}^2} \sin^2\left(\frac{\Omega_\mathrm{R}}{2}t\right), \tag{B.10}$$

where

$$\Omega_\mathrm{R} = \sqrt{|A_\mathrm{R}|^2 + (k_\mathrm{R} - \omega_\mathrm{R})^2} \tag{B.11}$$

is known as Rabi frequency. The detuning, which is defined by $k_\mathrm{R} - \omega_\mathrm{R}$, determines how off-resonance the system is, and amplitude of driving field A_R determines the

resonance width,

$$\text{Detuning} = |k_{\text{R}} - \omega_{\text{R}}|, \tag{B.12}$$

$$\text{Resonance Width} = |A_{\text{R}}|, \tag{B.13}$$

which is also shown in Fig. B.3 and Fig. B.4. The transition probability oscillates with frequency Ω_{R}. However, the amplitude A_1 is the dominate factor for oscillation frequency when the system is close to resonance. The phase of the matter potential ϕ_{R} has no effect on the transition probability since it only determines the initial phase of driving Hamiltonian vector $\mathbf{H}_+$. We also notice that the transition amplitude is determined by relative detuning D, which is defined as

$$D = \left| \frac{k_{\text{R}} - \omega_{\text{R}}}{A_{\text{R}}} \right|. \tag{B.14}$$

Given a Rabi oscillation system with two driving frequencies

$$\begin{aligned} H_{\text{R}} = &- \frac{\omega_{\text{R}}}{2}\sigma_3 - \frac{A_1}{2}\left(\cos(k_1 t + \phi_1)\sigma_1 - \sin(k_1 t + \phi_1)\sigma_2\right) \\ &- \frac{A_2}{2}\left(\cos(k_2 t + \phi_2)\sigma_1 - \sin(k_2 t + \phi_2)\sigma_2\right) \end{aligned}$$

we decompose it into $\mathbf{H}_{\text{R}} = \mathbf{H}_3 + \mathbf{H}_1 + \mathbf{H}_2$, where

$$\mathbf{H}_1 = \begin{pmatrix} A_1 \cos(k_1 t + \phi_1) \\ A_1 \sin(k_1 t + \phi_1) \\ 0 \end{pmatrix}, \mathbf{H}_2 = \begin{pmatrix} A_2 \cos(k_2 t + \phi_2) \\ A_2 \sin(k_2 t + \phi_2) \\ 0 \end{pmatrix}.$$

Assume $\mathbf{H}_1$ is the on-resonance perturbation which requires $k_1 = \omega_{\text{R}}$. The most general condition that we can drop the new perturbation $\mathbf{H}_2$ is to make sure k_2 is far from the resonance condition compared to the resonance width,

$$D \equiv \frac{|k_2 - \omega_{\text{R}}|}{|A_2|} \gg 1. \tag{B.15}$$

The transition amplitude between the two states becomes

$$P(t) = \frac{1}{1 + D^2} \sin^2(\frac{\Omega_{\text{R}}}{2} t). \tag{B.16}$$

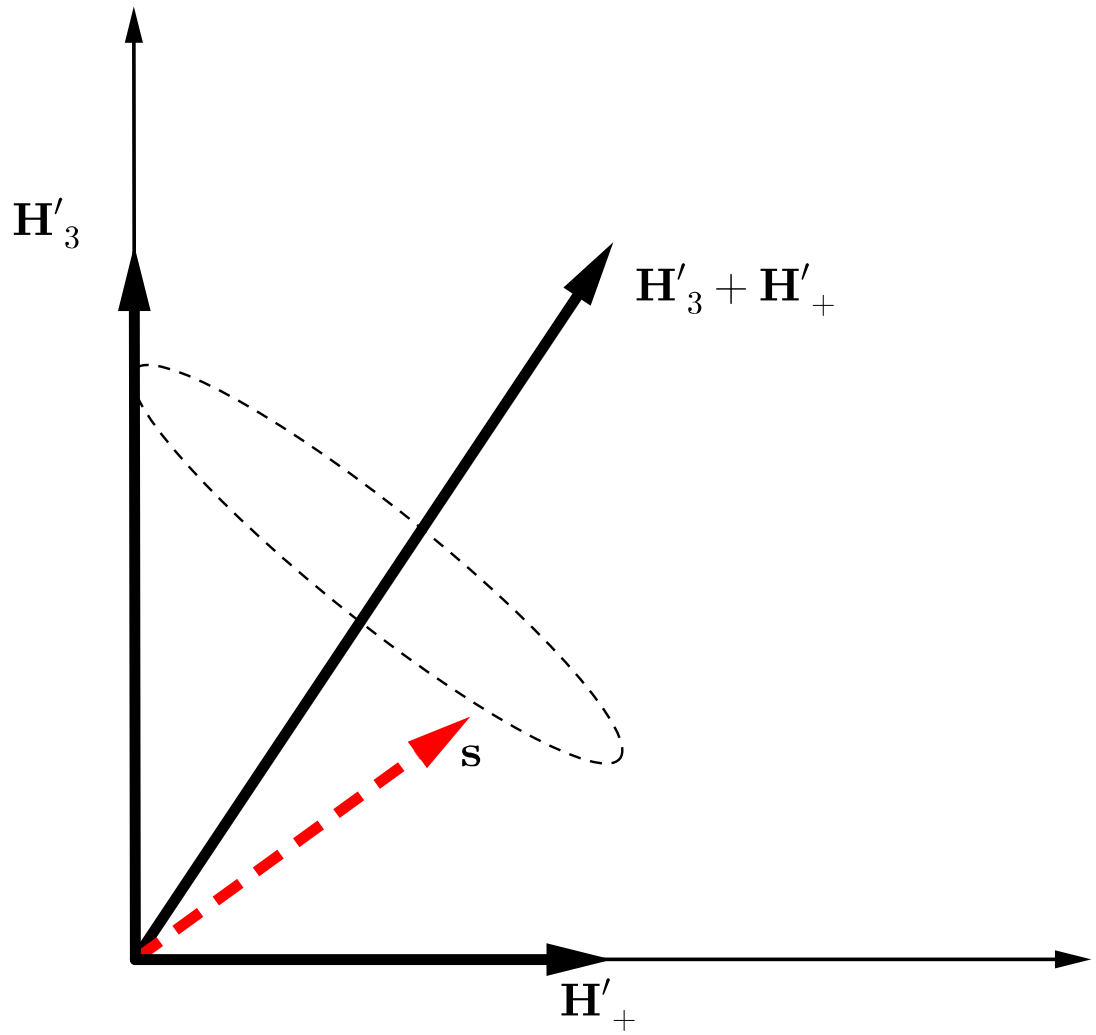

Figure B.2: Rabi oscillations in corotating frame. The red dashed vector is the flavor isospin, while the black solid vectors are the vectors of Hamiltonian. The flavor isospin vector is precessing around vector of total Hamiltonian $\mathbf{H}_3 + \mathbf{H}_+$.

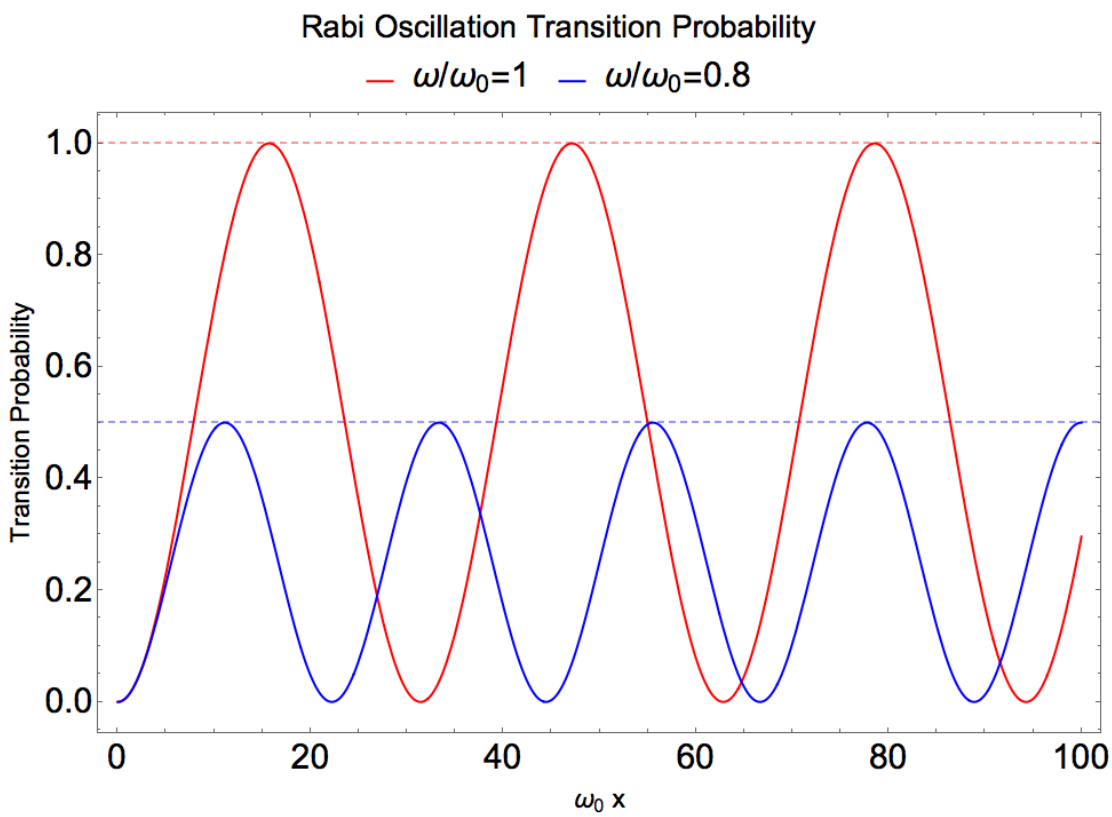

Figure B.3: Rabi oscillations for two different incoming light frequencies. $\omega/\omega_0 = 1$ is the resonance condition. As for $\omega/\omega_0 = 0.8$, the oscillation amplitude becomes 0.5.

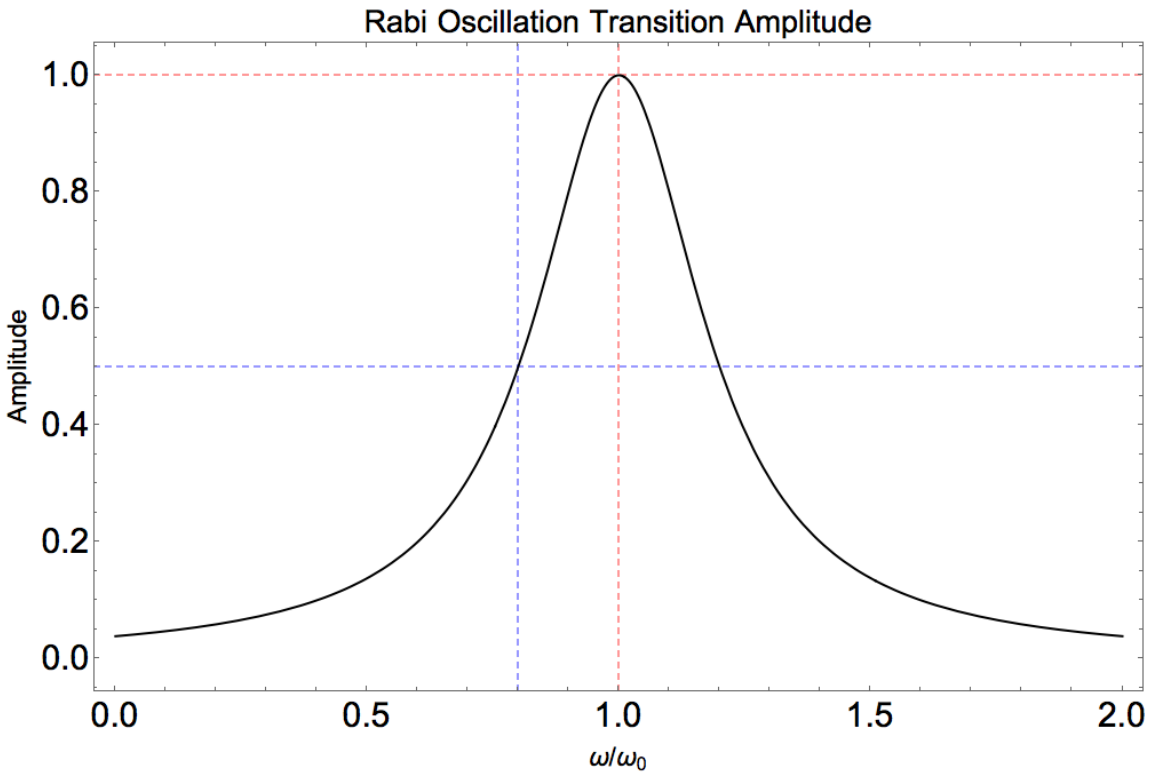

Figure B.4: Rabi oscillations for two different incoming light frequencies. $\omega/\omega_0 = 1$ is the resonance condition. The amplitude reach maximum when $\omega/\omega_0 = 1$. Resonance width is defined to be the width where amplitude becomes half of the maximum which is shown with blue dashed lines.

Appendix C

MSW Effect Revisited

C.1 Flavor Basis

In terms of formalism, vacuum oscillations is already a Rabi oscillation at resonance with oscillation width $\omega_v \sin 2\theta_v$. As derived, neutrino oscillations in matter are determined by Hamiltonian in flavor basis

$$H^{(f)} = \left(-\frac{1}{2}\omega_v \cos 2\theta_v + \frac{1}{2}\lambda(x)\right)\sigma_3 + \frac{1}{2}\omega_v \sin 2\theta_v \sigma_1, \tag{C.1}$$

with the Schröding equation

$$i\partial_x \Psi^{(f)} = H^{(f)}\Psi^{(f)}. \tag{C.2}$$

To make connections to Rabi oscillations, we would like to remove the changing σ_3 terms, using a transformation

$$U = \begin{pmatrix} e^{-i\eta(x)} & 0 \\ 0 & e^{i\eta(x)} \end{pmatrix}, \tag{C.3}$$

which transform the flavor basis to another basis

$$\begin{pmatrix} \psi_e \\ \psi_x \end{pmatrix} = \begin{pmatrix} e^{-i\eta(x)} & 0 \\ 0 & e^{i\eta(x)} \end{pmatrix} \begin{pmatrix} \psi_a \\ \psi_b \end{pmatrix}. \tag{C.4}$$

The Schrodinger equation can be written into this new basis

$$i\partial_x(T\Psi^{(r)}) = H^{(f)}T\Psi^{(r)}, \tag{C.5}$$

which is simplified to

$$i\partial_x\Psi^{(r)} = H^{(r)}\Psi^{(r)}, \tag{C.6}$$

where

$$H^{(r)} = -\frac{1}{2}\omega_v \cos 2\theta_v\sigma_3 + \frac{1}{2}\omega_v \sin 2\theta_v \begin{pmatrix} 0 & e^{2i\eta(x)} \\ e^{-2i\eta(x)} & 0 \end{pmatrix}, \tag{C.7}$$

in which we remove the varying component of σ_3 elements using

$$\frac{d}{dx}\eta(x) = \frac{\lambda(x)}{2}. \tag{C.8}$$

The final Hamiltonian would have some form

$$H^{(r)} = -\frac{1}{2}\omega_v \cos 2\theta_v\sigma_3 + \frac{1}{2}\omega_v \sin 2\theta_v \begin{pmatrix} 0 & e^{i\int_0^x \lambda(\tau)d\tau + 2i\eta(0)} \\ e^{-i\int_0^x \lambda(\tau)d\tau - 2i\eta(0)} & 0 \end{pmatrix}, \tag{C.9}$$

where $\eta(0)$ is chosen to counter the constant terms from the integral.

For arbitrary matter profile, we could first apply Fourier expand the profile into trig function then use Jacobi-Anger expansion so that the system becomes a lot of Rabi oscillations. Any transformations or expansions that decompose $\exp\left(i\int_0^x \lambda(\tau)d\tau\right)$ into many summations of $\exp(iax + b)$ would be enough for an Rabi oscillation interpretation. As for constant matter profile, $\lambda(x) = \lambda_0$, we have

$$\eta(x) = \frac{1}{2}\lambda_0 x. \tag{C.10}$$

The Hamiltonian becomes

$$H^{(r)} = -\frac{1}{2}\omega_v \cos 2\theta_v\sigma_3 + \frac{1}{2}\omega_v \sin 2\theta_v \begin{pmatrix} 0 & e^{i\lambda_0 x} \\ e^{-i\lambda_0 x} & 0 \end{pmatrix}, \tag{C.11}$$

which is exactly a Rabi oscillation. The resonance condition is

$$\lambda_0 = \omega_v \cos 2\theta_v. \tag{C.12}$$

C.2 Instantaneous Matter Basis

Neutrino oscillations can be calculated in instantaneous matter basis, where the Schrödinger equation is transformed to instantaneous matter basis by applying a rotation U,

$$i\partial_x \left(U\Psi^{(m)}\right) = H^{(f)}U\Psi^{(m)}, \tag{C.13}$$

where

$$U = \begin{pmatrix} \cos\theta_m & \sin\theta_m \\ -\sin\theta_m & \cos\theta_m \end{pmatrix}. \tag{C.14}$$

With some simple algebra, we can write the system into

$$i\partial_x \Psi^{(m)} = H^{(m)}\Psi^{(m)}, \tag{C.15}$$

where

$$H^{(m)} = U^\dagger H^{(f)} U - iU^\dagger \partial_x U. \tag{C.16}$$

By setting the off-diagonal elements of the first term $U^\dagger H^{(f)} U$ to zero, we can derive the relation

$$\tan 2\theta_m = \frac{\sin 2\theta_v}{\cos 2\theta_v - \lambda/\omega_v}. \tag{C.17}$$

Furthermore, we derive the term

$$iU^\dagger \partial_x U = -\dot{\theta}_m \sigma_2. \tag{C.18}$$

We can calculate $\dot{\theta}_m$ by taking the derivative of $\tan 2\theta_m$,

$$\frac{d}{dx}\tan 2\theta_m = \frac{2}{\cos^2 2\theta_m}\dot{\theta}_m, \tag{C.19}$$

so that

$$\dot{\theta}_m = \frac{1}{2}\cos^2(2\theta_m)\frac{d}{dx}\tan 2\theta_m \tag{C.20}$$

$$= \frac{1}{2}\frac{(\cos 2\theta_v - \lambda/\omega_v)^2}{(\lambda/\omega_v)^2 + 1 - 2\lambda\cos 2\theta_v/\omega_v}\frac{d}{dx}\frac{\sin 2\theta_v}{\cos 2\theta_v - \lambda/\omega_v} \tag{C.21}$$

$$= \frac{1}{2}\frac{(\cos 2\theta_v - \lambda/\omega_v)^2}{(\lambda/\omega_v)^2 + 1 - 2\lambda\cos 2\theta_v/\omega_v}\frac{\sin 2\theta_v}{(\cos 2\theta_v - \lambda/\omega_v)^2}\frac{1}{\omega)v}\frac{d}{dx}\lambda(x) \tag{C.22}$$

$$= \frac{1}{2}\sin 2\theta_m \frac{1}{\omega_m}\frac{d}{dx}\lambda(x). \tag{C.23}$$

C.3 Bipolar Model

The nature of this section is to provide the linear stability analysis of bipolar model. Bipolar model is a model of neutrino oscillations with the presence of neutrino and antineutrinos. It is also called bimodal oscillations [11], which means two frequencies in the context. An example of such instability happens in a system composed of equal amounts of neutrinos and antineutrinos.

Neutrino oscillations has a small amplitude inside a SN core (suppressed by matter effects) [4], which basically pins down the flavour transformation. As the neutrinos reaches a further distance, matter effect could drop out. Neutrino self-interaction becomes more important. S. Samuel considers a system of neutrinos and antineutrinos with only vacuum and neutrino self-interactions [11]. The neutrinos and antineutrino forms a bipolar vector in flavor isospin space. The flavor isospin of neutrinos and that of antineutrinos are coupled.

The equation of motion is

$$i\partial_t\rho = \left[-\frac{\omega_v}{2}\cos 2\theta\sigma_3 + \frac{\omega_v}{2}\sin 2\theta\sigma_1 - \mu\alpha\bar{\rho}, \rho\right]$$
$$i\partial_t\bar{\rho} = \left[\frac{\omega_v}{2}\cos 2\theta\sigma_3 - \frac{\omega_v}{2}\sin 2\theta\sigma_1 + \mu\rho, \bar{\rho}\right].$$

For the purpose of linear stability analysis, we assume that

$$\rho = \frac{1}{2}\begin{pmatrix} 1 & \epsilon \\ \epsilon^* & -1 \end{pmatrix}$$
$$\bar{\rho} = \frac{1}{2}\begin{pmatrix} 1 & \bar{\epsilon} \\ \bar{\epsilon}^* & -1 \end{pmatrix}.$$

Plug them into equation of motion and set $\theta = 0$, we have the linearized ones,

$$i\partial_t \begin{pmatrix} \epsilon \\ \bar{\epsilon} \end{pmatrix} = \frac{1}{2}\begin{pmatrix} -\alpha\mu - \omega_v & \alpha\mu \\ -\mu & \mu + \omega_v \end{pmatrix}\begin{pmatrix} \epsilon \\ \bar{\epsilon} \end{pmatrix}.$$

To have real eigenvalues, we require

$$(-1+\alpha)^2\mu^2 + 4(1+\alpha)\mu\omega_v + 4\omega_v^2 < 0,$$

which is reduced to

$$\frac{-2\omega_v(1+\alpha) - 4\sqrt{\alpha}|\omega_v|}{(1-\alpha)^2} < \mu < \frac{-2\omega_v(1+\alpha) + 4\sqrt{\alpha}|\omega_v|}{(1-\alpha)^2}.$$

It is simplified to

$$\sqrt{-2\omega_v}(1-\sqrt{\alpha})^2 < \mu < \sqrt{-2\omega_v}(1+\sqrt{\alpha})^2,$$

assuming normal hierarchy, i.e., $\omega_v > 0$. We immediately notice that this can not happen.

For inverted hierarchy, we have $\omega_v < 0$, so that

$$\sqrt{2|\omega_v|}(1+\sqrt{\alpha})^2 < \mu < \sqrt{2|\omega_v|}(1-\sqrt{\alpha})^2,$$

Within this region, neutrinos experience exponential growth.

For completeness, we also write down the formalism in flavor isospin picture.

$$i\partial_t \mathbf{s} = \mathbf{s} \times (\eta\mathbf{H}_v + \alpha\mu\bar{\mathbf{s}}) \tag{C.24}$$
$$i\partial_t \bar{\mathbf{s}} = \bar{\mathbf{s}} \times (\eta\mathbf{H}_v + \mu\mathbf{s}), \tag{C.25}$$

where η is the hierarchy, and α is the ratio of neutrino number density and antineutrino number density.

Glossary

$\nu_{e,\mu,\tau}$	Electron, muon, tao flavor neutrinos
IH	Inverted hierarchy
NH	Normal hierarchy
DUNE	Deep Underground Neutrino Experiment
AGN	Active Galactic Nuclei
CNO	Carbon-Nitrogen-Oxygen
RWA	Rotating Wave Approximation

Bibliography

[1] C L Cowan et al. "Detection of the Free Neutrino: a Confirmation." In: *Science (New York, N.Y.)* 124.3212 (July 1956), pp. 103–4.

[2] B Pontecorvo. "Neutrino experiments and the problem of conservation of leptonic charge". In: *Sov. Phys. JETP* 26.5 (1968), pp. 984–988.

[3] J.N. Bahcall. "The solar neutrino problem". In: *Nuclear Instruments and Methods* 110 (July 1973), pp. 381–384.

[4] L. Wolfenstein. "Neutrino oscillations in matter". In: *Physical Review D* 17.9 (May 1978), pp. 2369–2374.

[5] L. Wolfenstein. "Neutrino oscillations and stellar collapse". In: *Physical Review D* 20.10 (Nov. 1979), pp. 2634–2635.

[6] S. P. Mikheev and A. Yu. Smirnov. "Resonance Amplification of Oscillations in Matter and Spectroscopy of Solar Neutrinos". In: *Sov. J. Nucl. Phys.* 42 (1985). [Yad. Fiz.42,1441(1985)], pp. 913–917.

[7] P.I. Krastev and A.Yu. Smirnov. "Parametric effects in neutrino oscillations". In: *Physics Letters B* 226.3-4 (Aug. 1989), pp. 341–346.

[8] T. K. Kuo and James Pantaleone. "Neutrino oscillations in matter". In: *Reviews of Modern Physics* 61.4 (Oct. 1989), pp. 937–979.

[9] F. N. Loreti and A. B. Balantekin. "Neutrino oscillations in noisy media". In: *Physical Review D* 50.8 (Oct. 1994), pp. 4762–4770. arXiv: 9406003 [nucl-th].

[10] G. G. Raffelt. *Stars as laboratories for fundamental physics*. 1996. ISBN: 9780226702728.

[11] Stuart Samuel. "Bimodal coherence in dense self-interacting neutrino gases". In: *Physical Review D* 53.10 (May 1996), pp. 5382–5393. arXiv: 9604341 [hep-ph].

[12] S. T. Petcov. "Diffractive-like (or parametric-resonance-like?) enhancement of the Earth (day-night) effect for solar neutrinos crossing the Earth core". In: *Physics Letters B* 434.3-4 (Aug. 1998), pp. 321–332. arXiv: 9805262 [hep-ph].

[13] T. Totani et al. "Future Detection of Supernova Neutrino Burst and Explosion Mechanism". In: *The Astrophysical Journal* 496.1 (Mar. 1998), pp. 216–225.

[14] E.Kh. Akhmedov. "Parametric resonance of neutrino oscillations and passage of solar and atmospheric neutrinos through the earth". In: *Nuclear Physics B* 538.1-2 (Jan. 1999), pp. 25–51. arXiv: hep-ph/9805272 [hep-ph].

[15] E. Kh Akhmedov. "Parametric resonance in neutrino oscillations in matter". In: *Pramana* 54.1 (Jan. 2000), pp. 47–63. arXiv: 9907435 [hep-ph].

[16] Michael F Altmann, Rudolf L Mößbauer, and Lothar J N Oberauer. "Solar neutrinos". In: *Reports on Progress in Physics* 64.1 (Jan. 2001), pp. 97–146.

[17] S.T. Petcov and M. Piai. "The LMA MSW solution of the solar neutrino problem, inverted neutrino mass hierarchy and reactor neutrino experiments". In: *Physics Letters B* 533.1-2 (May 2002), pp. 94–106. arXiv: hep-ph/0112074 [hep-ph].

[18] Mathias Th. Keil. "Supernova Neutrino Spectra and Applications to Flavor Oscillations". PhD thesis. 2003. arXiv: 0308228 [astro-ph].

[19] Georg G. Raffelt et al. "Supernova neutrinos: Flavor-dependent fluxes and spectra". In: *Neutrino oscillations and their origin. Proceedings, 4th International Workshop, NOON2003, Kanazawa, Japan, February 10-14, 2003*. 2003, pp. 380–387. arXiv: `astro-ph/0303226 [astro-ph]`.

[20] Huaiyu Duan, George M. Fuller, and Yong-Zhong Qian. "Analysis of collective neutrino flavor transformation in supernovae". In: *Physical Review D* 74.12 (Dec. 2006), p. 123004. arXiv: `0703776 [astro-ph]`.

[21] Huaiyu Duan, George M. Fuller, and Yong-Zhong Qian. "Collective neutrino flavor transformation in supernovae". In: *Physical Review D* 74.12 (Dec. 2006), p. 123004. arXiv: `0703776 [astro-ph]`.

[22] Alexander Friedland and Andrei Gruzinov. "Neutrino signatures of supernova turbulence". July 2006.

[23] J. P. Kneller and G. C. McLaughlin. "Monte Carlo neutrino oscillations". In: *Physical Review D* 73.5 (Mar. 2006), p. 056003.

[24] R. W. Boyd. *Nonlinear Optics*. Third. Elsevier, 2008. ISBN: 978-0-12-369470-6.

[25] I. Ploumistakis, S. D. Moustaizis, and I. Tsohantjis. "Towards laser based improved experimental schemes for multiphoton e+e-pair production from vacuum". In: *Physics Letters, Section A: General, Atomic and Solid State Physics* 373.32 (2009), pp. 2897–2900. arXiv: `0907.2555v1`.

[26] I. Ploumistakis, S.D. Moustaizis, and I. Tsohantjis. "Towards laser based improved experimental schemes for multiphoton pair production from vacuum". In: *Physics Letters A* 373.32 (2009), pp. 2897–2900.

[27] James Kneller and Cristina Volpe. "Turbulence effects on supernova neutrinos". In: *Physical Review D* 82.12 (Dec. 2010), p. 123004. arXiv: `1006.0913`.

[28] Eg Adelberger and a García. "Solar fusion cross sections. II. The pp chain and CNO cycles". In: *Reviews of Modern …* 83.March (2011). arXiv: arXiv:1004.2318v3.

[29] James P. Kneller, Gail C. McLaughlin, and Kelly M. Patton. "Stimulated neutrino transformation with sinusoidal density profiles". In: *Journal of Physics G: Nuclear and Particle Physics* 40.5 (May 2013), p. 055002. arXiv: arXiv:1202.0776v1.

[30] Ilídio Lopes and Sylvaine Turck-Chièze. "Solar Neutrino Physics Oscillations: Sensitivity To the Electronic Density in the Sun's Core". In: *The Astrophysical Journal* 765.1 (2013), p. 14.

[31] Kelly M. Patton, James P. Kneller, and Gail C. McLaughlin. "Stimulated neutrino transformation through turbulence". In: *Physical Review D* 89.7 (Apr. 2014), p. 073022. arXiv: arXiv:1407.7835v1.

[32] Sean M. Couch and Christian D. Ott. "The Role of Turbulence in Neutrino-driven Core-collapse Supernova Explosions". In: *The Astrophysical Journal* 799.1 (Jan. 2015), p. 5.

[33] B. Muller and H.- T. Janka. "Non-radial instabilities and progenitor asphericities in core-collapse supernovae". In: *Monthly Notices of the Royal Astronomical Society* 448.3 (Feb. 2015), pp. 2141–2174.

[34] Hans-Thomas Janka, Tobias Melson, and Alexander Summa. "Physics of Core-Collapse Supernovae in Three Dimensions: A Sneak Preview". In: *Annual Review of Nuclear and Particle Science* 66.1 (2016), pp. 341–375. arXiv: 1602.05576.

[35] C. Patrignani et al. "Review of Particle Physics". In: *Chin. Phys.* C40.10 (2016), p. 100001.

[36] Hans-Thomas Janka. *Neutrino Emission from Supernovae*. Ed. by Athem W. Alsabti and Paul Murdin. Cham: Springer International Publishing, 2017, pp. 1575–1604. ISBN: 978-3-319-21846-5.

[37] E. Kemp. "The Deep Underground Neutrino Experiment: The precision era of neutrino physics". In: *Astronomische Nachrichten* 338.9-10 (2017), pp. 993–999.